Department of Precision and Microsystems Engineering

Metrology design for improving the beam stability in an e-Beam Lithography machine

S. A. van den Boogaart

Report no : 2020.007
Coach : Dr. ir. L. Cacace
Professor : Ir. J.W. Spronck
Specialisation : Opto-mechatronics
Type of report : Master of Science Thesis
Date : February 6, 2020

TU Delft Delft University of Technology

RAITH NANOFABRICATION

Challenge the future

Metrology design for improving the beam stability in an e-Beam Lithography machine

by

S. A. van den Boogaart

For obtaining the degree of

Master of Science
in Mechanical Engineering

at the Delft University of Technology,
to be defended on Thursday February 6, 2020 at 13.45 PM.

Student number:	4189957	
Supervisor:	Dr. ir. L. Cacace	
Thesis committee:	Ir. J. W. Spronck,	TU Delft
	Dr. ir. L. Cacace,	TU Delft
	Dr. ir. A. Sakes,	TU Delft
	Ir. R. van der Pluijm,	Guest

An electronic version of this thesis is available at `http://repository.tudelft.nl/`.

TU Delft Delft University of Technology

RAITH NANOFABRICATION

Abstract

There is an increasingly demand for higher performing e-beam lithography machines. An important user requirement is the beam stability, this is defined for the short and long term. This thesis focuses on improving the beam stability with the use of a new metrology design. The e-beam machine has the potential to real-time correct for all correctly measured mechanical displacements, which makes the metrology a powerful tool in ensuring high beam stability. In the current system the main contributors to displacement measurement errors are vibrations and thermal drift present on/in the metrology system. These measurement errors decrease the beam stability. The proposed metrology design makes use of a differential displacement measurement between the electron optical column and the stage. This makes the displacement measurement almost insensitive to vibrations and thermal drift. The short term beam stability is improved from < 5 nm to < 3.5 nm and the long term stability is improved from < 50 nm to < 9 nm.

Acknowlegdements

Thank you to Ricardo for the unlimited amount of support and feedback. And thank you to Lennino and Pieter for their guidance and enthusiasm for the field.

S. A. van den Boogaart

Contents

1 Introduction **1**
1.1 Relevance 1
1.2 E-beam lithography 1
1.3 Current system 3
1.4 Thesis aim and scope 10

2 System evaluation **11**
2.1 Mechanical system 11
2.2 Metrology 12
2.3 Conclusion 13

3 Requirements **14**
3.1 User requirements 14
3.2 Mechanical constraints 17
3.3 Environmetal conditions 19
3.4 Operational conditions 19
3.5 Other requirements/specifications 20

4 Error sources **21**
4.1 Static errors 21
4.2 Dynamic errors 28
4.3 Error budgets current system 39

5 Concepts **43**
5.1 Focus areas 43
5.2 Distance measurement principles 43
5.3 Strategies 45
5.4 Filtering solutions 49
5.5 Generating concepts 51
5.6 Comparing concepts 52

6 Detailed concept **58**
6.1 Design overview 58
6.2 Optical design 59
6.3 Opto-mechanical design 62
6.4 Design issues and solutions 69

7 Column mirror design **75**
7.1 Flexure design 75
7.2 Alignment system 78
7.3 Mirror design 80

7.4 Dynamic behaviour analysis 80

8 Concept analysis: error budget **84**
8.1 Beam stability 84
8.2 Other user requirements 85

9 Conclusion **86**

10 Recommendations **87**

List of Figures

1.1 SEM image of a pattern with a feature size < 6 nm written with the Raith EBPG5200 e-beam lithography machine[3] . . . 2
1.2 The EBPG5200 . . . 3
1.3 Electron optical column overview . . . 4
1.4 Vacuum setup . . . 5
1.5 Connection vacuum cover and top plate stage suspension . . . 5
1.6 Inside the stage suspension stage suspension: the x-y stage with the superplate on top and the x-y mirrors for the interferometers . . . 6
1.7 Overview metrology . . . 7
1.8 Metrology system . . . 7
1.9 Metrology system . . . 8
1.10 Working principle of a double pass heterodyne interferometer . . . 9

2.1 Force loop . . . 11
2.2 Metrology loop . . . 12
2.3 Coupled metrology and force loop . . . 13

3.1 Beam stability . . . 15
3.2 Stage move . . . 16
3.3 Stage step time . . . 17
3.4 Working distance final lens . . . 18
3.5 Parallelism . . . 18
3.6 Z-stage edition . . . 18

4.1 System overview mechanical connections . . . 22
4.2 Cosine error . . . 22
4.3 Cosine error alignment procedure . . . 23
4.4 Mirror form error . . . 24
4.5 Example of the mirror surface profile . . . 24
4.6 Mirror non-orthogonality . . . 25
4.7 Two measurements on a marker mask plate with a 90° rotation of the mask between them . . . 25
4.8 Yaw abbe error arising from the moment arm between the axis of measurement and the axis of movement . . . 26
4.9 Pitch/roll abbe error arising from the moment arm between the axis of measurement and the axis of movement . . . 27
4.10 Marker Intensity curvature . . . 28
4.11 Example data set of beam error feedback data . . . 29
4.12 Example data set of beam on edge data, raw data in blue and filtered data in black . . . 30
4.13 Frequency spectrum of the beam error feedback data, peaks are in Volts . . . 30
4.14 Frequency spectrum of the beam on edge data . . . 31
4.15 Frequency comparison between pull in data and beam-on-edge data . . . 31

4.16 Column swing error . . . 33
4.17 An example of the accelerometer frequency spectrum of the optical column after a stage step in x . . 34
4.18 Thermal drift for stage position measurement . . . 35
4.19 Thermal centre of the interferometer brackets . . . 36
4.20 Thermal centre of the top plate of the suspension . . . 36
4.21 Thermal drift of the x-interferometer and the ΔT of the room temperature over time . . . 38
4.22 Beam stability: error sources . . . 39
4.23 Error budgets beam stability . . . 40

5.1 Two different optical encoders, one using a 1D optical grating the other a 3D optical grating . . . 44
5.2 Strategies for improving the short term dynamic behaviour . . . 45
5.3 Reduce vibrations . . . 45
5.4 Decouple force frame and metro frame . . . 46
5.5 Add stiffness in the system . . . 46
5.6 Compensate vibrations . . . 47
5.7 Strategy for improving long term dynamic behaviour . . . 47
5.8 Strategy and solutions tree for improving long term dynamic behaviour . . . 48
5.9 Filtering reduce vibrations solution . . . 49
5.10 Filtering solutions of decouple force frame and metro frame . . . 49
5.11 Filtering solutions of add stiffness . . . 50
5.12 Filtering solutions of compensate vibrations . . . 50
5.13 Differential interferometer with a measurement between stage and optical column . . . 51
5.14 Optical surface encoder measurement system with an optical grating on both sides of the stage and a interferometer on the electron beam column . . . 52
5.15 Sensitivity of a differential interferometer . . . 53
5.16 Sensitivity in pitch direction: cosine error . . . 54
5.17 Approximation of a plate-with-hole that is clamped on all outer edges as a beam that is clamped on one side with a width b that is equal to the perimeter of the hole . . . 55
5.18 Loads on the beam with the moment $M = P \cdot \Delta x$ . . . 55
5.19 Displacement of the vacuum setup . . . 57

6.1 Overview concept . . . 59
6.2 Differential interferometer design (based on the Keysight 10719A) . . . 60
6.3 Keysight 10721A two-axes differential interferometer . . . 60
6.4 Retro-reflector: 3 reflecting surfaces at 90 degrees to each other . . . 61
6.5 Interfero mount . . . 62
6.6 Height meter ring and final lens assembly . . . 63
6.7 Mounting mirror directly to final lens . . . 63
6.8 Mounting the mirrors to the optical column with three notched leaf springs in two different ways. The thermal centre coincides with the optical axis . . . 63
6.9 **Mirror mount concept 3:** looking from below to the optical column, two stiff rods reference the the mirrors to the centre of the optical column. Looking from the side a wire flexure connects the mount to the column. . . . 64
6.10 Angles α_{cs} and β_{cs} between the mirror set on the stage and mirror set on the column . . . 65
6.11 Yaw and pitch movements . . . 65
6.12 Yaw and pitch movements sensitivity vs alignment angle . . . 66
6.13 Alignment strategy . . . 69
6.14 Current situation . . . 70
6.15 New situation . . . 70
6.16 Prism . . . 71
6.17 Error column swing . . . 71
6.18 First six eigenmodes of the original column assembly . . . 72

6.19 First eigenmodes of the different supported column assemblies . . . 73
6.20 The first six eigenmodes that correspond with the first six eigenmodes of the original column assembly and the relative increased stiffness, mass and eigenfrequency. . . . 74

7.1 Mirror mount design . . . 75
7.2 Two screws with opposite rotational freedom together constraint 6 DOF's . . . 76
7.3 The required constraint lines and different mechanisms that fulfill the constraints . . . 76
7.4 Flexures orientation and dimensions . . . 77
7.5 Alignment ring of the column mirror mount . . . 78
7.6 Mounting the alignment ring of the mirror mount . . . 78
7.7 Mirror mount integrated in current system . . . 79
7.9 Mirror design . . . 80
7.10 First eigenmodes of the two different flexures . . . 81
7.11 Steady state thermal expansion with $\Delta T = 0.1$ K for the mount with aluminum flexures . . . 82
7.12 Deformation due to gravity with the aluminum flexures . . . 82
7.13 Stress in the flexure due to a 0.05 mm lateral displacement . . . 83

List of Tables

3.1 User requirements . . . 14
3.2 Mechanical constraints . . . 17
3.3 Environmental conditions . . . 19
3.4 Operational conditions . . . 19

4.1 Writing parameters . . . 37
4.2 Error in OPL for the x-interferometer due to an isothermal temperature increase of $\Delta T = 0.1$ K . . . 38
4.3 Error in OPL for the y-interferometer due to an isothermal temperature increase of $\Delta T = 0.1$ K . . . 38
4.4 Static non-repeatable errors with error source e_3 . . . 40
4.5 Short term beam stability error budget . . . 41
4.6 Long term beam stability error budget . . . 41
4.7 Static error sources of the accuracy . . . 42

5.1 Comparison between concept 1 and concept 2 . . . 53
5.2 Total optical path length error due to static loads . . . 56

6.1 Comparison between Mirror mount concepts 1 and 2 . . . 64
6.2 Dynamic yaw and pitch movements . . . 67
6.3 Pitch tolerance for β_{cs}: pitch angle between the mirrors on the stage and on the optical column . . . 67
6.4 Yaw tolerance for α_{cs}: yaw angle between the mirrors on the stage and on the optical column . . . 67
6.5 Tolerance for pitch angle between the interferometer and mirrors . . . 68

7.1 Flexure materials . . . 77
7.2 Flexure dimension for different materials . . . 77
7.3 First six eigenfrequencies of the mirror mount . . . 81

8.1 Non-repeatable static errors with error source new system . . . 84
8.2 Total yaw angle between optical components . . . 84
8.3 Short term beam stability error budget new system . . . 85
8.4 Long term beam stability error budget new system . . . 85

Abbreviations

ϵ	Error
λ	Wavelength
ΔOPL	Change in optical path length
AC	Alternating current
BB	Beam bender
BS	Beam splitter
CD	Critical dimension
CSR	Column support ring
CTE	Coefficient of thermal expansion
DC	Direct current
DOF	Degree of freedom
e-beam	Electron beam
EBPG	Electron beam pattern generator
HeNe	Helium Neon
HMR	Height meter ring
Metro	Metrology
OPL	Optical path length
OTS	Of the shelf
RSS	Root sum square
SEM	Scanning electron microscope

Chapter 1

Introduction

Raith nanofabrication is a leading company when it comes to nanofabrication, especially e-beam lithography machines. Because of the high demand for increasingly better e-beam machines, Raith puts a lot of resources in research and development. To boost the research even more, Raith collaborates with universities and this thesis project is a consequence of this. This thesis project is a collaboration between the TU Delft and Raith nanofabrication.

1.1 Relevance

Every day new technologies are developed which almost always make use of electronic chips in some way or another. Because of this there is an urge to make chips smaller and faster. Right now, this is ability is started to reach a limit. New technologies are necessary to advance technologically. Optical wave guides are an example of such a new promising technology. This requires a lot of research and this creates a high demand for high resolution nanofabrication that makes fabrication of 1 prototype easy. E-beam lithography makes a huge contribution in this regard, because at the moment it is the only method to produce such specific and ultra high resolution chips. There are also many new promising technologies in the biomechanical industry/life sciences such as NEMS devices or lab-on-a-chip devices.

1.2 E-beam lithography

E-beam lithography is a nano-fabrication method that arises in the 1960's around the same time optical lithography arises[2]. The two fabrication processes are very similar as they both use particles to transfer energy to a resist. Even the optics used in both systems are very similar in their working principle. The main difference however, is that in optical lithography photons are used and in e-beam lithography electrons are used as the energy carrier. In optical lithography lenses are used to focus light by using the difference in refraction of different media, while in e-beam lithography electrostatic or magnetic lenses are used to focus the electron beam. This works based on the fact that electrons are charged particles. When a charged particle moves through an electric or magnetic field, the particle experiences a force. This is described by the Lorentz force[1]:

$$\boldsymbol{F} = q\boldsymbol{E} + q(\boldsymbol{v} \times \boldsymbol{B}) \tag{1.1}$$

Where q is the charge of the particle $\boldsymbol{E}$ is the electric field vector, $\boldsymbol{v}$ is the speed vector of the charged particle and $\boldsymbol{B}$ is the magnetic field vector. This force is used to change the trajectory of the particle. The $q\boldsymbol{E}$ part represents the electrostatic force, while the $q(\boldsymbol{v} \times \boldsymbol{B})$ part represents the magnetic force. Because electron optics is based on this principle, a few significant differences between optical lithography exist. The first difference is that electrons repel each other, because their charge has the same sign. If the electron beam has a high current density this repelling force will have a defocusing effect and this needs to be taken into account, this is called Coulomb interaction. This repelling effect is not present in optical lithography. Another phenomena that only occurs in e-beam lithography is

that when the electrons are deflected using a magnetic lens a rotation effect will occur. When taking a closer look at the magnetic force part of equation 1.1, one can see that if the velocity vector $\boldsymbol{v}$ and the magnetic field vector $\boldsymbol{B}$ are not parallel and not orthogonal to each other the electrons will have a helical trajectory with its axis parallel to the magnetic field. This happens because the Lorentz force in that case will have a component orthogonal to the magnetic field and a component parallel to the magnetic field. This will lead to a rotation of the image on the resist when it is not corrected for. Another difference is the way patterns are 'written' on the resist. Because electron optics use electric and magnetic lenses, the electric potential or magnetic field can be changed directly by either changing the voltage or the current. In using this the electron beam can be actively deflected and instead of using a mask as is done in optical lithography to write a pattern, the beam can write a pattern directly by deflecting the electron beam. This is called "direct write". This has its advantages and disadvantages. An advantage is of course that no separate (expensive) mask is needed and writing patterns are extremely flexible. But a disadvantage is that it is very challenging to increase throughput. An optical lithograpy machine such as the Extreme Ultra Violet (EUV) machine from ASML has a throughput of up to 170 wafers an hour. At the moment this is way out of reach for current e-beam lithography systems. Therefore the main market for e-beam lithography machines is not to mass produce integrated circuits, but as stated before is mainly used in the fabrication of research and specialty nanotechnology. Also, still half of the production of photomasks used for optical lihography is done with an e-beam[2]. One of the big advantages of e-beam lithography compared to optical lithography is that much higher resolutions and smaller feature sizes can be achieved.[2] The main limiting factor in optical lithography is that the critical dimension (CD) is limited by the optical wave length of light (λ) as described by Equation 1.2.

$$CD \propto \lambda \tag{1.2}$$

So the smaller wavelength can be used, the smaller the CD can be. For optical lithography machines the state-of-the-art ASML EUV lithography scanner uses deep UV light with a wave length of 13.5 nm and going much smaller than this wavelength is very difficult. As electrons can also be described as a wave, in e-beam lithography there is an equivalent way of describing the wavelength of an electron[2]:

$$\lambda_e = \frac{1.226}{\sqrt{V}} \text{ (nm)} \tag{1.3}$$

λ_e is the wavelength of the electron and V is the energy of the electrons given in the unit electron volt (eV). Equation 1.3 shows that the higher the energy of the electron, the shorter the wavelength will be. This already indicates that e-beam lithography could have a much higher resolution, as the electron wavelength could be up to a factor 10^5 smaller than is possible with the wavelength of light. But in e-beam lithography the limiting factor for the CD is not the electron wavelength, but electron scattering in the resist and electron aberrations[2]. Still, feature sizes < 10 nm are possible. Figure 1.1 even illustrated a pattern with a feature size of below 6 nm!

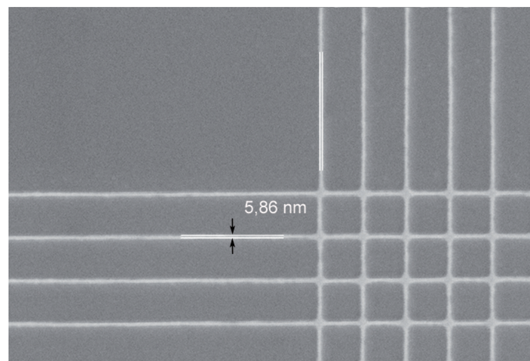

Figure 1.1: SEM image of a pattern with a feature size < 6 nm written with the Raith EBPG5200 e-beam lithography machine[3]

1.3 Current system

1.3.1 EBPG5200

One of the state-of-the-art e-beam lithography machines on the market is the EBPG5200 from Raith nanofabrication. The EBPG, or Electron Beam Pattern Generator, has a Gaussian beam shape that writes the pattern. This means the current of the electron beam has a Gaussian distribution across its diameter. The EBPG consists of several subsystems. Perhaps the most important part of the machine is the electron optical column. In this part of the machine the electron beam is generated and shaped. This electron beam is then aimed at the substrate located in the vacuum chamber. To move this substrate inside the vacuum chamber a linear x-y-stage is actuated. The vacuum chamber is supported by a large frame which is connected to the ground with four dampers. A system overview can be seen in Figure 1.2.

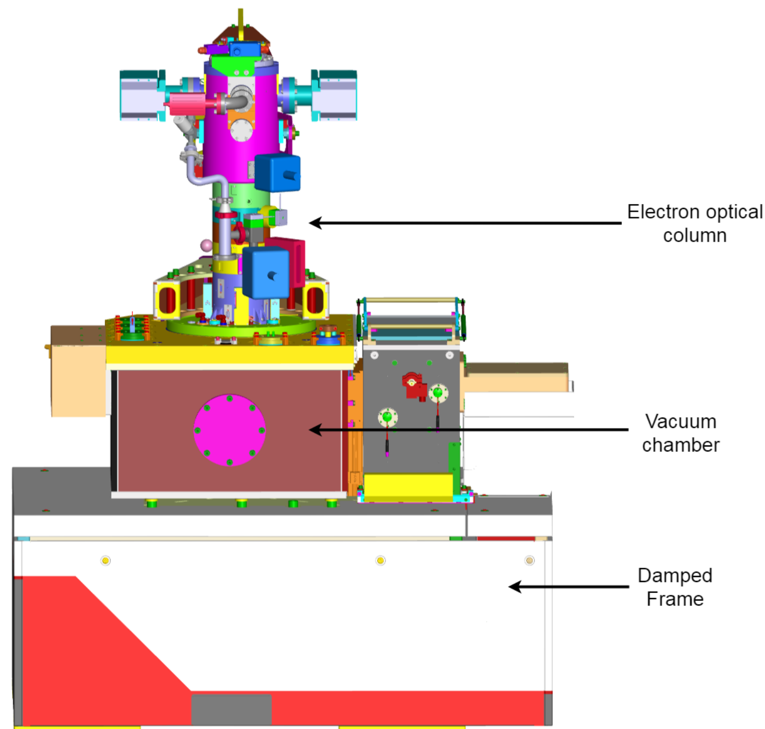

Figure 1.2: The EBPG5200

1.3.2 Electron optical column

The electron optical column is the heart of the machine. In this part the electron beam is created, shaped and deflected. Figure 1.3 shows an overview of the column. In the top part of the column the source is located. The source is a Schottky-type field emission gun[4], consisting of a tungsten wire heated filament with a very fine tip that has a radius $< 1\mu m$ from which the electrons are emitted. The combination of heating the filament and using an electric potential (up to 100 kV) makes sure electrons are emitted and accelerated. At the same time C1, an electrostatic lens, focuses the beam to the first cross over. After the beam is accelerated the beam is tilted and shifted using alignment coils such that the beam is co-axial with the optical axis in the centre of the column. With a second lens (C2), this time an magnetic lens, the beam is focused again to the second cross over located in the optical centre of the beam blanker. The beam blanker can blank the beam during writing when necessary, by deflecting the beam of electrons sideways away from the optical axis.

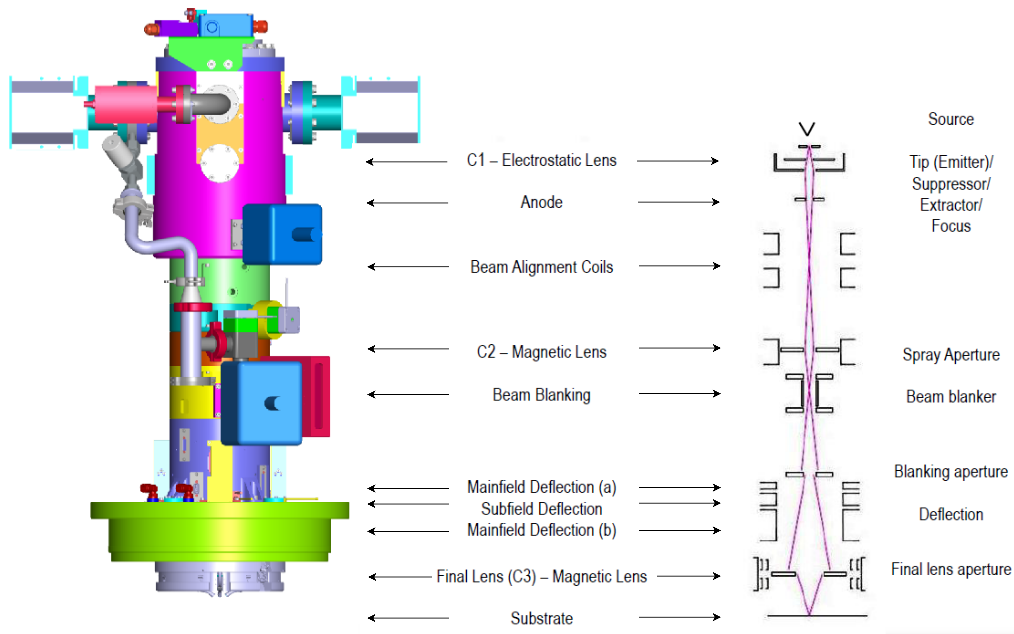

Figure 1.3: Electron optical column overview

After the beam blanker it enters the part of the column where the beam is deflected. This is the part where the writing pattern is generated by deflecting the electron beam. It exists of a coarse deflection and a fine deflection part. The coarse deflection deflects the beam within a main field (maximum area of $1024\mu m$ x $1024\mu m$), whereas the fine deflection deflects the beam in a sub-field within the main field (maximum area of $4.5\mu m$ x $4.5\mu m$). Then finally, the beam is focused on the substrate with the final lens (C3), also an magnetic lens. In the final lens an aperture is present that can be mechanically changed between three different sizes. The spotsize and beam current can be varied by changing the ratio between the voltage in C1 and the current in C2 and/or by changing the aperture in the final lens. The spotsize can range from 2 nm all the way to $\sim$ 200 nm and the beam current can be varied between 100 pA - 200 nA.

1.3.3 Vacuum setup

To make writing with an electron beam possible, a vacuum should be present. Otherwise all the electrons would bump into/interact with other atoms and the beam will be incoherent and loose all focus. This means that from the point the e-beam is formed until it reaches the substrate a vacuum should be ensured. For the e-beam source in the column this vacuum is very critical and a pressure lower than 10^{-9} mbar is necessary[4]. Such a high level vacuum is necessary to ensure a low enough work function and therefore high emission of electrons. It is also necessary to prevent electric potential breakdown and to lengthen the filament lifetime. In the vacuum chamber attached to the column a pressure of 10^{-7} mbar is sufficient.

The vacuum chamber

Figure 1.4a shows a cross section of the CAD drawing of the vacuum setup and Figure 1.4b shows a more schematic overview of the vacuum setup. The column is connected to the vacuum chamber by the column support ring (or CSR). As the name suggest, this ring serves as a connection that supports the weight of the column on the vacuum chamber. Both the vacuum cover plate and the CSR are made of Invar36®, this material is chosen to reduce the thermal expansion (Invar36 has a CTE of $1.2 \cdot 10^{-6} K^{-1}$[6]) and the errors it gives for the metrology. Both are also water cooled around the perimeter of the column to minimise the heat conducting from the surroundings to the

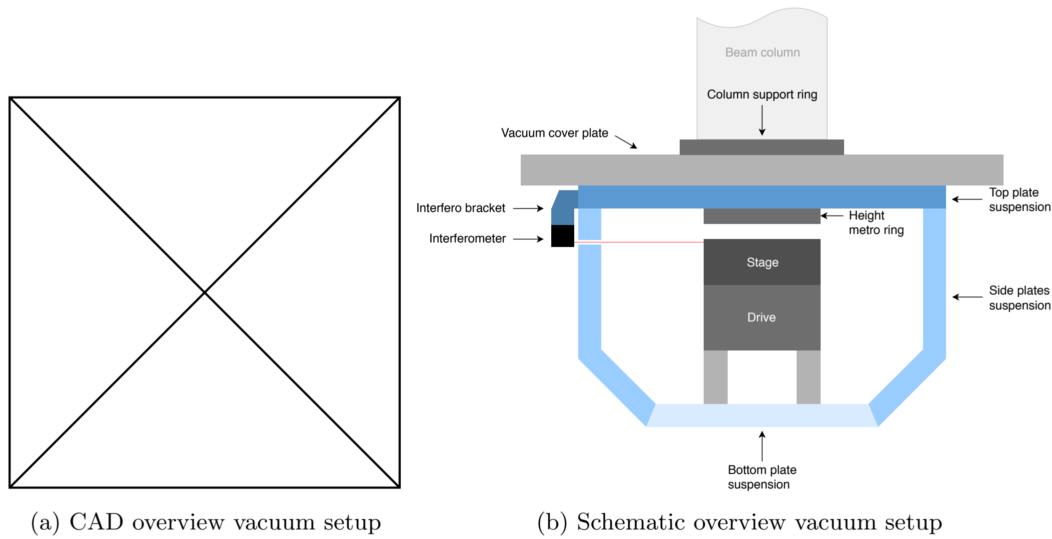

(a) CAD overview vacuum setup

(b) Schematic overview vacuum setup

Figure 1.4: Vacuum setup

metrology and stage. The vacuum chamber is closed off with side and bottom plates which are made of steel. In one of the side plates a slit valve is located through which the substrate holder can be loaded unto the stage. This slit valve is connected to an airlock. The airlock makes sure the vacuum in the vacuum chamber is maintained while loading a new substrate on the stage. To the bottom plate a turbomolecular pump is attached.

Inside the vacuum chamber multiple systems are located, namely the stage suspension, stage mount, stage and metrology. The stage suspension is a closed box that exists of a top plate, four side plates and a bottom plate. The closed box design adds stiffness to the stage suspension and to make it even more stiff the side plates are made slightly slanted towards the bottom of the suspension. In the side plates a lot of holes are present, this is not only to make the suspension lighter, but also to ensure a clear path for air molecules to be guided away from the vacuum chamber. The stage is mounted to the bottom plate of the stage suspension and most of the metrology is attached to the top plate. Both the top and bottom plate are made of Invar, while all the side plates are made of Aluminum. The top plate is made of Invarto reduce thermal expansion in this plate and therefore reduce errors in the metrology. For the side plates the expansion due to variations in temperature has less influence on the metrology so for this aluminum has been chosen. It is not exactly clear why the bottom plate of the stage suspension is made out of Invar, it could be to also reduce lateral thermal expansion parallel to the measurement axis. The top plate is attached to the vacuum cover with 4 small stainless steel struts on each corner and bolts around the column opening. There is a small gap between the cover and this plate starting a few centimeter from the column opening and reaching all the way to the edge of the plate. This is illustrated in Figure 1.5. This gap should reduce the amount of thermal conduction into the system by reducing the contact area between the two plates and therefore increasing the thermal resistance.

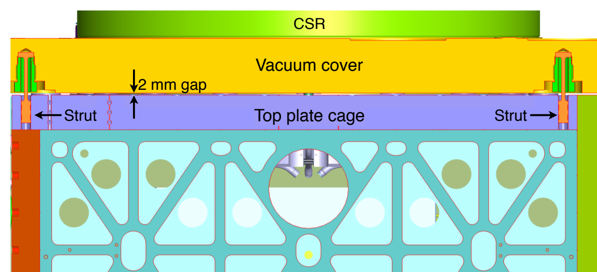

Figure 1.5: Connection vacuum cover and top plate stage suspension

To the top plate of the stage suspension the brackets of the interferometers in x- and y-direction are attached. Also the bracket for the beamsplitter and reference arm are attached to this top plate. There are multiple reasons that the stage suspension is made as a box hanging from the vacuum cover. The first reason is to make maintenance inside the vacuum chamber an easier process. A crane can be attached to the CSR which (when the vacuum cover is decoupled from the sides) can lift the optical column + vacuum cover and stage suspension in one movement. This makes sure maintenance can be done in the vacuum chamber while ensuring alignment is kept between the optical column and the stage/metrology setup. The other reason is to reduce the influence from the surroundings on the stage and metrology, in particular thermal noise. If temperature differences between different parts in the vacuum chamber are small, the main way of heat flux inside the vacuum chamber will be through conduction. This is reduced by creating only a small contact area around the column opening (as discussed before) and the stage suspension setup creates a long thermal path, further increasing the thermal resistance.

1.3.4 Stage setup

The stage is used to position the substrate with respect to the column. The stage exists of two separate linear stages, one for the x- and one for the y-direction. The two stages are stacked on top of each other, hence the y-stage also has to move the x-stage when it is actuated. Each stage consists of a steel plate with two linear bearing guides and is actuated using a rack and pinion and a DC motor. The stage is attached to the bottom plate of the stage suspension with three rigid connections. The mounting consists of a bolting mechanism which can be adjusted in height for alignment. When the correct position is achieved, a preload ensures any play is minimized. On top of the stage the 'superplate' is located. This is a Zerodur® block which provides a kinematic mounting interface for the substrate holders and in which two mirrors for the metrology are integrated. Zerodur is a glass-ceramic with an extremely low coefficient of thermal expansion of $\sim 0.02 \cdot 10^{-6} K^{-1}$[7]. So the reason Zerodur has been chosen is to reduce any expansion of the mirrors and therefore reduce metrology errors.

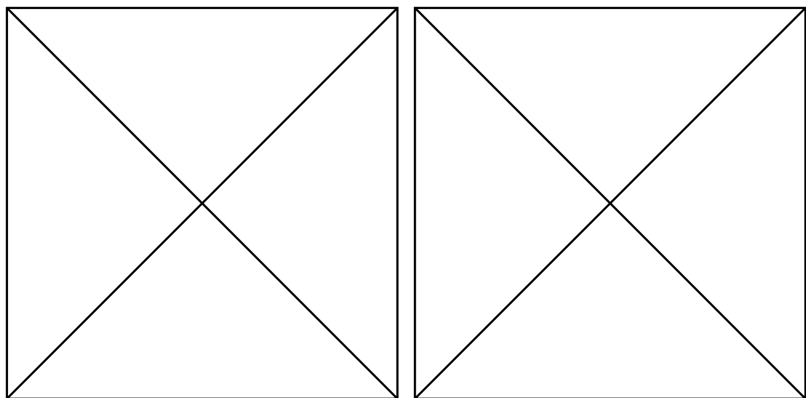

(a) Picture of the inside of the stage suspension stage suspension

(b) CAD drawing of the inside of the stage suspension stage suspension

Figure 1.6: Inside the stage suspension stage suspension: the x-y stage with the superplate on top and the x-y mirrors for the interferometers

1.3.5 Metrology system

In Figure 1.7 all the metrology components are displayed. The metrology exists of a laser, a beam dump, three beamsplitters, two interferometers, two mirrors, optical fibres and electronics. Also all the mounts of the components are part of the metrology.

The metrology uses two heterodyne double pass interferometers, which are explained in detail later in the chapter. They measure the displacement of the mirrors located on the stage. Heterodyne means that the intereferometers use laser light that is comprised of a spectrum of two frequencies, f_1 and f_2, that are linearly polarized with an

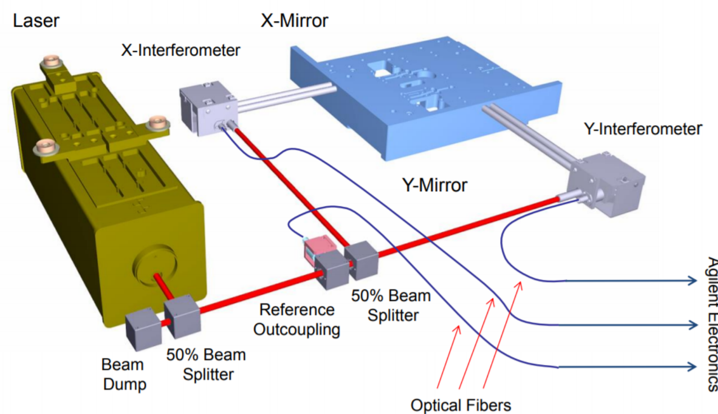

Figure 1.7: Overview metrology

angle of 90 degrees between them (orthogonally polarized). The two frequencies only have a slight shift Δf of about 2MHz between them. This small frequency shift is created inside the laser with the use of the Zeeman effect. The laser used by the interferometers is a Helium Neon (HeNe) laser that produces light with a wavelength of 632.99137 nm ≈ 633 nm and a beam diameter of 6 mm. The laser is mounted outside of the vacuum chamber to the side of the vacuum cover plate, as depicted in Figure 1.9c. After the light exits the laser it will enter a 50% beamsplitter that dumps half of the light in a beam dump to reduce the light intensity. The beamsplitter and beamdump are mounted to the same bracket as the laser outside the vacuum chamber and the setup is shown in Figure 1.9d. The mount is made of Invar. It is not completely clear why this mount is made of this material, as thermal expansion of this part is not very critical (the two different frequencies in the laser beam are not separated at that point and both get the same Doppler shift). The mount has an alignment mechanism that can align yaw and tilt. It consists four line contacts between a concave and a convex surface. The two parts of the mount can be rotated relative to each other and then bolted down. After this, the light enters another two beamsplitters mounted on a bracket as can be seen in Figure 1.9b. The bracket is made of stainless steel and the mount of the beamsplitters is made of Invar. Again, why the mounts are made out of Invar is not completely clear, because at this point expansion of the mount has no effect on the actual measurement of the stage displacement. And if it would, the advantages of the Invar would be nullified by using a stainless steal bracket. The first beam splitter splits 15% of the light to a reference signal, while the second is a 50% beam splitter. The two beamsplitters have the same alignment mechanism as the first beamsplitter. After this, the light enters both of the interferometers, one on the x- and one on the y-axis. Figure 1.9a shows the mounts that connect the x- and y-interferometers to the top plate of the stage suspension. The mounts are made of Invar and have the same alignment mechanisms as the other optical components.

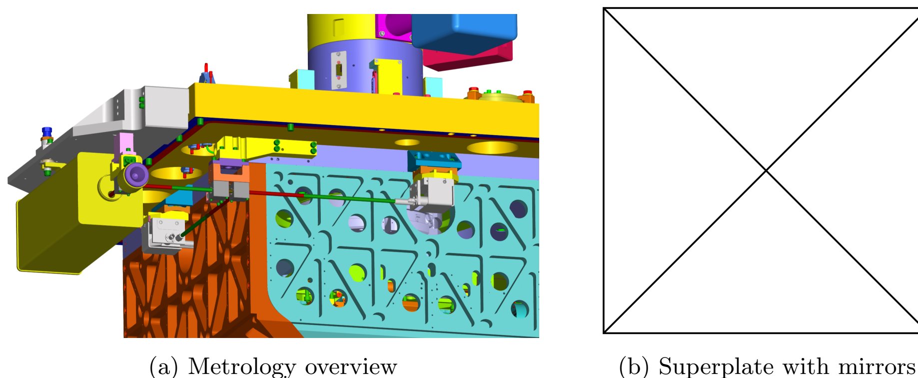

(a) Metrology overview

(b) Superplate with mirrors

Figure 1.8: Metrology system

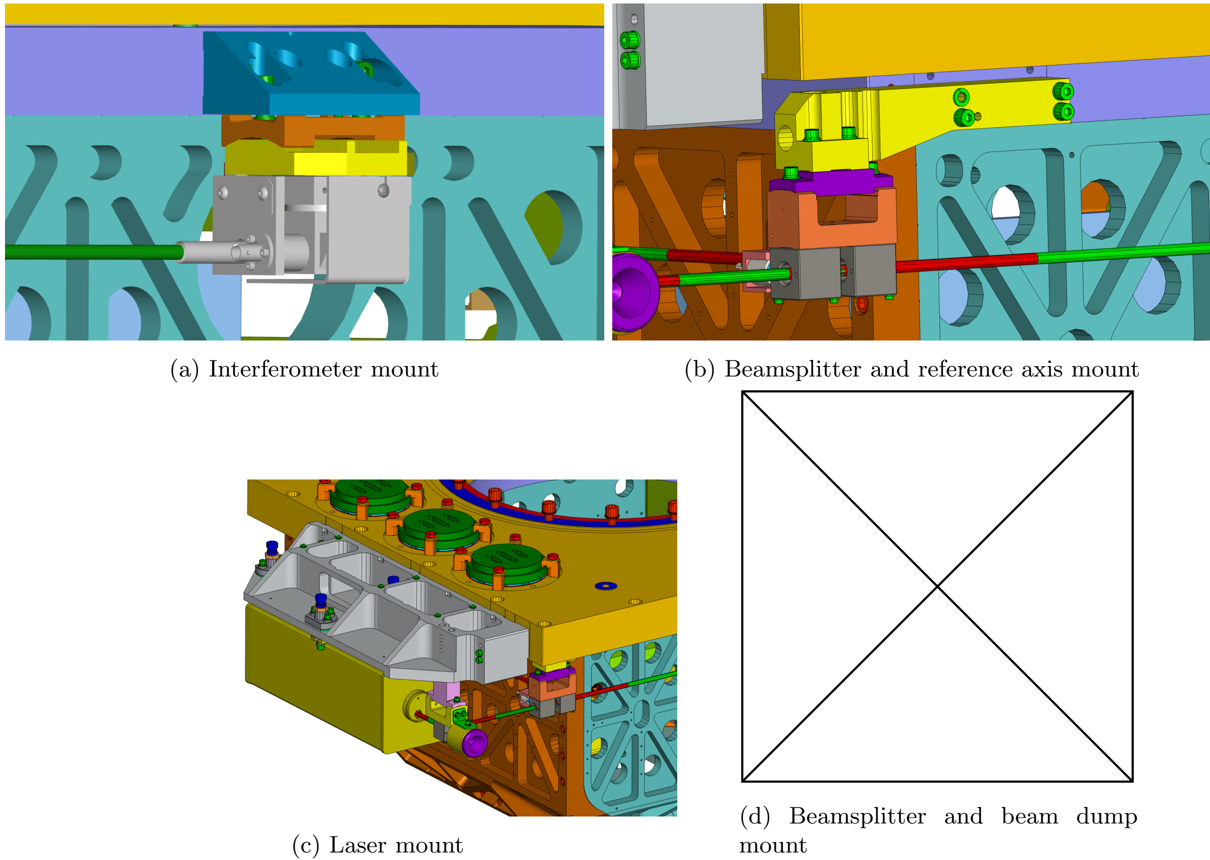

(a) Interferometer mount

(b) Beamsplitter and reference axis mount

(c) Laser mount

(d) Beamsplitter and beam dump mount

Figure 1.9: Metrology system

These mounts do make sense that they are made of a material with a low thermal expansion coefficient, because this does effect the measurement stability. After the laser beam leaves the interferometer the two frequencies are split and only one of the frequencies gets a Doppler shift, namely the one that is reflected on the stage mirror. The interfered light enters the optical fibres and is processed using electronics and software. These mounts do make sense that they are made of a material with a low thermal expansion coefficient, because this does effect the measurement stability.

Interferometer working principle

As shown in Figure 1.10, the light from the laser exists of two frequencies f_1 and f_2 that are orthogonal polarized. In the interferometer itself the light enters a polarizing beamsplitter which reflects the part of the beam with frequency f_2, which is polarized 90 degrees to the transmission axis. The other part of the beam with frequency f_1 will be transmitted. The reflected beam will pass through a quarter wave plate and will be right handed circular polarized. It then reflects off the mirror on the stage and will be left handed circular polarized. After passing through the quarter wave plate again it will be linear polarized, but with a 90 degrees phase shift (compared to the beam before the first quarter wave plate). As it encounters the polarizing beamsplitter again, this time it will be passed through. The beam will then encounter a corner cube after which it will be passed through the polarizing beamsplitter again. Then it will pass through the quarter wave plate, making the beam left handed circularly polarized. The beam will reflect again at the stage mirror making it right handed circular polarized. As it passes through the quarter wave plate, the beam will be phase-shifted again and will have a 180 degrees phase shift (compared to the original beam with f_2). As it encounters the polarizing beamsplitter again, this time it will be reflected. The beam with

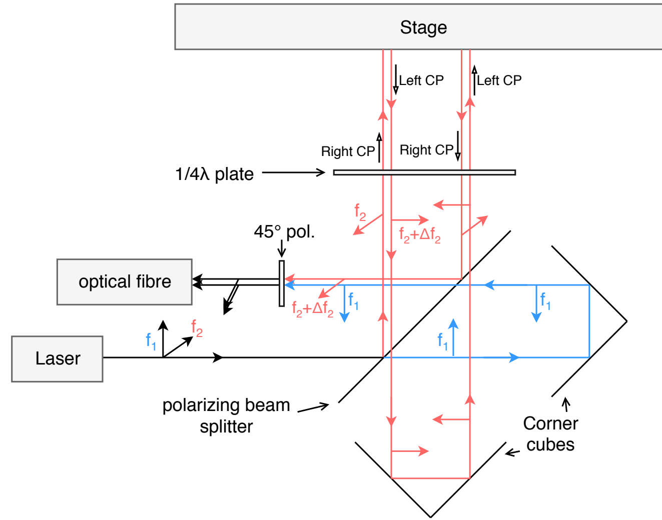

Figure 1.10: Working principle of a double pass heterodyne interferometer

frequency f_1 (after passing through the polarizing beamsplitter) will be reflected in a cube corner. It then passes through the polarizing beamsplitter again. The two beams with frequencies f_1 and f_2 are at this point combined. They will pass through a 45 degrees polarizer, which will project the two beams on the 45 degree axis, making both of the beams linearly polarized with the same polarization state. This will make the two beams interfere and the signal will be collected in a optical fiber. As the stage moves, the Doppler effect will introduce a frequency shift Δf_2 to frequency f_2. The two beams combined as they enter the optical fiber will then have a frequency difference of: $\Delta f_M = f_2 + \Delta f_2 - f_1$. The maximum measurable velocity is dependent on the beat frequency $f_1 - f_2$ and is equal to 500 mm/s in this system.

The interferometer is a double pass interferometer. This means, as depicted in Figure 1.10, that the light is reflected two times by the measurement mirror. Because of this the light has to travel the distance of the measurement arm four times, hence the optical resolution of the system is $\frac{\lambda}{4} \approx 158$ nm. Fortunately, with interpolation software this can be improved to an electronic resolution of $\frac{\lambda}{4 \cdot 1024} = \frac{\lambda}{4096} \approx 0.155$ nm.

1.3.6 Writing strategy

General writing process

As stated before, the beam has a Gaussian shape which is focused on the substrate and the writing is done by deflecting the beam. This writing process is done in steps. The basic principle is the following. The stage moves the substrate to a new location, then the pattern is written in a certain area on this location. then the stage is moved to a new location again, etc. So the substrate is divided into areas that are called main write fields. The maximum main write field area is 1x1 mm. The stage is moved each time to the middle of the main write field. This field is then again subdivided into so-called sub write fields. Recalling in Section 1.3.2, in one part of the optical column the beam is deflected with the main deflection. This main deflection is used to deflect the electron beam to each center of the sub write field. When the beam is located at the center of the sub write field, the sub field deflection is used to deflect the beam on the sub write field. At this point the writing starts and the pattern is written on the sub write field. If this is done, the main field deflection deflects the beam to the center of the next sub write field, then writing on the new sub write field starts again, etc. If the pattern on the whole main write field is written, the stage moves the substrate to the centre of the next main write field. In this way the pattern is written over the whole substrate.

Another key element of the EBPG is that it can also be used as a SEM (Scanning Electron Microscope). There are scintillators on the bottom surface of the optical column that collect 'back scattered' electrons (and convert them to a photon signal). These are electrons that are reflected back from the surface when the electron beam hits

the substrate. The photon signal is converted to a voltage which can be processed digitally. This principle can be used to calibrate the system. To do this, so-called 'markers' are used. A marker is a tiny square written on the substrate ($\sim \mu$m) that has a high contrast in reflectance compared to the substrate. By 'scanning' over the marker in a systematic way and given the size (and possible location) of the marker a local calibration can be done that has a repeatability and accuracy in $\sim$nm. This is very useful and often markers are used to calibrate before writing a main write field.

Stage positioning

During the writing process the stage has to be moved to each center of the main write field. This is done by actuating the stage based on measurements of the interferometers. The feedback used to position the stage is called 'beam error feedback'. This is the difference between the set-point position and the measured position by the metrology:

$$\text{Beam error feedback} = X_{setpoint} - X_{measured} \tag{1.4}$$

If the stage is within a certain range from the set point position the beam error feedback is used to deflect the electron beam. So the beam error feedback in that case is added as a correction on the main field deflection. This ensures writing can start before the stage is exactly on the set point, but is also used to correct for position deviations. The sampling frequencies of the interferometers is 10 MHz. Every sample either x- or y-direction is read out, leaving the sampling frequency per axis to 5 MHz. Then only 1 in 5 measurements is used, so the sampling frequency is equal to 1 MHz. This means any vibrations with a frequency lower than half of this (given Shannon-Nyquist sampling theorem), so <0.5 MHz, can be used for correction on the main field deflection.

The fact that the electron beam can be corrected for with a frequency of 0.5 MHz with the measurements of the interferometers has very important consequences. This means that pretty much all mechanical vibrations, if measured correctly(!), can be compensated for by deflecting the electron beam. This is because all mechanical vibrations that have any significant amplitude have a frequency << 0.5 MHz. This also means the system does not have to be perfect, mechanically speaking. The stage will have finite accurate guiding, with non-repeatability errors. If this can be measured with the interferometers, it can be corrected for.

Writing speed

The speed or time that is needed to write a main write field is dependent on many variables. Examples of these variables are: the pattern density one writes, which substrate is used, what dose is needed for the substrate, what beam current and beam spot size are used, what high voltage is used and what the desired edge roughness is. The maximum writing frequency is equal to 125 MHz.

1.4 Thesis aim and scope

Because the use of beam error feedback is so powerful, the metrology is a very important aspect in the performance of the system. Users are expecting and demanding an increasingly higher performance. An important user requirement is the beam stability for the short and long term (so for multiple typical user cases). Since the beam stability is for a great extend dependent on correct metrology measurements, a way to improve the performance is by improving the metrology. The aim of this thesis therefore is:

> Improve the short and long term beam stability through improving the metrology design.

The short term beam stability should be improved from 5 nm to 3.5 nm and the long term beam stability should be improved from 50 nm to 10 nm. The scope includes every relevant aspect to the metrology and all other aspects that are relevant for the opto-mechanical functioning of the metrology. The scope does not include other parts of the system, such as the electron optics of the electron optical column, the stage design and the stage controller.

Chapter 2

System evaluation

To achieve a better understanding of the possible problems present in the current system, a short design evaluation will be done. This will be more of a qualitative evaluation than a quantitative one (a quantitative evaluation will be done later in the report).

2.1 Mechanical system

When applying a force to an element, the element will exert an equal amount of force back with opposite direction. This is described by Isaac Newton's third law of motion. This means that a force applied to any part of a structure that is in equilibrium ($\sum F = 0$) will be transmitted by a closed loop of structural elements connected to this part. This is called a 'force loop'[5]. The force loop in manufacturing machines is defined as the path of structural elements going from the machining tool (in this case the electron beam) to the effective point on the work piece (in this case the point of interest on the substrate). Forces in the force loop will deform the structural elements. This leads to a displacement between the machining tool and the work piece, so in this case to a displacement between the electron beam and the desired position on the substrate. To minimise this displacement, the deformation of the force loop should be minimised. This can be achieved by decreasing forces and moments on the loop and by keeping stiffness high. In Figure 2.1 the force loop of the current system is drawn. It can be seen that the loop runs through the stage guiding, stage legs, stage suspension, vacuum cover, CSR and finally through the center of the electron beam to the substrate and stage. A number of observations can be made about the current force loop:

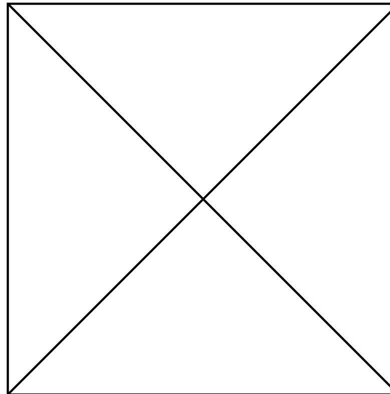

Figure 2.1: Force loop

- The stage suspension is a closed box which in principle is a stiff construction. Deformation of the box itself when a stage step is done is less likely.

- The way the stage suspension is connected to the vacuum cover gives rise to large moment arms.
- This connection between the suspension and vacuum cover also lacks stiffness, since the top plate of the suspension is only connected along the column circumference and with four small struts.
- When the stage is actuated the acceleration of the stage creates a force that is applied in lateral direction to the stage suspension.
- This force is multiplied with a large moment arm (the distance from the bottom to top plate of the suspension).
- The combination of the large moment arm and the lack of stiffness of the connection between the vacuum cover and suspension, leads to large deformations. This will mainly be a rotation of the suspension around the column opening.
- Another thing that can be noticed is that the legs that support the stage are relatively long. A force generated by the stage motors will be horizontal and this is exactly the direction the legs lack the most stiffness.

All these factors can lead to high deformations in the system and displacement between the electron beam and the substrate. If this is correctly measured in some way this does not have to be a problem. Other observations about the current mechanical system that can be made is that the system is very complex and a lot of expensive materials are being used (a significant amount of huge parts made of Invar are being used). This makes the overall system expensive.

2.2 Metrology

In the same way that a force loop was defined, also a 'metrology loop' can be defined. The metrology loop is defined as the closed loop that includes all the structural elements connecting the measurement device to the point of interest[5]. The point of interest in this case is the position of the electron beam on the substrate. In this case it consists of the interferometer with measurement mirror on the stage and the mechanical elements going from the interferometer to the electron beam on the substrate. The metrology loop of the current system is drawn in Figure 2.2. In general a few notes can be made about the current metrology. The first is that displacement on the point

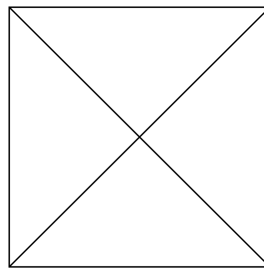

Figure 2.2: Metrology loop

of interest is not what is measured:

- Desired measurement: the displacement between the electron beam and the desired location on the substrate.
- Actual measurement: displacement between the interferometer and the mirror on the stage.

The fact that the interferometer measures the displacement between the interferometer and the stage mirror, makes it very sensitive (with a sensitivity of 1!) to any movements of the interferometer itself parallel to the measurement axis.

A second observation is that the force loop and the metrology loop are connected, as depicted in Figure 2.3. To make accurate measurements the deformation of the metrology loop should be as little as possible. Connecting the

metrology loop to the force loop is not the best way to reach that goal. As seen before, there are some concerns with the elements in the force loop leading to potential large deformations. This is concerning when it comes to possible deformations on the metro loop.

A final observation about the metrology is about the way the interferometers are mounted. The mounting mechanism is shown in Figure 1.9a. The mount used is made of stack of multiple parts, this is done such that alignment is possible and the right distance is spanned from the top plate of the suspension to the measuring height. The top part is a rigid bracket on which the first alignment piece is bolted down. The second piece that is used for the alignment is bolted to the interferometer housing and the two alignment pieces are connected to each other, first loosely and after alignment they are bolted down. The way the two alignment pieces are connected to each other is with 4 line contacts. This makes the interferometer mount overconstrained. The fact that the mount consists of a stack of numerous elements and of which a part is connected with overconstrained line contacts, does not ensure a stiff and rigid way of mounting and therefore leads to a lack of stiffness of the interferometer mount. This is not desirable as this probably means the mount has a low eigenfrequency. This frequency is potentially exited during operating the EBPG and this will lead to measurement errors.

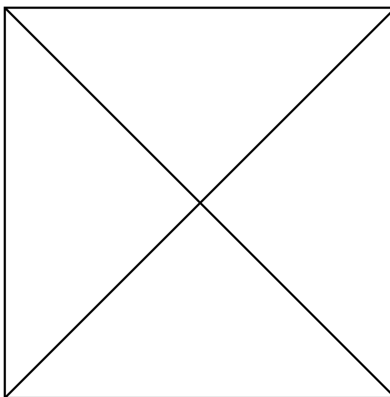

Figure 2.3: Coupled metrology and force loop

2.3 Conclusion

The following conclusions have been drawn:

- Some structural elements in the force loop implicitly lack stiffness in design and large moment arms are present. This can lead to large deformations.
- The metrology measures the displacement between the interferometer and the mirror on the stage. For accurate measurements of the actual point of interest (which is not measured) the system relies heavily on the fact that the metrology loop should not deform.
- The metrology loop and the force loop are connected and this can lead to high deformations of the metrology loop, giving rise to measurement errors.
- The way the interferometers are mounted lacks stiffness, which leads to higher deformations of the mount and a more easily exited eigenfrequency, both leading to measurement errors.

Chapter 3

Requirements

One key element in designing a new system is formulating the requirements. These are of the utter most importance, as they will greatly determine which solutions and concepts are feasible and therefore what the final design will look like. Different types of requirements can be thought of, but the most important requirements to meet are the user requirements. The user requirements will be described in section 3.1. Other types of requirements are defined by some form of constraints or working conditions. This means that these requirements are types of conditions that should be taken into account when designing a new system. They can be mechanical constraints, environmental conditions or operational conditions. The mechanical constraints will be discussed in section 3.2, the environmental conditions in 3.3 and the operational conditions in section 3.4.

3.1 User requirements

The user requirements are of great importance as they are the drive of designing a new system. They should clearly state what it is that the user desires. In this case the main goal of the project is to improve the beam stability, so the requirements about the beam stability are the most important ones. Besides improving the beam stability, also the overlay and throughput should be improved, although these will be less of a focus in this project. All the user requirements can be found in Table 3.1.

The challenging part of the user requirements is the fact that user cases are highly divergent. In some user cases the machine is used to write patterns for hours to even days on end without inbetween calibration, while in other user cases only a few very small features are written per main write field. Some user cases demand absolute placing accuracy while in other user cases the user only cares about relative placement of features. These variable users cases make it challenging to design a system that complies to all, but this variability is also what sets Raith apart from competition. The following sections will go into greater detail.

Table 3.1: User requirements

User requirement	**Value**	**Remarks**
Short term stability	≤ 3.5 nm/s	
Long term stability	≤ 10 nm/h	
Overlay	≤ 5 nm	For a write field of 1x1 mm
Throughput	-	

Beam stability

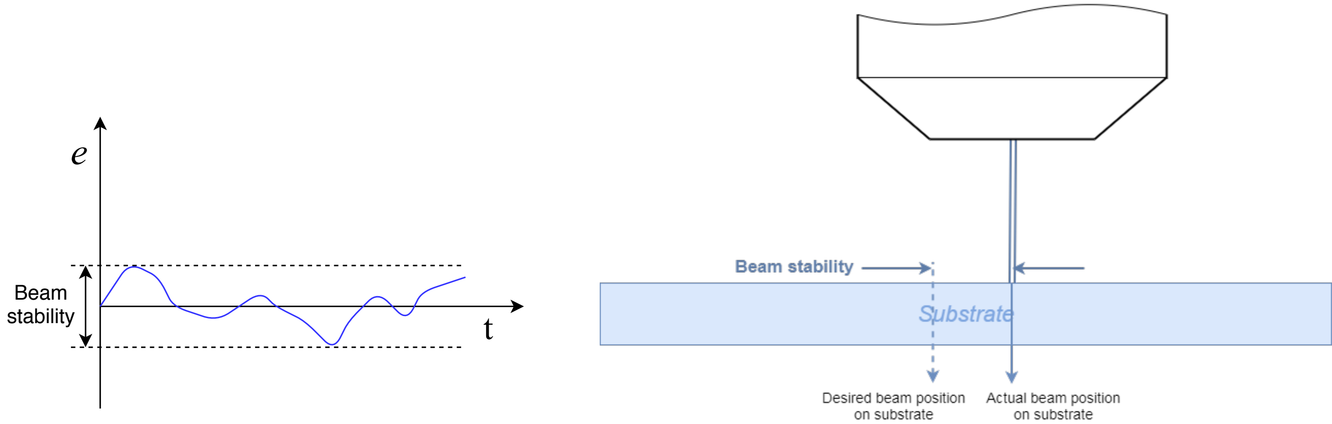

Figure 3.1: Beam stability

As said before the main focus of this project is to improve the beam stability. The beam stability is defined as:

> "The maximum displacement error of the electron beam on the substrate over a certain amount of time."

So the beam stability indicates the potential increase in the beam position-error in a certain amount of time. One could see this as a measure for the ability of the system to keep the electron beam stationary at a certain location. This is illustrated in Figure 3.1. The stability can be divided into two categories:

- the short term beam stability: within one second
- the long term beam stability: within one hour

The following sections will discuss the short and long term stability separately. Both the short and long term stability are determined by a variety of factors. Errors could arise for example from beam placement within the electron column, all kinds of noise in and on the system or due to measurement errors in the metrology. Especially the latter, so error due to the metrology, is the scope of this project and will therefor be the focus for improving the beam stability. Improving other error sources that will lead to beam instability will not be considered part of this project.

Short term stability

A significant part of the EBPG users are using the machine to write sparse patterns. This means a low pattern density per writing area, so relatively short writing times. For example if a 50 nm beam diameter is used with a 10 nA beam current and the resist needs a dose of 150 μC/cm^2, then writing a 100 μm long line (50 nm wide) per mainfield takes only 590 μs. Compared to the time needed for a stage step, which can take up to 200 ms, the writing time only takes up 0.3% of the total time. For this reason the short term stability will be a very important requirement to meet. Figure 3.1 shows that the requirement for the short term stability should be smaller than or equal to 3.5 nm. This means an improvement of 1.5 nm compared to the current system, as right now the short term stability is estimated to be about 5 nm.

Long term stability

The long term beam stability is also important as another substantial part of EBPG users write patterns for hours on end. The current long term beam stability is about 50 nm, given that the cleanroom is compliant with the specifications. This specification is measured with the beam stability acceptance test, a test that needs to be passed as part of commissioning. In this test the beam deviation is measured by measuring the position of a marker every 10 minutes for 8 hours long. To meet the increasing demand for higher long term stability, this should be improved by a factor of 5 to 10 nm.

Overlay
The overlay performance is defined as how well the system is able to write the exact same feature twice on top of each other, so how well these twice written features overlap. It is highly dependent on a number of different variables. It is for example determined by beam the quality/aberrations, noise, beam current, resist type, etc. Most of these variables originate from sources that fall outside the scope of this project. However, one of these variables is the metrology and the errors it gives, so in this way the overlay could be improved. This requirement is more of a secondary focus. The overlay is currently $\leq$ 10 nm and should be improved to 5 nm.

Throughput
Several factors determine the throughput. A number of variables that determine the throughput are highly dependent on the application such as the writing pattern, the substrate used, the spot size and beam current used, the writing frequency, stage setup, stage controller, etc. One variable in this equation is the time needed to perform a stage move and this is something the metrology could help improve. As discussed above sparse pattern writing is an important element in using the EBPG. When very little writing has to be done per area, stage move time dominates exposure duration. In this case the largest contributor to the total writing time is the stage move time. In the current system this time can take up to 99% of the total writing time. Therefore any reduction in this time can increase throughput significantly. But because this is so highly dependent on factors outside the scope of this project and the performance is hard to verify this requirement will be more of a secondary focus. Moreover, it will almost certainly be implicitly improved when improving the short-term beam stability. Still, improving the throughput will be taken into account during the design process.

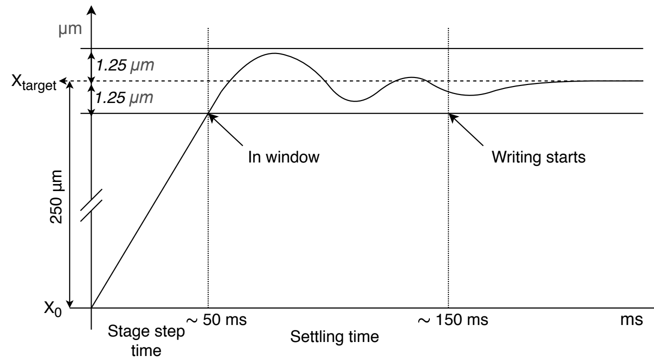

Figure 3.2: Stage move

Part of the reason that a stage move can take up so much time is due to the settling behaviour of the system and therefore the settling time needed. In Figure 3.2 a typical stage move of 250 μm has been visualized. The stage step time is defined as the time needed from $t = 0$ when the stage starts moving to the moment the stage is first "in window". "In window" means the first time the targeted position minus the interferometer measurement is within this value. At that moment beam error feedback can be used to actively compensate the position error before the stage position converges to the desired position and writing could theoretically start at this moment. The window is set to $\pm 1.25 \mu m$. This value originates from the measurement resolution of the interferometer and the available DAC (Digital to Analogue Converter) steps. The stage step times are given for different step sizes in Figure 3.3. If a stage move is done, the stage step time should be within this specification. The reason why for the y-direction a larger step time is specified is because the y-stage has to move the extra weight of the x-stage when actuated. The settling time is defined from the moment the stage is in window to the moment that writing will start. This time can be chosen/changed, but is recommended (and defaulted) to be 100 ms if writing errors are to be reduced within the current specifications.

Step size	X direction	Y direction
(µm)	(msec)	(msec)
250	≤ 50	≤ 80
500	≤ 70	≤ 120
1000	≤ 100	≤ 150

Figure 3.3: Stage step time

The part the metrology can contribute in improving the throughput is through the use of beam error feedback. From the moment the stage is in window, every displacement the metrology measures accurately can be compensated for accordingly. This can be done with the use of the high bandwidth (∼0.5 MHz) of the deflection of the electron beam. All mechanical vibrations present on the stage could in theory be corrected for, as long as they can be measured effectively. Right now if a stage step is done much faster than the stage step time specified, vibrations on the metrology cause large measurement errors and a longer settling time is needed before these vibrations are damped out. If measurement errors in the metrology are reduced during stage moves, the stage could have a higher acceleration hence the stage step time could be reduced. Also the settling time needed before the writing starts could be reduced or even set to zero, because now the metrology can measure the stage displacement accurately and the beam error feedback can correct for this. This all leads to a higher throughput.

3.2 Mechanical constraints

Table 3.2: Mechanical constraints

Mechanical constraint	Value	Remarks
Volume vacuum chamber	696x760x385mm	Soft constraint
Optical working distance	40mm $\pm 50\mu m$	Height between stage & final lens
Parallelism	$\leq 10\mu$m/200mm	Between stage and column bottom reference surface
Space underneath stage	$\geq$ 70mm	Space needed for optional z-stage

Volume

When designing a system it should fit into a reasonable volume. One of the volumes it potentially has to fit in is the vacuum chamber. The volume of the vacuum chamber can be found in Table 3.2 and is a constraint that preferably is complied with. However, it is a soft constraint so when necessary this can be altered by some amount, ensuring consequences have been thought through and negative side effects are kept to a minimum.

Optical working distance

One very important mechanical constraint is the defined height between the stage and the final lens pole gap centre. In Figure 3.4 this is illustrated. The first number of the constraint (40 mm) is the nominal focus distance from the final lens to the substrate. The second number ($\pm 50\mu m$) is the fine focus range of the final lens. There are multiple reasons this height should always be kept in this range. The first reason is because of defocus. If the substrate is outside of the specified range, the electron beam cannot be focused anymore and the image becomes blurry. A second reason is because of the rotational trajectory the electrons get in the optical column. This is the effect described in Chapter 1.3. A height outside of the requirement will lead to a rotation of the image which is not corrected for. But the most dominant effect of violating this constraint is the gain that happens during deflection of the beam. If the height difference is Δh and the deflection angle of the electron beam is θ, then the deflection gain error that occurs is $\epsilon = \Delta h \cdot tan(\theta)$. So the error scales linearly with the height difference.

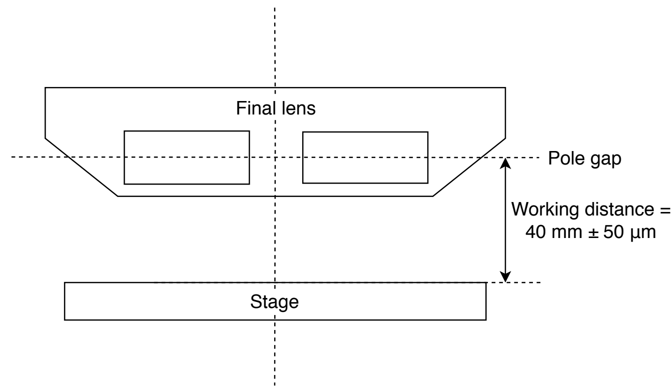

Figure 3.4: Working distance final lens

Parallelism
Another very important constraint is the parallelism between the stage and the reference plane on the bottom of the optical column. It defines the parallelism between the plane defined by the kinematic mount on which the substrate holder is loaded and the plane spanned by the bottom reference surface of the optical column. Much of the same effects as violating the working distance constraint occur, although to a lesser extent, like defocus of the image, rotation of the image and the deflection gain effect. Also the image gets a tilt if the parallelism constraint is violated.

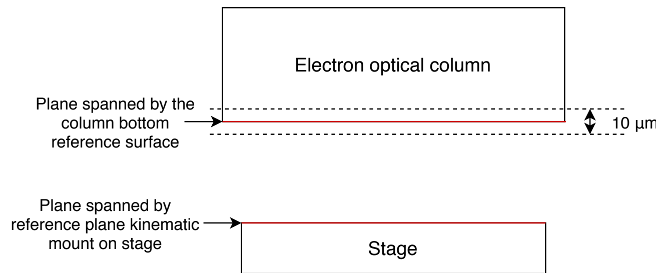

Figure 3.5: Parallelism

Space underneath stage
A second height constraint indicates the space needed for a potential z-stage. The EBPG5200 can be ordered with an additional z-stage option located under the x- and y-stage. A picture of this option is shown in Figure 3.6. This additional z-stage would take up some space underneath the current stage, namely 70 mm, and this space should be reserved for this. During the design project the z-stage itself will not be taken into account.

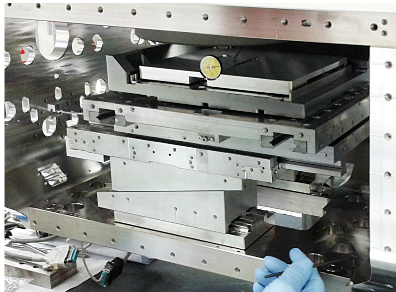

Figure 3.6: Z-stage edition

3.3 Environmetal conditions

The environmental conditions are all the constraints that are set by the surroundings, or better said the requirements that are set for the surroundings. They comprise of all the cleanroom specifications and these include mostly thermal conditions, noise specifications and ground specifications. These conditions are of great influence on how the system behaves during operation and what the potential performance is. All the environmental conditions are stated in Table 3.3. The most important conditions to take in mind for designing the metrology are the temperature conditions. These will be elaborated further.

Table 3.3: Environmental conditions

Environmental conditions	**Value**	**Remarks**
Temperature	21 °C	Preferred temperature
Temperature deviation ΔT	±0.25 °C	
Temperature gradient $\frac{\partial T}{\partial t}$	$\leq$ 0.1 °C/h	
Relative humidity	$40 - 70\%$	
Acoustic noise	$\leq$ 65 dBA	
Magnetic field deviation (DC)	$\leq$ 0.4 mG/h	0.8 mG over 2 hours
Magnetic stray-field	$\leq$ 0.5 mG	Peak-peak for both vertical and horizontal plane
Ground stiffness	$\geq 53 * 10^6$ N/m	
Ground flatness	$\leq$ 1.5 mm	Over an area of 1260x1654 mm
Ground vibrations	$\leq 10\mu$m/s	for all frequencies

Temperature and humidity
Temperature behaviour of the cleanroom can be of great influence of the long term ($\sim$ hour) performance of the system. High or sudden temperature changes are generally better avoided to decrease the temperature variation in the system itself and with that potential performance decline. The preferred set temperature is 21°C and from this a maximum deviation of ± 0.25°C is allowed. To ensure the temperature is not changed to sudden, a maximum temperature gradient of 0.1°C over the time span of an hour is allowed.

Finally the relative humidity should be within 40-70%. The lower limit is mainly determined by the fact that people have to operate in the cleanroom and any lower humidity levels are experienced as uncomfortable. Also the rate in which skin flakes are formed is increased with lower humidity levels. The upper limit is mainly set to prevent creating a suitable climate for fungus and bacteria and to prevent any condensation on cooled parts in the cleanroom.

3.4 Operational conditions

The operational conditions are the constraints that are set during operation. These include all the loads present in the system. In Table 3.4 the relevant operational loads are displayed. These include conditions such as the vacuum presence, some mechanical vibrations and dissipated heat in the system.

Table 3.4: Operational conditions

Operational conditions	**Value**	**Remarks**
Vacuum	10^{-7} mbar	
Turbo pumps	350-600 Hz	
Temperature final lens ΔT	±0.01 °C	120 W dissipation, water-cooled
Heat stage motors	0-3 W	Motors are air cooled
Heat dissipation laser	23 W	

Vacuum
As stated earlier, operating in a vacuum setup is necessary. When designing a new system this is something very important to keep in mind. All parts and materials used inside the vacuum chamber should be vacuum compatible. The pollution with particles that are released from the parts used should be minimized. This can mean that certain materials should not be used, for example materials that demonstrate out-gassing under vacuum. But it can also mean that certain shapes should be avoided to allow particles to be removed out of the chamber more easily. For example use bolts that do not create trapped air pockets or put holes in large surfaces.

Turbomolecular pumps
A source of noise on the system during operation is the noise that is generated by the turbo pumps. The turbo pumps are connected to the vacuum chamber and airlock. They rotate with a certain frequency (normally between 250 and 600 Hz) and this creates mechanical vibrations on the system.

Heat dissipation
During operation several heat sources are present and they introduce noise on the system as well. The biggest heat source is the heat generated by the deflection in the final lens. This produces 120 W. Fortunately the final lens is water-cooled, creating a relatively stable temperature on the outside of the final lens with a variation of $\Delta T = \pm 0.01$ °C. Other important heat sources are the heat dissipation of the laser of 23 W and the heat dissipation of the stage motors of up to 3 W. As the stage motors are quite close to the substrate, they are air cooled to decrease the heat flow to the substrate and the rest of the system.

3.5 Other requirements/specifications

Material requirements
Besides the fact that materials should be vacuum appropriate, there are also some other requirements to take into consideration. As electrons are charged particles, they are influenced by magnetic fields. This means that materials used near the substrate or electron beam are not allowed to be magnetic. Also to prevent interference near the electron beam, materials should have a high permeability to not interfere with the magnetic fields used in the electron optical column. A third requirement concerns the electric charge that can occur because of scattered electrons. When the beam hits the substrate part of the electrons are either reflected directly of the surface (back scattered electrons) or are re-emitted from other molecules inside the substrate (secondary electrons). These electrons then hit other surfaces present in the vacuum chamber. If these materials are not able to (easily) conduct electrons, electric charge can build up. This build up will create an electric potential, that will interact with the electron beam and therefore distorts the beam shape/deflection. To prevent this either the material used should be conducting, or a conducting layer that is grounded should be put on top of this material. Another thing to take into consideration, although this is not really about material choice, is the shape of parts around the column. These should preferably be rotational symmetric to minimise the effects described above on the electron beam.

Costs and manufacturability
For a requirement about costs there is no real specific number that should be adhered to, but of course the costs should not be out of proportion. Costs are taken into account and are preferably lowered where possible while still meeting the requirements. This also ties in with the manufacturability. How easy or hard, and therefore how expensive, a part is to manufacture is something that should be taken into account when designing a new system. Also lead time and availability are important design factors.

Maintainability
Performing maintenance is part of the life cycle of a Raith lithography machine. This is a fact that has to be taken into consideration with the new design. This means maintenance should be possible and although the ease in which this maintenance can be done is not a priority, it is preferably high.

Chapter 4

Error sources

For improving the current system according to user requirements it is insightful to evaluate the current performance. The goal is to gain insight into which error sources contribute the most (and the least). Errors are defined as:

> "The inadmissible difference between the as-designed nominal system and the as-built system."

As the main focus of this thesis to meet the requirements is on improving the metrology, most attention will be given to the error sources caused by the metrology. An estimate of the contribution of these errors to the total performance will be made. Two types of error sources can be identified, namely:

- Static errors
- Dynamic errors

Static errors are errors that do not change over time. Examples are alignment and finite manufacturing accuracy. Dynamic errors on the other hand are errors that do change over time. Examples are vibrations or noise on the system and thermal drift. In Section 4.1 the static errors will be evaluated and in Section 4.2 the dynamic error sources. Using this information, in Section 4.3 the error budgets of the current system for the different user requirements will be formulated and evaluated.

4.1 Static errors

Static errors can be subdivided into three categories:

- Finite manufacturing accuracy
- Alignment errors
- Calibration errors

When producing and assembling all the parts that comprise the metrology loop, only a finite accuracy can be achieved. In Figure 4.1 an overview of all the mechanical connections of the metrology loop can be seen. Every part has its manufacturing tolerances and between every mechanical connection certain tolerances are present. Luckily, by means of alignment and/or calibration procedures, these can mostly be compensated for. So in the end the static errors that stay present are mostly alignment and calibration errors. All the different metrology error sources discussed in the next sections. These include a cosine error that originates from an alignment error, the mirror tolerances that are partly finite manufacturing accuracy errors and partly calibration errors and Abbe errors that originate from the finite manufacturing accuracy. Finally some instrumentation errors are discussed that do not really fall in either of the three categories.

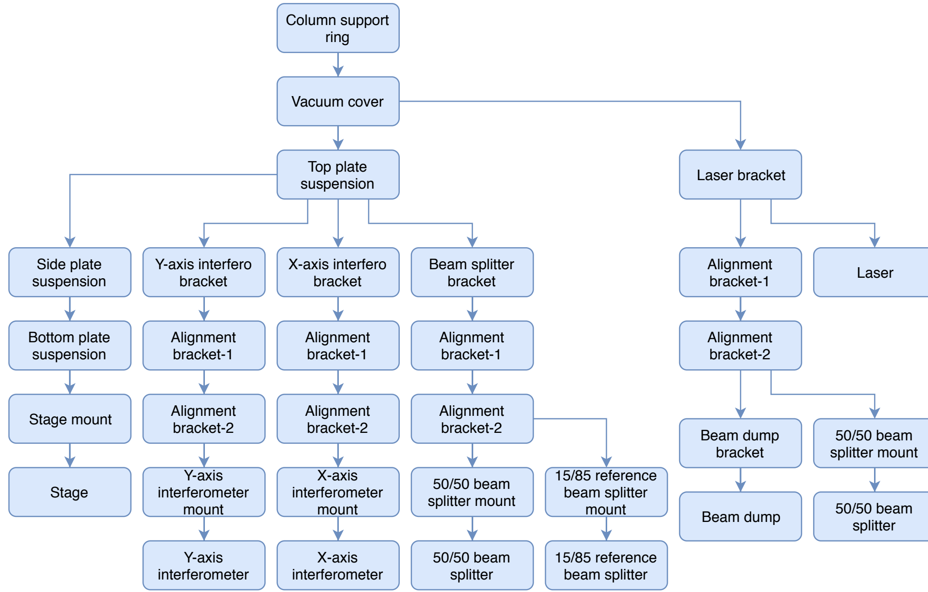

Figure 4.1: System overview mechanical connections

4.1.1 Cosine error

The cosine error is an error in optical path length that arises when the measurement axis does not co-inside with axis of motion. This can have multiple origins with one of them being the alignment between the optical components. In Figure 4.2 this is visualized. Angle α causes the laser to travel with a measurement distance L_M instead of the real distance L_R. The ratio between L_R and L_M is the cosine of the offset angle (see equation 4.1), hence the name.

$$L_R = L_M cos(\alpha) \tag{4.1}$$

The error in optical path length therefore becomes:

$$\epsilon_{cos} = L_M - L_R = \frac{L_R}{cos(\alpha)} - L_R = L_R\left(\frac{1}{cos(\alpha)} - 1\right) \tag{4.2}$$

Angle α can have multiple causes, namely:

1. The plane spanned by the mirror is not aligned perpendicular to the axis of movement.
2. The laser beam from the interferometer is not perpendicular to the mirror.

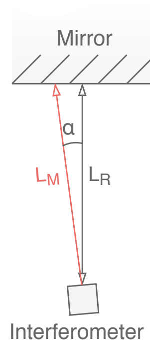

Figure 4.2: Cosine error

The mirror offset will be dealt with in section 4.1.2 about mirror tolerances. For now only the perpendicularity of the laser to the mirror will be discussed. The offset angle α is caused by misalignment between the optical components in the optical path. The laser, the three beam splitters and the interferometer all have certain alignment tolerances resulting in the combined offset angle α. The optical components are aligned using the alignment mechanisms described earlier, which can rotate the component perpendicular to the mirror on the stage (in yaw and pitch). So the type of error source category the cosine error falls into is an alignment error.

Alignment procedure

The alignment procedure in the current system is an iterative process by adjusting different optical components at a time. The laser and beamsplitters all should be aligned with respect to the interferometer and the interferometer should be aligned with respect to the mirror on the stage. If one components orientation is adjusted, this influences the alignment of the other optical components and should therefore be corrected again. This process evolves until the residual error is within a certain range.

The procedure to minimize the alignment offset α consists of holding a piece of white paper at the output of the interferometer. If the angle $\alpha \neq 0$ two laser spots will occur on the sheet of paper. This is caused by the fact that α causes a lateral displacement between the beam leaving and re-entering the interferometer, but the reference arm inside the interferometer will not have this displacement. Therefore the two beams will not completely overlap when going to the output of the interferometers. This can be seen in 4.3. If $\alpha = 0$ the spots will perfectly overlap, but if $\alpha \neq 0$ the middle points of the two spots will have a distance Δ_{spots}. Hence to make angle α as small as possible, Δ_{spots} should be made as small as possible. During the procedure the stage will be moved to amplify Δ_{spots}. The amount that Δ_{spots} will change by moving the stage is called the 'runout'. As this is done by eyesight, the alignment will have a finite accuracy. The assumption will be made that the runout, or the deviation of Δ_{spots}, can be reduced within a margin of about 0.5 mm over a distance of 360 mm. If $\Delta_{spots} = 0.5$ mm in Figure 4.2, then the angle α becomes:

$$\alpha = tan^{-1}\left(\frac{0.5/2}{360}\right) \approx 0.7 \text{ mrad} \tag{4.3}$$

With a maximum distance $L_R = 360$ mm this will lead to a absolute accuracy error of $360/cos(0.7E^{-3}) - 360 = 88$ nm. This is the maximum error over the full actuation range of the stage of 220 mm.

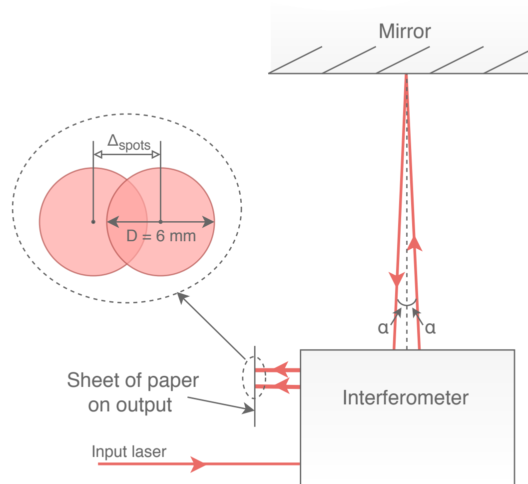

Figure 4.3: Cosine error alignment procedure

4.1.2 Mirror tolerances

During the production process of the superplate (the ZeroDur block described in Section 1.3.4), which has the two mirrors integrated in it, only a certain precision is achievable. These production tolerances give rise to measurement

errors. The two main errors in optical path length due to these tolerances are the form deviations of the mirror and the non-orthogonality of the two mirrors (how perpendicular the x and y mirrors are to each other). The form error is a finite manufacturing accuracy error and the non-orthogonality error is calibrated so therefore a calibration error.

1. Nominal mirror deviations
In a perfect world the mirror would completely coincide with a plane, the nominal mirror. Alas, in practice this will not be the case. During the production process in which the mirror is polished extensively, certain deviations from the nominal surface will occur. They are usually described using spatial frequencies, which can be roughly divided into three categories. The low spatial frequencies describe the form or flatness of the mirror, the mid frequency range describes the waviness of the mirror and the high frequencies describe the surface roughness. Because the beam diameter is 6 mm and the surface roughness[8] $R_a \sim 4\text{Å} \ll 6$ mm, they will be left out of the error source evaluation. In Figure 4.4 the flatness and the waviness of the mirror are visualised.

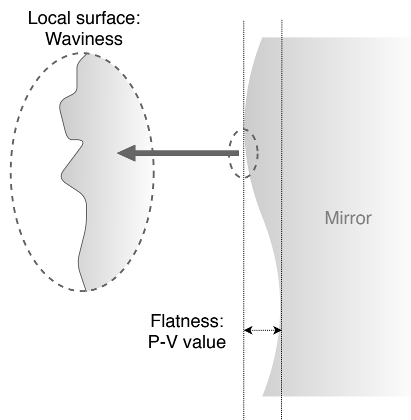

Figure 4.4: Mirror form error

In this case the flatness of the mirror is specified with the Peak-to-Valley (P-V) value. This means the complete mirror surface lies between two planes that have a distance between them equal to the P-V value. This value is usually given in terms of the wave length λ. Flatness for the mirrors is equal to $\lambda/10 \approx 63$ nm.

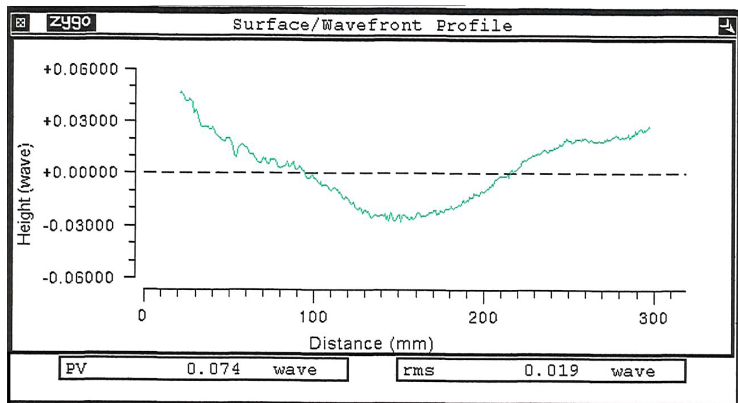

Figure 4.5: Example of the mirror surface profile

A example measurement of the mirror surface profile is shown in Figure 4.5. One can clearly see the lower spatial frequency component and the mid spatial frequency. To determine the waviness the local largest derivative

from the figure will be a good estimate. As the beam diameter is 6 mm, the largest deviation within a distance of 6 mm will be taken. This gives a waviness of $\sim \lambda/100 = 6.3$ nm.

2. Mirror non-orthogonality

In Figure 4.6 the mirror non-orthogonality is visualised. Introducing this non-orthogonality during the production process is unavoidable unfortunately. If the two mirrors used for the x- and y-interferometers are not completely orthogonal to each other measurement errors will occur when actuating the stage. When the stage is moved on one axis also a change in optical path length is measured on the other axis even though the stage does not physically move in that direction. In addition, because there is an offset angle between the two mirrors, the mirrors can not be orthogonal to both axes of movement and hence a cosine error will occur as discussed previously.

The orthogonality between the two mirror surfaces is < 0.02mm over a distance of 250 mm. This means the angular offset is $< 100\mu$rad.

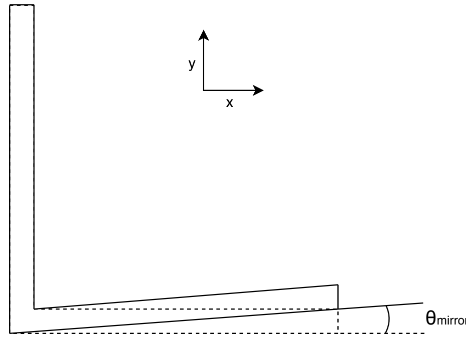

Figure 4.6: Mirror non-orthogonality

Calibration procedure

To reduces the errors given by the mirror non-orthogonality, a calibration procedure is being done. During this procedure a mask plate with two perpendicular rows of markers will be loaded in the machine. A marker search on all the markers of each row will be performed given a certain non-orthogonality error. Then the mask plate will be rotated by 90 degrees and again a marker search will be done on all the markers. The non-orthogonality angle between the mirrors should in both measurements be the same, but by rotating the mask plate by 90 degrees the non-orthogonality between the marker rows itself will be cancelled out. Therefore only the non-orthogonality of the mirror remains. With this information a simple first order correction will be done and a residual angle of $\sim 0.5\mu$rad will remain.

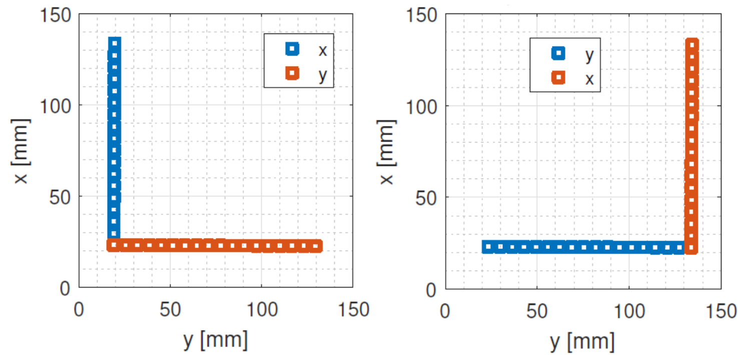

Figure 4.7: Two measurements on a marker mask plate with a 90° rotation of the mask between them

4.1.3 Abbe errors

Abbe errors are errors that occur when the axis of movement has an offset to the axis of measurement and when angular motion errors are present in the positioning system. Abbe errors cause the measured displacement to be shorter or longer than the actual displacement. The current system does obey the abbe design principle, so the nominal design does not have abbe offsets. However, manufacturing tolerances do introduce slight abbe offsets and since no calibration or alignment procedure is done currently to correct for these offsets, all the abbe errors of the current system fall into the error source category of finite manufacturing accuracy.

Yaw error

The yaw error is defined as the error that arises when the stage rotates around the z-axis. This leads to an error in the measurement in the x- and y-direction. This can be seen in Figure 4.8 as the angle θ_{yaw}. The stage has a repeatable yaw angle variation θ_{yawr} of 100 μrad and a non-repeatable yaw angle variation θ_{yawnr} of 10 μrad. The laser used by the interferometers should in theory be perfectly in line with in the x- and y-axis and meet in the middle of the optical centre of the column. In practice tolerances will tell how well this can be achieved. The tolerances will give rise to a moment arm and therefore the abbe error. This is illustrated in Figure 4.8. The position tolerances for the dowel pin holes the interferometer bracket is aligned to will be estimated to be 0.1 mm, so the maximum arm will therefore be estimated to be $L_{arm} = 0.1$ mm. This will lead to a repeatable and a non-repeatable yaw abbe error of:

$$\epsilon_{yawr} = L_{arm} sin(\theta_{yawr}) = 0.1E^{-3} \cdot sin(100E^{-6}) = 10 \text{ nm} \tag{4.4}$$

$$\epsilon_{yawnr} = L_{arm} sin(\theta_{yawnr}) = 0.1E^{-3} \cdot sin(10E^{-6}) = 1 \text{ nm} \tag{4.5}$$

The yaw angle of the stage also leads to a cosine error. For the repeatable yaw this will give a maximum absolute accuracy error of $360/cos(100E^{-6}) - 360 = 1.8$ nm and for the non-repeatable yaw error a maximum ΔOPL error of $360/cos(10E^{-6}) - 360 = 0.018$ nm.

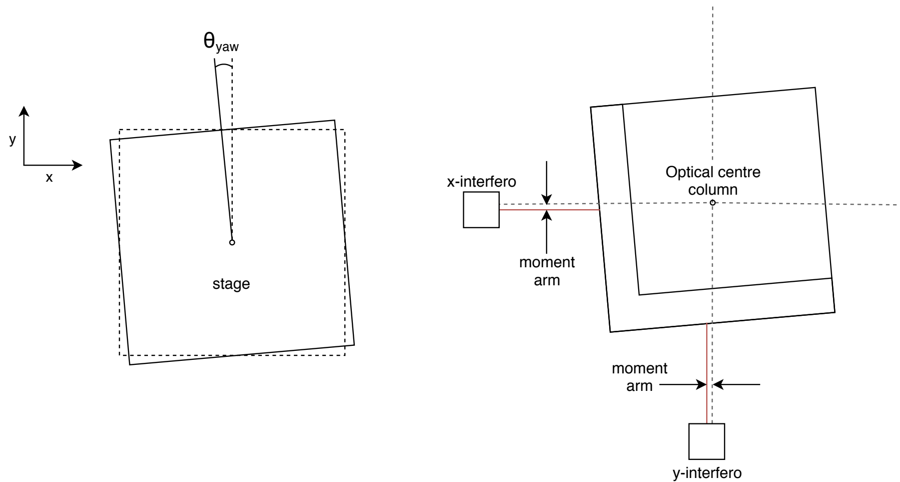

Figure 4.8: Yaw abbe error arising from the moment arm between the axis of measurement and the axis of movement

Pitch/Roll error

A pitch error arises when there is a rotation of the stage around the y-axis, this leads to a measurement error in the x-direction. A roll error on the other hand arises when there is a rotation of the stage around the x-axis, which leads to a measurement error in the y-direction. The angle $\theta_{pitch/roll}$ can be seen in Figure 4.9. The repeatable pitch/roll angle of the stage is $\theta_{pitch/rollr} < 20$ μrad and the non-repeatable pitch/roll angle is $\theta_{pitch/rollnr} < 10$ μrad. The offset in z-direction, so the moment arm, from the point of measurement on the mirror to the substrate

height is also based on manufacturing tolerances. If the same positioning tolerances as with the yaw error are used then $L_{arm} = 0.1$ mm. This leads to repeatable and non-repeatable pitch and roll errors of:

$$\epsilon_{pitch/rollr} = L_{arm} sin(\theta_{pitch/rollr}) = 0.1E^{-3} \cdot sin(20E^{-6}) = 2 \text{ nm} \tag{4.6}$$

$$\epsilon_{pitch/rollnr} = L_{arm} sin(\theta_{pitch/rollnr}) = 0.1E^{-3} \cdot sin(10E^{-6}) = 1 \text{ nm} \tag{4.7}$$

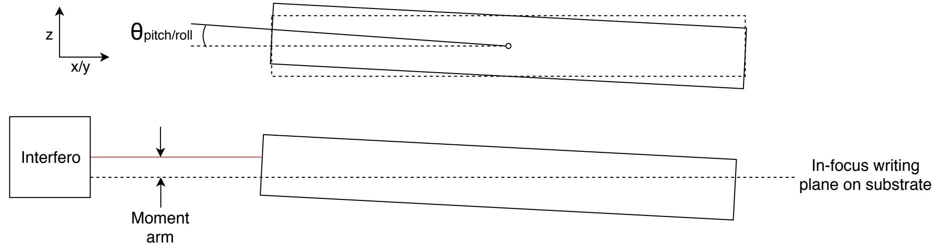

Figure 4.9: Pitch/roll abbe error arising from the moment arm between the axis of measurement and the axis of movement

The cosine error caused by the pitch/roll angle is for the repeatable angle equal to $360/cos(20E^{-6}) - 360 = 0.072$ nm and for the non-repeatable angle equal to $360/cos(10E^{-6}) - 360 = 0.018$ nm.

4.1.4 Instrumentation errors

Laser wavelength stability
Ideally the laser would create perfectly coherent light that stays coherent over time and distance. Unfortunately in practice this is not the case and the wavelength will have a certain stability over a certain amount of time/distance. In this case the laser has a distance stability of 0.002 ppm for the duration of one hour and a distance stability of 0.02 ppm over its lifetime[13].

Optics non-linearity
The optical system has finite accuracy too. Optical non-linearity is essentially caused by imperfect separation of the two different frequency components. This leads to frequency mixing, hence errors occur. The frequency mixing has several causes[11][12]:

- The laser beam is elliptically polarized instead of circularly polarized
- The polarization between the two frequencies is not completely orthogonal
- Finite alignment accuracy of the beam splitter
- Finite alignment accuracy of the 45° polarizer
- The two frequencies undergo different transmission coefficients in the beam splitter

The non-linearity caused by these effects are cyclic in nature and have a period of one wavelength change of the optical path length. Methods have been developed to model and largely compensate for these cyclic non-linearities[12]. However, these are not applied to the current system. The periodic non-linearity error of the current interferometry system is $\leq$1 nm peak-peak (L. Uittenbogaard, *Keysight technologies*, personal communication, August 13, 2019).

Electronic errors
During the displacement measurement of the stage mirrors, electronics and software are used to process the signal and extend the resolution beyond the optical resolution. This process gives rise to electronic errors. In the metrology used in the current system the electronic error equals the measurement resolution[9]. As seen in Chapter 1.3.5 the measurement resolution is equal to $\lambda/4096 \approx 0.155$ nm.

4.2 Dynamic errors

Dynamic errors are errors that change over time. Dynamic errors of the metrology will be largely mechanical in nature. The main error sources are mechanical vibrations and thermal expansion of materials in the system.

4.2.1 Mechanical vibrations

Mechanical vibrations on the system can lead to errors. If vibrations are present on the metrology, measurement errors (and therefore errors in the writing process) will be made and vibrations on/in the optical column will also lead to writing errors. An attempt is made to get a better understanding of what magnitude and sources the vibration errors have by means of a vibration test.

Vibration test setup
The test has been done on an EBPG5200 machine under vacuum. During the test the machine was exposed to an external impulse by using a free falling weight and letting it fall on the vacuum cover plate. The free weight (a ball) was released from a certain height that was kept constant over the multiple measurements to ensure the same impulse. During this impulse displacement measurements in x- and y-direction were taken. A combination of two measurement types were taken that combined could lead to some inside. The two types are:

1. Intensity measurement on the edge of a marker
2. Beam error feedback signal read out

As discussed before, what is unique to the EBPG machine is that marker searches can be done by measuring the back scattered electrons of the electron beam. This feature can also be used in a clever way to make beam displacement error measurements. The method works in the following way. The electron beam is set on a location on the substrate that lies on the edge of a marker in either x- or y-direction. At the marker itself the reflectance of the electron beam is high, but just outside the marker area the reflectance is very low. By assigning the beam position to the edge of the marker, vibrations will lead to differences in intensity reflected back from the surface. The back scattered electrons from the electron beam are collected by a scintillator that converts the electron signal into a photon signal. This signal is converted to a current via a photo-multiplier and then converted to a voltage. First a calibration sweep is done by starting from the outside of the marker where intensity is low, stopping at the inside of the marker where intensity is at its highest. This will lead to a curvature as seen in Figure 4.10. The assumption is made that the marker edge lies in the middle of the slope. Through a fitting process the slope in the middle of the graph can be determined. Now the sensitivity for nm/V is known. So this can then be used to determine the deviation in nm from the edge of the marker.

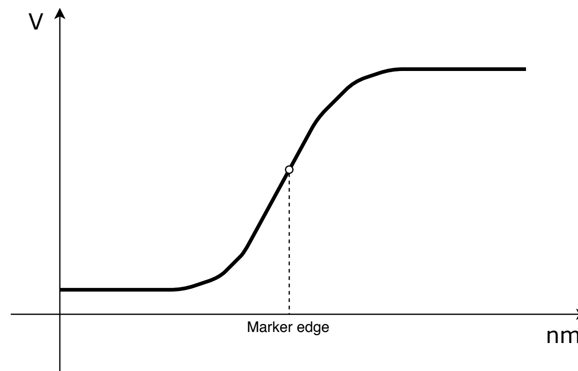

Figure 4.10: Marker Intensity curvature

The second measurement method was by using the beam error feedback signal. The beam error feedback signal measured in x- and y-direction was defined in Equation 1.4 as:

$$\text{Beam error feedback} = X_{setpoint} - X_{measured} \tag{4.8}$$

From this signal the value that the interferometers measure can be determined. The beam error feedback signal can be directly read out via a 16 bit oscilloscope that is connected with a laptop. The measurement resolution of the interferometer is $\frac{\lambda}{4096} = \frac{633}{4096}$. Therefore the sensitivity is about $\frac{2^{16}}{20} \cdot \frac{633}{4096} = 506.4$ nm/V.

The aim of this method is to compare these two signals and to see which errors are present on both signals and which are not. With this information an estimation can be made to which extend the metrology introduces errors, since these will show on both the measured signals.

Vibration test results

In total 9 measurement sets were taken. Each measurement set exists of two beam error feedback measurements (one in x and one in y) and one beam on edge measurement (either in x or in y as only one axis can be measured at a time). Of the 9, there are 5 measurement sets where the beam on edge is measured in x-direction and 4 in y-direction. There were also a number of measurements done with moving the stage as an impulse. In Figure 4.11 the data set of an example measurement of the beam error feedback is depicted. It should be said that

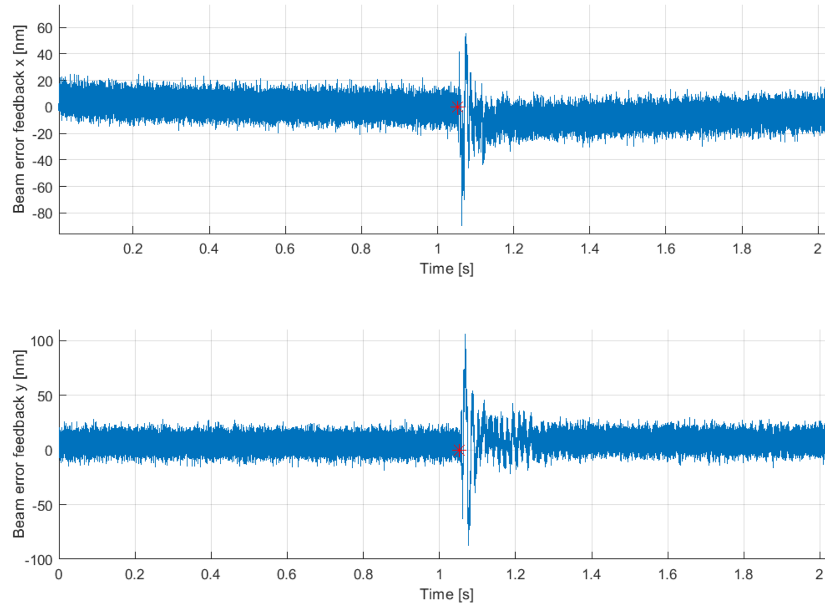

Figure 4.11: Example data set of beam error feedback data

measurement noise is likely present which is introduced by the oscilloscope and this should be taken into account when studying the Figure. The red stars in the graph indicate when the impulse is applied to the vacuum cover. Figure 4.12 shows the corresponding beam on edge measurement in the x-direction. In general the beam on edge displacement measured is about a factor 4 smaller than the measured displacement of the interferometers. This could indicate that the interferometers make sure a big part of the vibrations in the system are correctly corrected for, but this is not completely clear because of read out noise. The frequency spectra of the beam error feedback in x-direction from Figure 4.11 are given in Figure 4.13. In Figure 4.13a the frequency spectrum of the 'impulse' moment is shown. This means the spectrum is calculated of the data starting from the red star moment in Figure 4.11, the moment the ball hits the vacuum cover, till 2 seconds after this. There has no window function been applied so there is some spectral leakage.

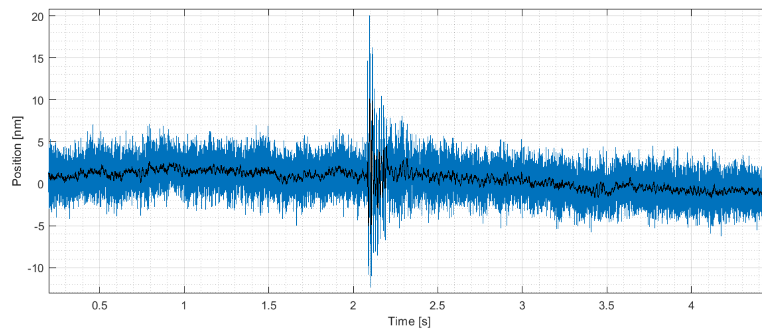

Figure 4.12: Example data set of beam on edge data, raw data in blue and filtered data in black

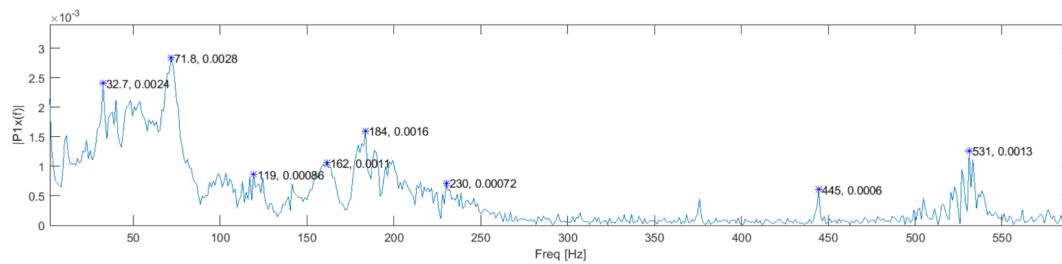

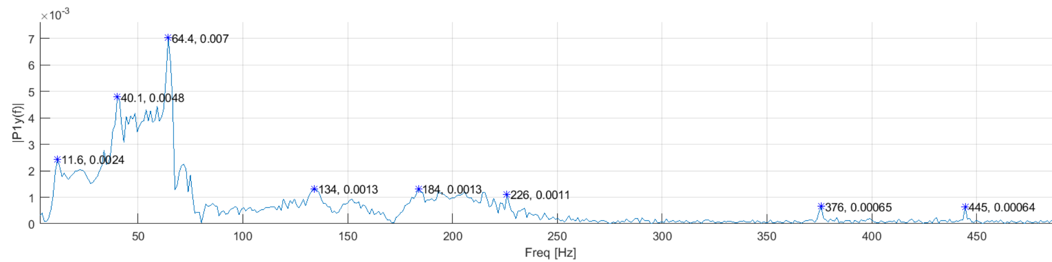

(a) The impulse vibrations

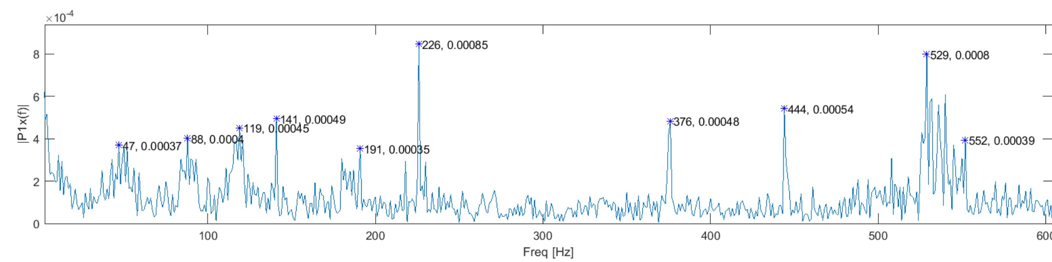

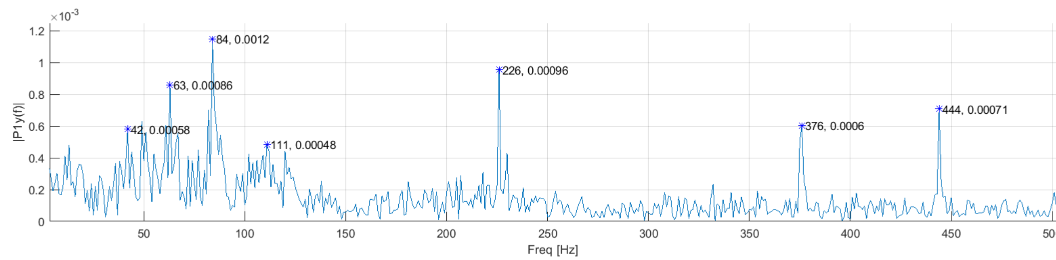

(b) The background vibrations

Figure 4.13: Frequency spectrum of the beam error feedback data, peaks are in Volts

Figure 4.13b gives the frequency spectrum of the 'background' vibrations. This spectrum is taken from $t = 0$ till the red star moment. The frequency spectrum of Figure 4.12 of the beam on edge data set is displayed in Figure 4.14. Figure 4.15 gives an overview of the peak frequencies of the beam error feedback and beam on edge

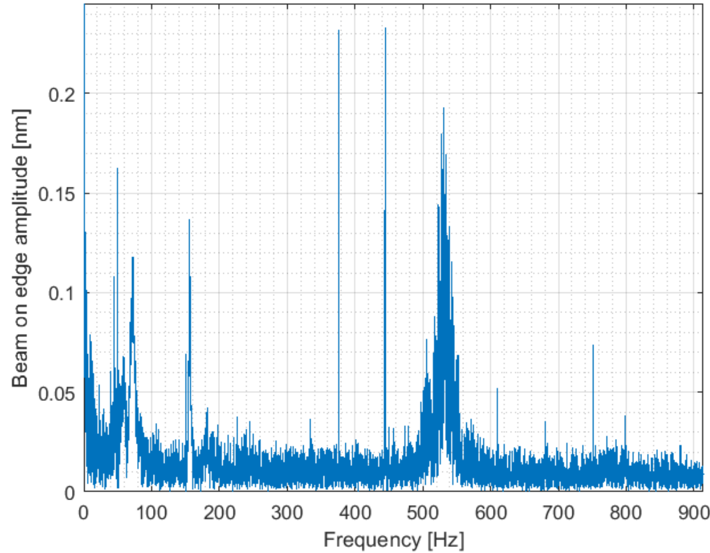

Figure 4.14: Frequency spectrum of the beam on edge data

measurements as seen in Figures 4.13a, 4.13b and 4.14. Next to the frequencies of all the peaks, the amplitude values are displayed. These amplitudes (in nm) should be evaluated very carefully and not taken too literally. Most of the peaks in the figures have wide bases. This means the vibrations are not nicely sinusoidal but noisy. Although the absolute amplitude may be not taken literally, the amplitude ratio between the different peaks inside the graph can be evaluated. The left part of the table displays the beam error feedback. It gives the peak frequencies for

Beam error feedback								Beam on edge	
Peak x [nm]	Hz	Peak y [nm]	Hz	Peak background x [nm]	Hz	Peak background y [nm]	Hz	Peak [nm]	Hz
1.22	33	1.24	12	0.19	47	0.29	42	0.11	45
1.44	72	2.42	40	0.20	88	0.44	63	0.16	50
0.44	119	3.55	64	0.23	119	0.58	84	0.12	72
0.54	162	0.67	134	0.25	141	0.24	111	0.14	156
0.81	184	0.67	184	0.18	191	0.48	226	0.04	182
0.36	230	0.56	226	0.43	226	0.31	376	0.03	197
0.23	376	0.33	376	0.24	376	0.36	444	0.04	226
0.31	445	0.32	445	0.27	444			0.04	333
0.64	531			0.40	529			0.23	375
				0.20	552			0.23	444
								0.19	530
								0.05	609
								0.04	681
								0.07	751
								0.04	798

Figure 4.15: Frequency comparison between pull in data and beam-on-edge data

the 'impulse' part in x- and y-direction and the frequencies for the 'background' part in x and y. The right side of the column shows the peak frequencies of the beam on edge data. The frequencies that overlap in both the right and left side of the table, so that are both present in the beam error feedback and beam on edge, are given the

same color. This indicates that those frequencies are most likely wrongfully corrected for by the electron beam and are actually vibrations on the metrology. Of course it could also be that the same vibrations on the metrology are also imposed on the electron optical column. This is hard to separate from each other. Another contribution is the imperfect stage guiding, however this probably has a negligible contribution. Either way, if frequencies are measured on both data sets it can be assumed that they are mechanical in nature and for the most part caused by the metrology.

When looking at the data sets of the beam on edge in x-direction, most of the highest peaks of the spectrum are ones that overlap with the beam error feedback and therefore are most likely mechanical. For the impulse caused by the free weight these frequencies include 45, 72, 375, 444 and 531 Hz. For the stage move measurements the frequencies include 12, 45, 375, 444 and 531 Hz. In the beam on edge data in the y-direction however this is different. Most of the highest peaks in this case are ones that do not overlap with the beam error feedback spectrum except from the frequency of 65 Hz which has a high peak and does overlap. The other frequencies with high peaks include 50, 150 and 156 Hz and especially 50 Hz is very high. This can indicate that in this direction other noise sources dominate and displacement errors are caused most likely in the electron optical column itself.

When a closer look is taken at which frequencies are observed on both measurements, some observations can be made. The turbo pumps on the vacuum chamber and airlock were set to a frequency of 376 and 444 Hz, so the peaks observed with these frequencies are most certainly mechanical vibrations. Also the peaks (with these frequencies) observed in Figure 4.14) are very narrow. This means the actual amplitude of the frequency can be taken as a truthful representation in this case. The amplitudes are both ~ 0.23 nm. The fact that they are present in both measurements indicates that are most likely caused by the metrology. In the x-direction the peak of the frequency of 531 Hz is also very high in both data sets. The origin for this frequency is unclear. A frequency from which the origin is likely known is the 50 Hz (and the 150 Hz which is an odd multiplication of 50 Hz) on the beam on edge measurement. This is the utility frequency of the power grid. This is therefor most certainly electromagnetic noise present on the optical column and not on the metrology. This frequency is especially highly present in the data from the y-direction of the beam on edge and as the peak is also very narrow the amplitude can be assumed to be a good representation. The amplitude is ~ 0.35 nm. When looking at the relative contribution of the frequency peaks that were observed in both the beam error feedback and beam on edge to the total amount of peaks, the contribution in the x-direction seems to be around than 75%. For the y-direction this is somewhat lower, around 55%.

Vibration test conclusion

- The frequencies that are measured on both the beam error feedback and the beam on edge are mechanical vibrations that are incorrectly compensated.
- Wrongful metrology measurements seem to be the main contributor to the total error with a contribution of $\sim$75% in x-direction and $\sim$55% in y-direction.
- Probably all the frequencies that are measured on both the beam error feedback and the beam on edge are mechanical vibrations.
- The turbo pump vibrations are large contribution to the measurement errors of the metrology and the utility frequency is a large electron optical error contribution.
- The fact that a significant part of the noise sources are mechanical vibrations shows that there is room for improvement with a new metrology system.

4.2.2 Column swing

Another type of error source in the form of mechanical vibrations is the swinging motion of the electron optical column after a stage step.

- The column is essentially a beam that is clamped at the interface of the vacuum cover.
- The first eigenmode of the column is likely a swinging motion as the column is a long heavy beam that is attached to a membrane. The membrane geometry is not very stiff in principle and its stiffness is mainly

determined by the material and thickness. So it will be relatively easy for the beam to rotate around the membrane and this will likely be the most dominant mode by far.

- In this mode the column assembly can be modelled as a stiff rod rotating around a point somewhere near the centre of the vacuum cover interface.
- As the column is a long beam (total length of ~ 1 m) and (top) heavy (total weight ~ 200 kg), this mode will probably have a low frequency.
- Actuating the stage triggers this mode.
- This decreases throughput if writing errors are supposed to be kept minimal.

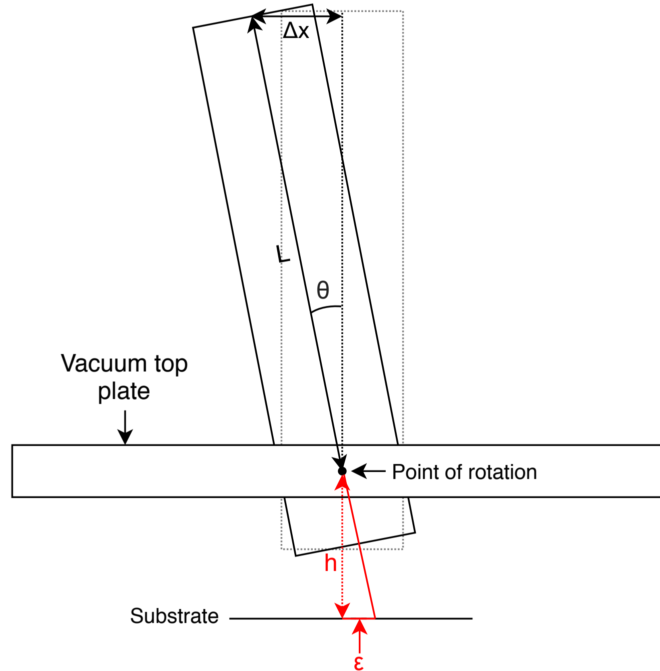

Figure 4.16: Column swing error

In Figure 4.16 the model is illustrated. The relation between Δx and ϵ when the column is modelled as a stiff beam with a rotation point is:

$$\begin{aligned} \theta &= sin^{-1}\left(\frac{\Delta x}{L}\right) \\ \epsilon &= h \cdot tan(\theta) \end{aligned} \tag{4.9}$$

Or described in a simpler way as a lever with the small angle approximation:

$$\frac{h}{L} = \frac{\epsilon}{\Delta x} \tag{4.10}$$

For now the rotation point is assumed to be at the height of the interface between the CSR and top side of the vacuum cover plate. This makes $L = 900$ mm in Figure 4.16 and $h = 120$ mm. From accelerometer tests done on the optical column while stage moves were performed, an estimate for Δx has been made. An example of the frequency spectrum of the accelerometer is visualised in Figure 4.17. Although not completely conclusive, the first eigenmode seems to have a frequency of around 13 Hz. A similar frequency of ~ 12 Hz was found in the vibration

analysis when a stage impulse was given. Looking at the raw data from the accelerometer, the excitation due to the stage step seems to be damped for the most part in about 250 ms and the excitation seems to have a particular frequency that is damped for a significant amount in about 2.5 periods. If one takes the observed frequency of 13 Hz, this means the settling time is about $\frac{1}{13} \cdot 3 \approx 230$ ms, which matches the observed settling time in reality pretty nicely (~ 200 ms). From the data an estimate has been made of what the amplitude of this frequency is likely to be. This is a tricky process because noisy data needs to be integrated twice. Although the specific number is not completely clear, the order of magnitude seems to be a couple of micrometers. Δx is estimated to be 4 micrometer. This displacement will lead to a error in beam position on the substrate of $\epsilon = 4E^{-3}\frac{120}{900} = 533$ nm.

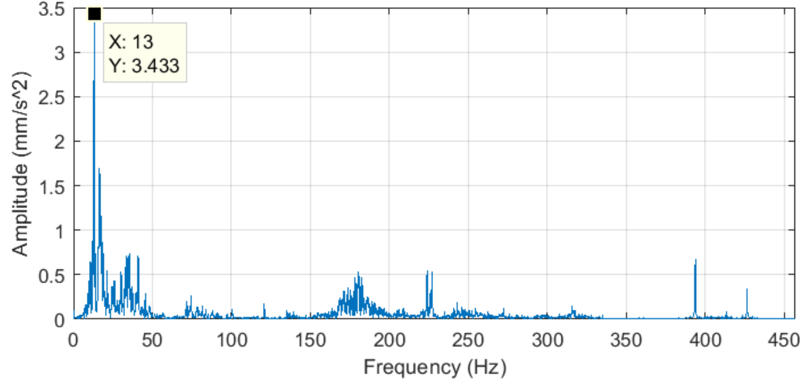

Figure 4.17: An example of the accelerometer frequency spectrum of the optical column after a stage step in x

4.2.3 Thermal drift

Figure 4.18 shows an overview of the current metrology. The optical path length of the x and y interferometers is subdivided in the sub-paths x_1, x_2, y_1, y_2, u and w. Only expansion of sub-paths x_1 and y_1, so Δx_1 and Δy_1, will lead to measurement errors. Only from the point the two different frequencies are separated from each other inside the interferometer (as explained in 1.3.5) do optical path length changes influence the measurement. So changes in any of the other sub-paths do not influence the measurement of the interferometers. The two sub-paths x_1 and y_1 will have thermal errors with different sources.

- Δx_1 is caused by thermal expansion of:
  1. Superplate in x-direction
  2. Bracket x-interferometer in x-direction
  3. Top plate suspension in x-direction
- Δy_1 is caused by thermal expansion of:
  1. Superplate in y-direction
  2. Bracket y-interferometer in y-direction
  3. Top plate suspension in y-direction

There is also thermal drift due to thermal expansion of the holder and substrate.

Steady state thermal drift

First the steady state thermal drift will be considered. At $t = 0 \Rightarrow T = T_0$ and at $t \gg 0 \Rightarrow T = T_0 + \Delta T = T_{new}$. So the assumption will be made that the system is isothermal with a temperature of T_{new} after some settling time. The temperature difference ΔT will the maximum allowed temperature difference within one hour given by the

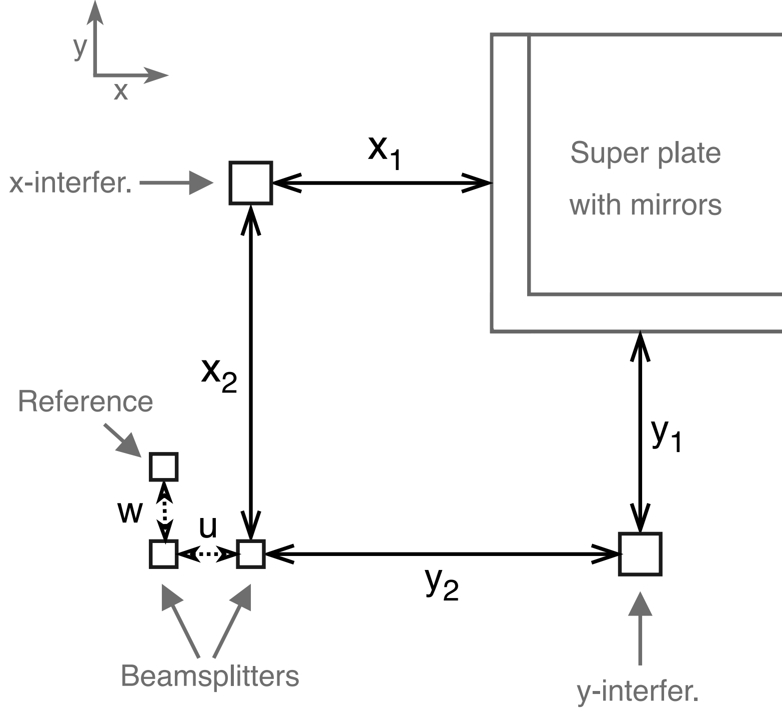

Figure 4.18: Thermal drift for stage position measurement

requirements. As the system is isothermal, the linear thermal expansion relation can be used to calculate changes in optical path length.

- $\Delta T = 0.1$ K
- Coefficient of thermal expansion of Zerodur = $\alpha_Z = 0.02E^{-6}$/K
- Coefficient of thermal expansion of Invar36 = $\alpha_I = 1.2E^{-6}$/K
- Coefficient of thermal expansion of Stainless steel AISI 304 = $\alpha_{SS} = 17.2E^{-6}$/K

Thermal expansion of the superplate
The superplate is assumed to be square with dimensions: LxL = 270x270 mm. The superplate is suspended with a Kelvin clamp with three balls in grooves under relative angles of 120 degrees. Therefore the thermal centre is assumed to be in the centre of the plate and expansion will occur in all directions evenly. The length that will be used to calculate the optical path difference is therefore half the length of the superplate: L_{sp} = 135 mm. The expansion of the superplate will influence Δx_1 and Δy_1.

$$\Delta L_{sp_{x1}} = \Delta L_{sp_{y1}} = L_{sp}\alpha_Z \Delta T = 135 \cdot 0.02E^{-6} \cdot 0.1 = 0.27 \text{ nm} \tag{4.11}$$

Thermal expansion of the interferometer brackets
The interferometer brackets are attached to the side of the top plate of the suspension. Therefore the bracket will be assumed to expand in all directions except in the direction towards the top plate of the suspension. The location of the thermal centre can be seen in Figure 4.19. The location of the interferometer is assumed to be in the middle of the bracket. This means that the net change in optical path length will be zero in the direction parallel with the side of the suspension, so both sub-paths x_1 and y_1 are influenced. Because the interferometer is attached

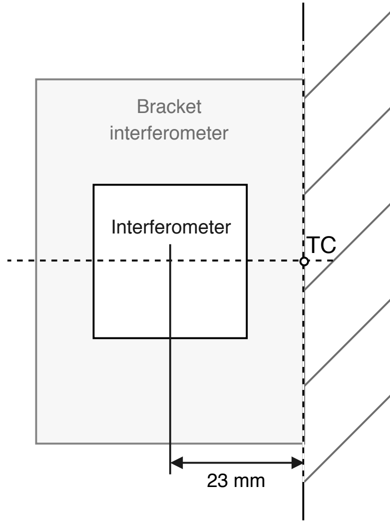

Figure 4.19: Thermal centre of the interferometer brackets

in the centre of the bracket, the thermal expansion for x_1 and y_1 will be calculated with half the length of the interferometer bracket. This is equal to L_{ib} = 23 mm.

$$\Delta L_{ib_{x1}} = \Delta L_{ib_{y1}} = L_{ib}\alpha_I \Delta T = 23 \cdot 1.2E^{-6} \cdot 0.1 = 2.8 \text{ nm} \tag{4.12}$$

Thermal expansion of the top plate of the suspension

The thermal centre of the top plate of the suspension is assumed to be in the centre of the plate because of the symmetric design of the attachment of the vacuum cover plate (16 bolts around the opening for the beam column and 4 small struts in each corner). This is illustrated in Figure 4.20. The thermal expansion in x-direction will

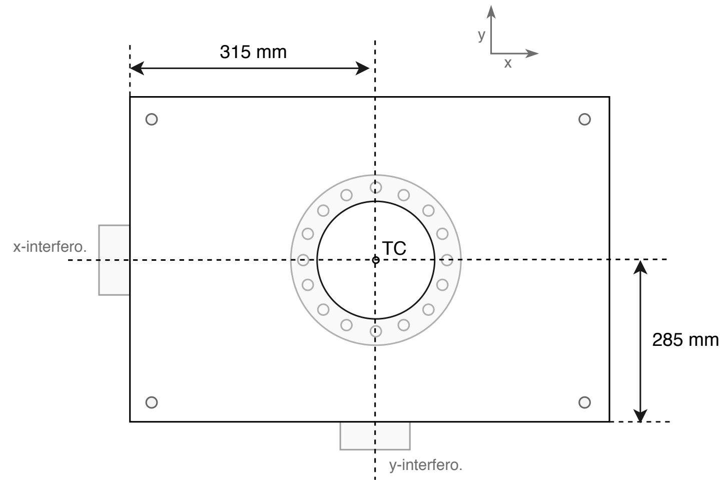

Figure 4.20: Thermal centre of the top plate of the suspension

influence the sub-paths x_1. The contribution of the thermal expansion of the suspension top-plate will be equal to:

$$\Delta L_{sus_{x1}} = \Delta L_{sus_{y2}} = L_{sus_x}\alpha_I \Delta T = 315 \cdot 1.2E^{-6} \cdot 0.1 = 37.8 \text{ nm} \tag{4.13}$$

Thermal expansion in the y-direction will influence the optical path length of y_1. This expansion is equal to:

$$\Delta L_{sus_{y1}} = \Delta L_{sus_{x2}} = L_{sus_y}\alpha_I \Delta T = 285 \cdot 1.2E^{-6} \cdot 0.1 = 34.2 \text{ nm} \tag{4.14}$$

Thermal expansion of the substrate

To calculate the expansion of the substrate the following estimation will be made. All the relevant parameters are given by Table 4.1. Writing one spot with the spot size of 50 nm, a current of 10 nA and a resist dose of 150 μC/sm^2

Table 4.1: Writing parameters

Variable	Value	Unit
Substrate material	Silicon	-
Spot size	50	nm
Beam current	10	nA
Beam voltage	100	kV
Resist dose	150	μC/sm^2
Writing percentage	60	%
Writing time	1	h
Substrate diameter	200	mm
Substrate thickness	0.5	mm
Substrate density	2320	kg/m^2
Substrate conductivity	760	J/kg·K
Substrate CTE	2.6E^{-6}	1/K

gives a writing time per spot of $150 \cdot \pi \cdot (25E^{-7})^2/10E-3 = 295$ ns. In one hour the area that can be written with these parameters is about 24 mm^2. If the writing percentage is 60%, the writing area will be 24/0.6=40 mm^2. The energy that is transferred to the substrate during this writing time is the power of the electron beam times the writing time and writing percentage: $10E^{-9} \cdot 100E^3 \cdot 3600 \cdot 0.6 = 2.1$ J. The mass of the substrate is equal to: $\pi \cdot 0.1^2 \cdot 0.5E^{-3} = 0.036$ kg. If the assumption is made that all the heat is absorbed by the entire substrate and is not further transferred in the system, then the temperature difference in the substrate is equal to:

$$\Delta T = \frac{2.1}{760 \cdot 0.036} \approx 0.08 \text{ K} \tag{4.15}$$

If the area of 40 mm is assumed to be square sides are $\sqrt{40} = 6.3$ mm. A temperature difference of 0.08 K will lead to an expansion error of $\epsilon = 0.08 \cdot 2.6E^{-6} \cdot 6.3E^{-3} = 1.3$ nm.

Thermal sensitivity optics

The optics used in the interferometer are sensitive to temperature changes. One of the reasons is the temperature dependence of the index of refraction of glass. The error in optical path length due to a temperature variation is ≤ 10 nm/K (L. Uittenbogaard, *Keysight technologies*, personal communication, August 13, 2019). For a $\Delta T = 0.1$ K an error in optical path length of $10 \cdot 0.1 = 1$ nm will be observed.

Changes in OPL of the x- and y-interferometer

For the x-interferometer arm the total change in optical path length due to an isothermal increase in temperature of 0.1 K is about 43 nm, see Table 4.2. As can be seen, the expansion of the superplate is negligible compared to the other components. The largest contributor seems to be the expansion of the top plate of the stage suspension.

Table 4.2: Error in OPL for the x-interferometer due to an isothermal temperature increase of $\Delta T = 0.1$ K

Thermal error source x-interferometer		Error in OPL Δx_1 [nm]
Superplate in x-direction:	$\Delta L_{sp_{x1}}$	0.3
Bracket x-interferometer in x-direction:	$\Delta L_{ib_{x1}}$	2.8
Top plate suspension in x-direction:	$\Delta L_{sus_{x1}}$	37.8
Thermal drift of optics in x-interferometer:	10nm/K	1
Thermal drift of the substrate:		1.3
	Sum	43.2

For the y-interferometer the error in optical path length is about the same as for the x-interferometer being ~ 40 nm, see Table 4.3. Also for the y-interferometer the main contributor is the expansion of the top plate of the stage suspension.

Table 4.3: Error in OPL for the y-interferometer due to an isothermal temperature increase of $\Delta T = 0.1$ K

Thermal error source y-interferometer		Error in OPL Δy_1 [nm]
Superplate in y-direction:	$\Delta L_{sp_{y1}}$	0.3
Bracket y-interferometer in y-direction:	$\Delta L_{ib_{y1}}$	2.8
Top plate suspension in y-direction:	$\Delta L_{sus_{y1}}$	34.2
Thermal drift of optics in y-interferometer	10nm/K	1
Thermal drift of the substrate:		1.3
	Total sum	39.6

Drift test results

A number of long term stability tests have been done on the EBPG5200 with the focus on thermal drift. Temperatures at different places around and in the machine have been measured, while simultaneously looking at the error in beam position. This error is determined by searching the position of a marker every 10 minutes. In Figure 4.21 an example measurement set is visualised, with the ΔT of the cleanroom temperature in blue and the registered drift given with the red plot. The drift is given as the 'interferometer' drift in the graph, but this is under the

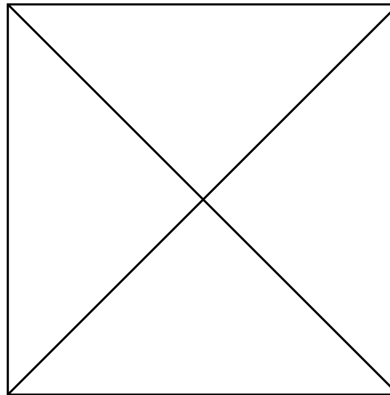

Figure 4.21: Thermal drift of the x-interferometer and the ΔT of the room temperature over time

assumption that drift of the substrate itself and drift inside the electron optical column are low. As the graph clearly shows a high correlation between the ΔT and the registered drift and given that the correlation between the cleanroom temperature and the temperature of the superplate is very low, this may be a valid assumption. The following conclusions can be drawn from the thermal drift tests:

- An sensitivity estimation of error for temperature change in cleanroom in x-direction: $\frac{\Delta\epsilon}{\Delta T} \approx 150$ nm/K. But there is quite a high differences between data sets.
- The sensitivity estimation of error for temperature change in cleanroom in y-direction: $\frac{\Delta\epsilon}{\Delta T} \approx 200$ nm/K. But there are also quite high differences between data sets.
- Cleanrooms are not always compliant with the cleanroom specs which leads to higher errors.
- There is a high correlation between temperature change in the environment and beam stability. This indicates that thermal errors are a very large contribution in the long term stability budget, probably up to 90%.

4.2.4 Magnetostriction

Invar is notorious for its expansion under a change in magnetic field strength as this effect can be quite significant (for precision engineering). Luckily in this case the magnetic field strength stays approximately constant during operation, so after an initial start-up period the expansion due to this magnetic field can be assumed constant as well.

4.3 Error budgets current system

4.3.1 Beam stability

In Figure 4.22 the beam stability is illustrated. The beam stability $\boldsymbol{e}$ can be roughly divided into three different error sources e_1, e_2 and e_3. The first error source e_1 is the error that occurs when a displacement of the electron beam position occurs, so electron beam drift. The beam inside the electron beam column can be different than anticipated and/or the actual column can be at a different position in space than anticipated. Error source e_2 is the drift that occurs between the mirror and the interferometer. The interferometers measure a certain cumulative displacement of the mirror based on the wavelength of light, but the actual displacement of the mirror can be different. Finally, a third error source (e_3) occurs due to drift of the substrate and substrate holder.

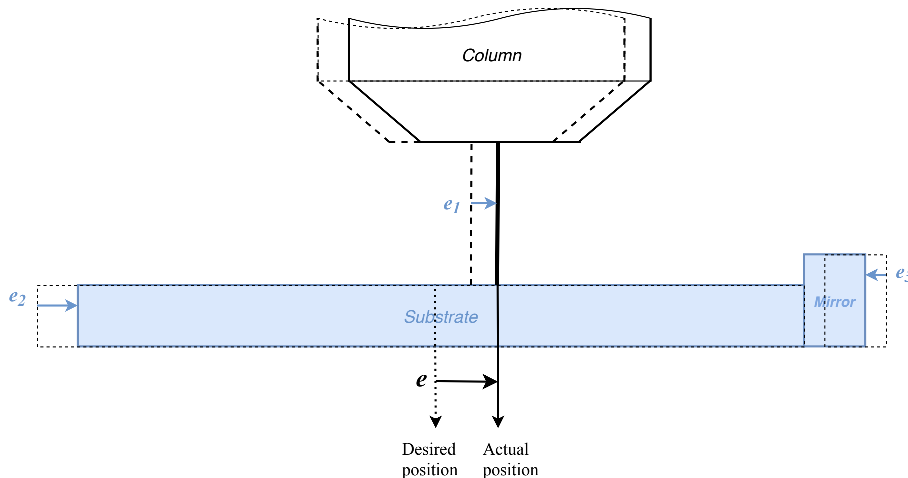

Figure 4.22: Beam stability: error sources

Inside the error budgets for the beam stability two categories can be thought of being the non-repeatable static errors and dynamic errors. These categories each include the three different error sources e_1, e_2 and e_3. A first assessment of the error budgets has been done in Figure 4.23. Figure 4.23a shows the error budget for the short term stability and Figure 4.23b shows the budget for the long term stability. It is likely that the non-repeatable static errors consist mostly of errors in measuring the right displacement of the mirrors on the stage (error source e_3),

Error budget short term stab.		
Non-repeatable static errors		
e_1	≈ 0	
e_2	≈ 0	
e_3		+ (rss)
e_{stat}	?	
Dynamic errors		
e_1		
e_2	≈ 0	
e_3		+ (rss)
e_{dyn}	?	+
$\mathbf{e_{tot}}$	**≈ 5 nm**	

(a) Short term beam stability error budget

Error budget long term stab.		
Non-repeatable static errors		
e_1	≈ 0	
e_2	≈ 0	
e_3		+ (rss)
e_{stat}	<< 50 nm	
Dynamic errors		
e_1		
e_2		
e_3		+
e_{dyn}	≈ 50 nm	+
$\mathbf{e_{tot}}$	**≈ 50 nm**	

(b) Long term beam stability error budget

Figure 4.23: Error budgets beam stability

although some part may be due to the electron beam having non-repeatable 'static' errors such as deflection errors. The non-repeatable static errors with error source e_3 were discussed in Section 4.1. Table 4.4 gives an overview. The total root sum square is equal to 1.64 nm. The non-repeatable static errors and the dynamic errors should be added linearly, as they are correlated in the sense that the static errors give an offset on the dynamic errors. This means for the short term error budget the $e_{dyn} = e_{tot} - e_{stat} = 5 - 1.4 = 3.6$ nm. This number is divided in some unknown way between e_1 and e_3, as e_2 will have no contribution in this time scale. The vibration analysis in Section

Table 4.4: Static non-repeatable errors with error source e_3

Contributor	**Unc.**	**unit**	**Prob. dist.**	**Div.**	**Sens.**	**Perf.**	**unit**	**[%]**	**Remarks**
Alignment/Abbe errors	0.87	nm						38.3	
Pitch error non-repeatable	10	μrad	Normal, 2s	2.00	0.14	0.70	nm	12.8	0.1 mm offset
Roll error non-repeatable	10	μrad	Normal, 2s	2.00	0.14	0.70	nm	12.8	0.1 mm offset
Yaw error non-repeatable	10	μrad	Normal, 2s	2.00	0.14	0.70	nm	12.8	0.1 mm offset
Instrumentational errors	1.1	nm						61.7	
Laser stability	0.002	ppm	Uniform	1.73	800.00	0.92	nm	43.5	
Optics cyclic error	1	nm	Uniform	1.73	1.00	0.58	nm	17.0	Periodic error
Measurement resolution	0.155	nm	-	1.00	1.00	0.16	nm	1.2	$\lambda/4096$
Non-repeatable static errors	1.40	nm						100.0	

4.2.1 indicated that mechanical vibrations had a higher contribution to the total dynamic errors than other noise sources. If they are estimated to have a 65% contribution (average of the x- and y-axis contribution), this means that the error due to mechanical vibrations is $\sqrt{0.65 \cdot 3.6^2} = 2.9$ nm. An overview of the short term beam stability error budget is shown in Table 4.5. For the long term error budget this means that the e_{dyn} is indeed approximately equal to 50 nm. As indicated by the thermal analysis, thermal errors are likely to have a very large contribution in this budget, probably up to 90%. As these errors are correlated and added linearly this means thermal noise causes an error of about $0.9 \cdot 50 = 45$ nm. This is similar from what was found in the steady state thermal drift analysis of Section 4.2.3. The 45 nm is divided over e_1, e_2 and e_3, but a large part seems to be caused by the metrology (e_3). An overview of the error budget can be seen in Table 4.6.

Table 4.5: Short term beam stability error budget

Error source	**nm**	[%]
Non-repeatable static error	1.40	28.0
Dynamic errors	3.60	72.0
- Metrology	2.9	46.8
- Other noise sources	2.1	25.2
Total error	5	100

Table 4.6: Long term beam stability error budget

Error source	**nm**	[%]
Thermal drift	45	90
Other error sources	5	10
Total error	50	100

4.3.2 Overlay

The part of the overlay that is determined by metrology errors consists of all the non-repeatable static errors as described in Table 4.4, but the non-repeatable stage errors also rotate and shift the image and therefore additionally contribute to the overlay error in the following way. On a write field area of 1x1 mm the overlay error due to non-repeatable yaw is:

$$\frac{1}{2}\sqrt{2}E^{-3} \cdot 10E^{-6} = 7 \text{ nm} \tag{4.16}$$

This is using the small angle approximation. $\frac{1}{2}\sqrt{2}$ is the arm in mm from the middle of a 1x1 mm square and the $10E^{-6}$ is the non-repeatable yaw angle of the stage. This is already a large contribution of the current overlay budget. The non-repeatable yaw error is based on the specifications of the stage. This does not match what is seen in practice and it seems that in practice this number is better than the specifications show. This could have multiple reasons. One of the reasons is that the stage in practice has better non-repeatabilities than specified. But more plausible is that the effect is largely reduced because of the calibration with marker locations around the 1x1 mm area that is done before the overlay test is performed. When calculating the overlay error contribution of the yaw for the total actuation range of the stage of 220 mm, the error is equal to: $110E^{-3} \cdot 10E^{-6} = 1.1\mu$m! This is also way worse than seen in practice. However this does indicate that non-repeatable yaw errors can be a significant contribution to the overlay budget, for both on a write field of 1x1 mm or on the entire actuation range of the stage. For the non-repeatable pitch and roll errors the contribution is less pronoun. The roll and pitch movement of the stage mainly lead to gain errors when the electron beam is deflected. The maximum deflection angle for a write field of 1x1 mm is $tan^{-1}(0.5\sqrt{(2)}/40) = 0.018$ rad. This gives a maximum pitch/roll overlay error (the gain error) of:

$$\frac{1}{2}\sqrt{2}E^{-3} \cdot 10E^{-6} \cdot tan(0.018) = 0.125 \text{ nm} \tag{4.17}$$

So the total overlay contribution of the errors due to the metrology is $\sqrt{1.4^2 + 7^2 + 0.125^2} = 7.14$ nm. This is on a write field of 1x1 mm and according to the stage specifications, which may or may not be completely accurate.

4.3.3 Throughput

As evaluated in Section 4.2.2, the estimated error directly after a stage step is equal to 533 nm. This potentially decreases throughput by a significant amount because there has to be waited for the column swing to damp out in order to keep the errors caused by this to a minimum. As discussed before it is hard to put specific numbers on the throughput, but for the sparse patterns the settling time can be up to 99% of the total write time. In the current system the settling time should be set $<$ 100 ms if the settling errors are supposed to be minimum. This settling

time is determined by a number of variables, but the column swing is estimated to be a large contributor to this time.

4.3.4 Accuracy

The accuracy of the system is not a user requirement right now, but could become one in the future since the demand for absolute accuracy is rising. A short evaluation will be done of the contribution of the metrology errors to the accuracy performance. In the accuracy budget all the previously discussed error sources play a role. Dynamic effects such as thermal drift and vibrations will be left out of the equation, only the static repeatable and non-repeatable errors over the full actuation range of the stage will taken into account in this evaluation. An overview of all the static errors are given in Table 4.7. The errors added linearly give a total accuracy error due to the metrology of 266 nm.

Table 4.7: Static error sources of the accuracy

Static error source	nm
Cosine error	88
Mirror form error	63
Mirror non orthogonality	100
Repeatable yaw error	10
Repeatable yaw cosine error	1.8
Repeatable pitch/roll error	2
Repeatable pitch/roll cosine error	0.072
Non-repeatable static errors	1.4

Chapter 5

Concepts

The goal of the concept phase is to come up with a general concept idea. This will be done in the following way. First via brainstorming/reading literature some general strategies and solutions will be formulated to meet the requirements. After this a filtering process will take place in which, based on simple reasoning and/or quick calculations, some solutions will be eliminated. With the remaining solutions a few (about three) general concepts will be composed. These different concepts will be compared to each other with some simple assessments. Based on this evaluation eventually one general concept will be chosen. This way of approaching the concept phase is based on the method described by (*K. Bustraan.*, 2010 [14]).

5.1 Focus areas

In Chapter 4 the error sources were evaluated. From the error budgets the following problem/improvement areas can be indicated:

1. Short term beam stability budget: significant part is mechanical vibrational noise
2. Long term beam stability budget: significant part is thermal drift of the interferometers
3. Overlay budget: non-repeatable yaw leads to big errors
4. Throughput budget: column swing decreases throughput significantly
5. Accuracy budget: cosine and abbe errors lead to big accuracy errors

5.2 Distance measurement principles

Various measurement principles exist to measure position (relative or absolute). The most relevant methods will be shortly discussed here and are the following[15]:

- Capacitive sensors
- Laser interferometers
- Optical encoders

Capacitive displacement sensor measures the changes in capacitance (due to a change in distance between the two plates) in an electric field. Capacitive sensors are only suited to measure displacement of a very short distance (≤ 1 mm), so they are not suited to measure the displacement of the stage. They could be potentially used to measure displacement of other parts of the system, such as the electron optical column or the metrology frame.

Laser interferometers base their measurement on the wavelength of light. This measurement can be either a relative or an absolute position. For relative displacement homodyne or heterodyne interferometers can be used. The homodyne interferometer uses laser light with a single wavelength and determines the displacement with quadratic phase detection. The heterodyne interferometer has been discussed already in Chapter 1.3.5. The performance (looking at high precision systems) of a heterodyne interferometer is superior to that of a homodyne, because the AC signal used in heterodyne is less sensitive to noise sources (for example laser power fluctuation) than the DC signal used in the homodyne. Added to that is the fact that only one receiver is necessary in a heterodyne interferometer to determine both displacement and direction, compared to homodyne where two different receivers are necessary to determine this. It is also possible to measure absolute displacement with interferometers. This can be done by using laser light that has multiple wavelengths. The measuring range for interferometers can be up to tens of meters.

Optical encoders are rising in popularity in precision positioning systems as the resolution possible is now matching that of what is possible with interferometers (< 10 pm)[15] and because they can potentially reduce the air path used in non-vacuum systems. Optical encoders are based on graduated scales that diffract the light and this is than interfered. They too can be either absolute or incremental, for now the focus will be put on the incremental type. The type of encoder that is suitable for precision positioning are optical encoders that use interferential scales. Different arrangements can be used in an optical encoder, but a basic example is shown in Figure 5.1a and is type of optical encoder called a Canon laser linear encoder[18]. The optical encoder uses a laser to reflect light on an optical grating scale. The first order diffraction is reflected back again at the grating with use of a 50% mirror and then is interfered with itself and enters a photo detector. The grating has a certain pitch and the final signal is sinusoidal with four periods per pitch (because the light is reflected twice by the grating). The resolution measured is equal to[18]:

$$d = \frac{g}{k \cdot f} \tag{5.1}$$

With d the measured displacement, g the grating pitch, f the optical multiplication factor and k the electronic interpolation factor. Without going into detail, with 2D optical gratings 2DOF up to 6DOF can be measured[17]. An example of such a system is displayed in Figure 5.1b. The accuracy is mainly dependent on calibration of

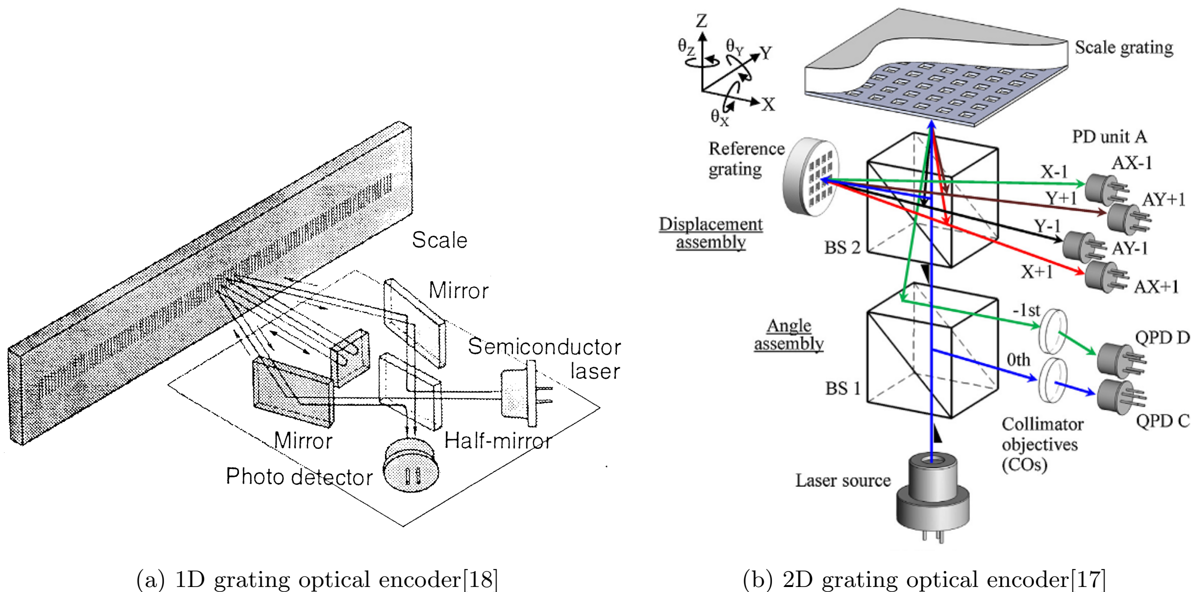

(a) 1D grating optical encoder[18]

(b) 2D grating optical encoder[17]

Figure 5.1: Two different optical encoders, one using a 1D optical grating the other a 3D optical grating

the grating, which is definitely necessary in a high precision system. So the main error sources of this type of measurement are the calibration errors (which can be low if done correctly) and thermal expansion of the grating (which could be reduced by using Zerodur).

5.3 Strategies

5.3.1 Improving short term dynamic errors

For decreasing the short term dynamic errors in the system and improving the short term dynamic behaviour, three general strategies are formulated. The first strategy is to decrease the vibrations in the metrology system (or in the overall system). The second strategy is to compensate the vibrations that are on the metrology system. So vibrations are present in the system but the system is insensitive to it. The two strategies can be seen in Figure 5.2. Of course a combination of the two strategies is also a solution. Solutions to each strategy can be formulated.

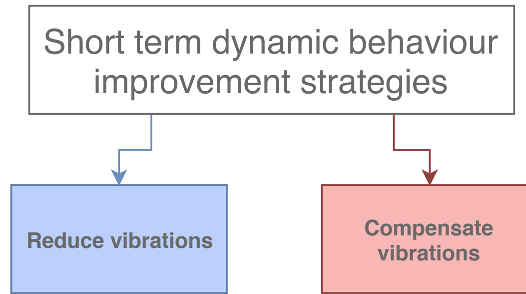

Figure 5.2: Strategies for improving the short term dynamic behaviour

5.3.2 Short term dynamic error solutions

Reduce vibrations

In Figure 5.3 four different solutions are presented to reduce the vibrations in the system. The first one is mode shaping in which mass and stiffness are added in ways which increases vibrations in areas that are not important and decreases vibrations in areas that are important. The second solution is to decouple the metrology frame from the force frame. If separation is successful all the forces act on the force frame and forces and deformations are reduced on the metrology frame. A third solution is to make some parts in the system stiffer, this can decrease the amount of displacement due to vibrations. The final solution is dynamic balancing. In this solution a second mass is actuated at the same time that the stage is actuated creating a counter moment which reduces the overall moment on the system and therefore reduces vibrations due to the stage moving.

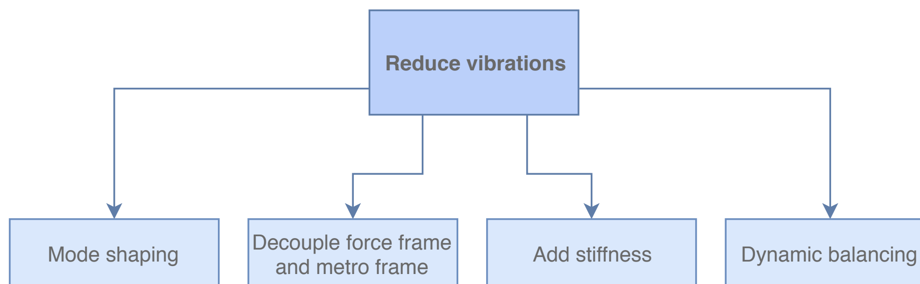

Figure 5.3: Reduce vibrations

In Figure 5.4 the solution 'Decouple force frame and metro frame' is worked out into sub-solutions. A possible solutions is to have a metro frame inside or outside the vacuum chamber. Inside the vacuum chamber one could have a suspended frame that is attached to the vacuum chamber or that goes through it with bellows. The metrology frame attached to the vacuum chamber could be either damped or attached with a very low stiffness connection. Inside the vacuum chamber active vibration compensation is also a way to decouple the force and metro frame.

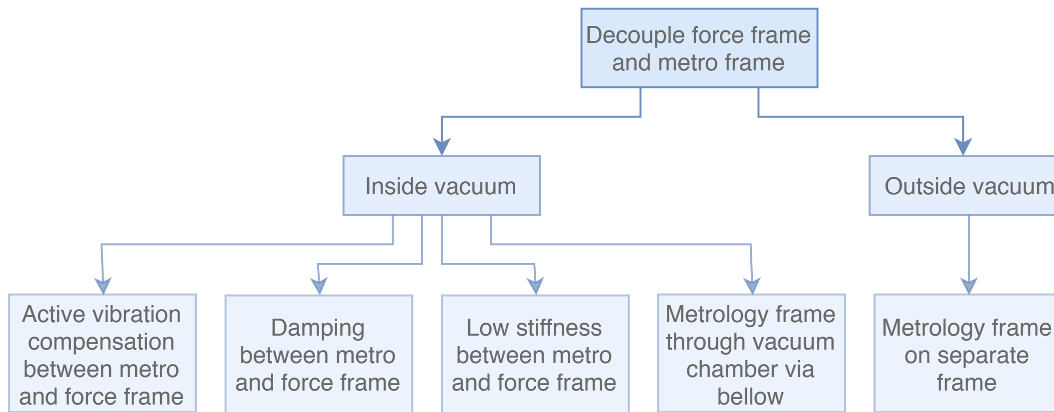

Figure 5.4: Decouple force frame and metro frame

In Figure 5.5 the sub-solutions for the 'Add stiffness' solution are presented. There are three main sub-solutions: a stiffer geometry, stiffer materials and a stiffer column assembly (which is technically also a stiffer geometry). Sub-solutions of a stiffer geometry can be different ways to mount the stage and mount the metrology and reduce the force loop present in the current system. Sub-solutions to make a stiffer column assembly are attaching the column at different points and in different ways to the vacuum chamber and make a horizontal column assembly in which the stage moves vertical.

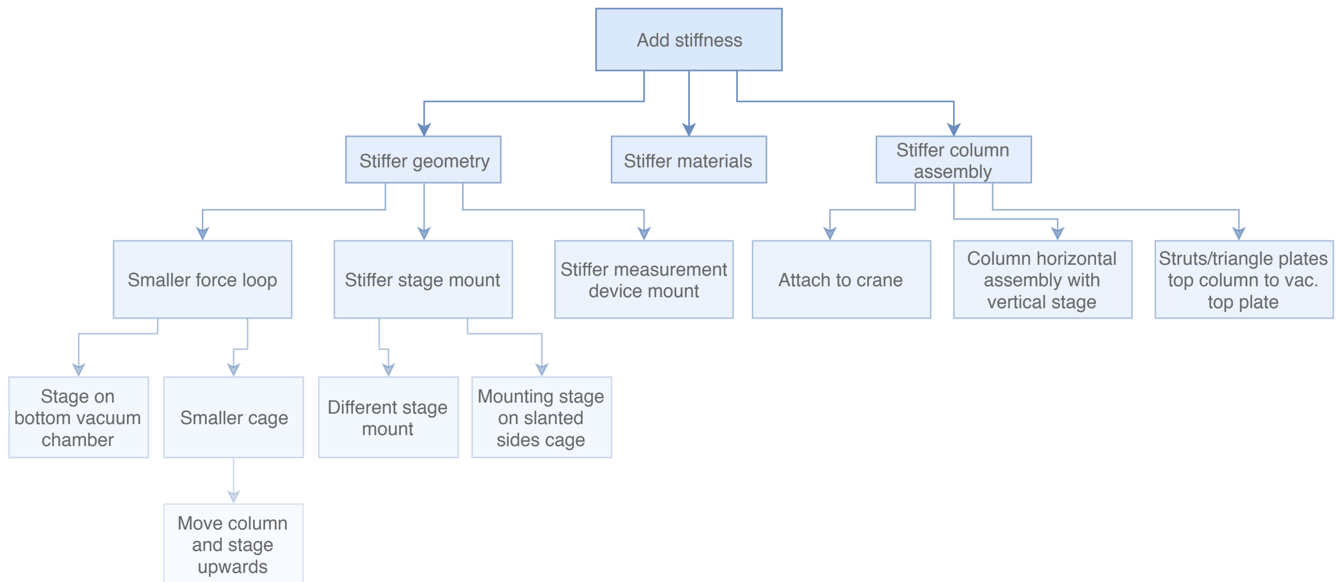

Figure 5.5: Add stiffness in the system

Compensate vibrations

In Figure 5.6 the sub-solutions for compensating the vibrations are shown. One way of 'compensating' is by using differential interferometry. In this solution one could place a mirror on the electron beam column and use this as the 'reference mirror'. Then a difference in position between this mirror and the mirror on the stage is measured, leaving any horizontal vibration of the interferometer itself irrelevant. The same principle could also be done mechanically by attaching the interferometer via some stiff connection to the electron column ensuring the interferometer moves with the column and so the distance measurement is done between the column and the stage mirror. The third

option is to use a optical surface encoder, measuring directly from the optical column to the stage. This means on either the optical column or the stage a phase grating grid is attached and on the other part the surface encoder.

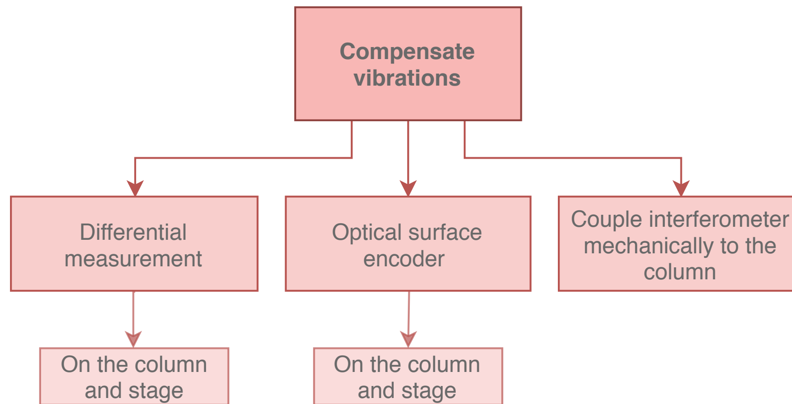

Figure 5.6: Compensate vibrations

Combination: reduce and compensate vibrations
For the third strategy (the combination of the two) no solutions have been separately drawn in a block diagram, as this could be numerous combinations of the red and blue blocks. As one can see, a lot of the solutions can all be combined with each other. This combining of solutions to make different concept ideas will be done in Section 5.5.

5.3.3 Improving long term dynamic errors

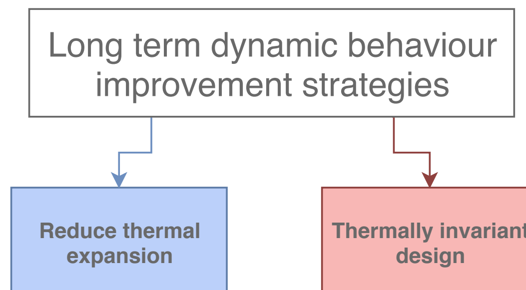

Figure 5.7: Strategy for improving long term dynamic behaviour

5.3.4 Long term dynamic error solutions

The long term dynamic behaviour is dominated by thermal drift as was seen from the long term beam stability error budget. For improving thermal behaviour two main strategies can be distinguished. The first strategy is reducing thermal expansion in the system and the second strategy is making the system thermally invariant. This is illustrated by Figure 5.7 as the first two darker colored blocks. Of course a third strategy is a combination of the two strategies: reduce the expansion and make the system thermally invariant.

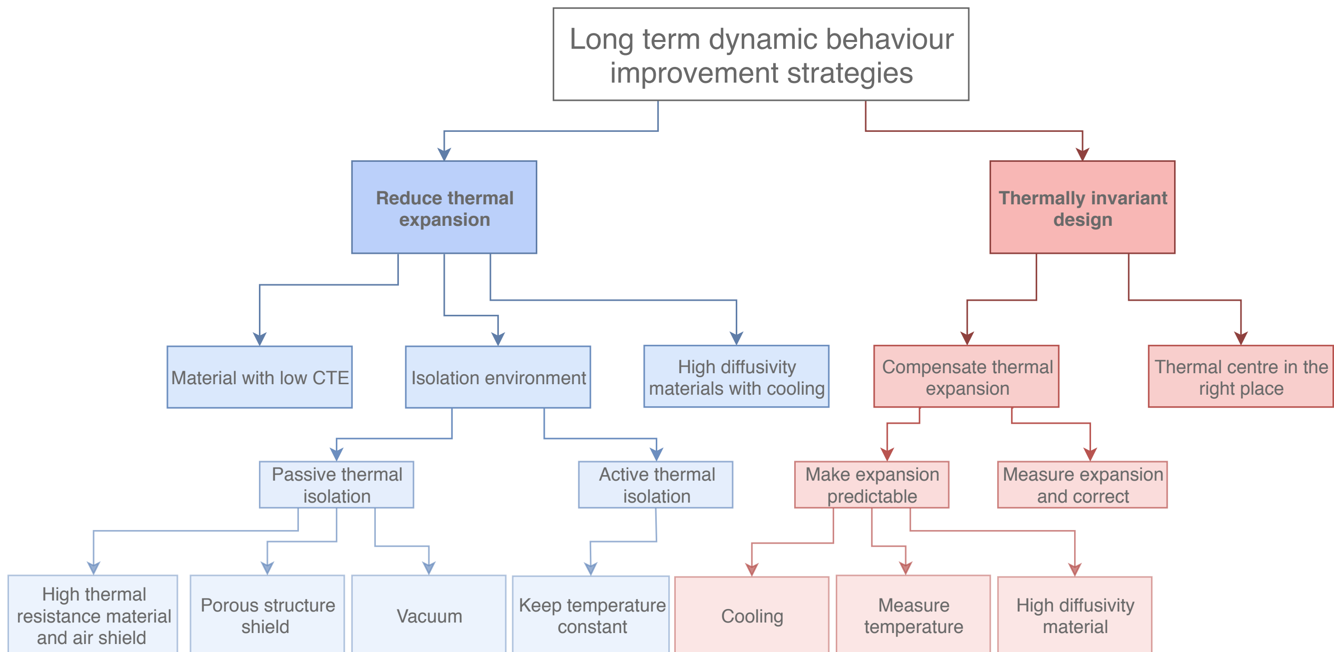

Figure 5.8: Strategy and solutions tree for improving long term dynamic behaviour

There are three main solutions to reduce thermal expansion. One is to use materials that have a low coefficient of thermal expansion. This makes sure that even if there is heat variation present in the system, this does not lead to huge dimensional variations. Another solution is to reduce the amount of heat that goes into the system, so to isolate it from its surrounding (or from heat sources). This can be done passively by using a high thermal resistance surrounding the system, or actively by using cooling fluid. A third solution is to let heat dissipate easily in the system but use cooling and the high diffusivity to keep the temperature relatively constant and homogeneous throughout the system. This makes sure the amount of thermal expansion is limited. The second strategy is making the system thermally invariant. Two main solutions are illustrated: compensate the thermal expansion or place the thermal centre at a convenient location at which thermal expansion does not influence it. To compensate for thermal expansion one could either predict it by measuring temperature and correct accordingly or measure the expansion itself and correct for it.

5.3.5 Improving static errors

Yaw error

The most noticeable static errors were the repeatable and non-repeatable yaw errors. To improve this, two displacement measurements on one axis (either the x- or y-axis) could be made to measure the yaw. Or with the use of an optical surface encoder, with a measurement looking down on the xy-plane of the stage, also a yaw measurement could be made. The implementation of yaw-correction is something that has to be thought of too. This could either be corrected electron-optically in the electron beam, or by actuating/rotating the stage/substrate accordingly.

Calibration

A lot of repeatable static errors that exist in the system originate from the fact that little calibration is being done currently. The cosine error, all the abbe errors and mirror tolerances could be compensated for if a calibration would be done on the system. This could for example be done by using a marker mask plate from which a very precise measurement has been done from all the marker positions and orientations, also called a golden standard. The optics periodic non-linearity is another example which could be compensated for by using compensation methods described in [12].

5.4 Filtering solutions

A number of solutions thought of in Section 5.3, can be eliminated based on simple reasoning or assessment. For the 'reduce vibrations' solution in Figure 5.3 the sub-solutions 'Mode shaping' and 'Dynamic balancing' can be eliminated based on the fact that they are out of the area of expertise. The solutions that are left are shown in Figure 5.9. For the sub-solution 'Decouple force frame from metro frame' in Figure 5.4 the solution 'Outside vacuum'

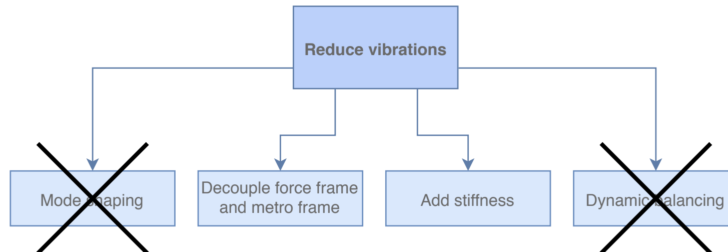

Figure 5.9: Filtering reduce vibrations solution

can be eliminated. Making a separate metroframe outside the vacuum chamber will maybe decrease the forces on the metroframe, but probably lead to significant higher errors due to refractive index changes that turbulent air introduces. Also the system is more exposed to environmental loads such as temperature changes. For the branch 'Inside vacuum' 'active vibration compensation' can be eliminated based on the fact that is outside of the area of expertise and 'metrology frame through vacuum' can be eliminated because this makes the system unnecessarily complex. This is because in this case one works in the interface between vacuum and non-vacuum. To ensure the vacuum a connection has to be made between the vacuum chamber and the frame, this can be done by using bellows and these have a certain (although fairly low) stiffness. But in that case you basically have the same situations as 'low stiffness between metro and force frame' connecting the metro frame to the vacuum with a low stiffness connection, but more complex. Figure 5.10 displays the remaining solutions.

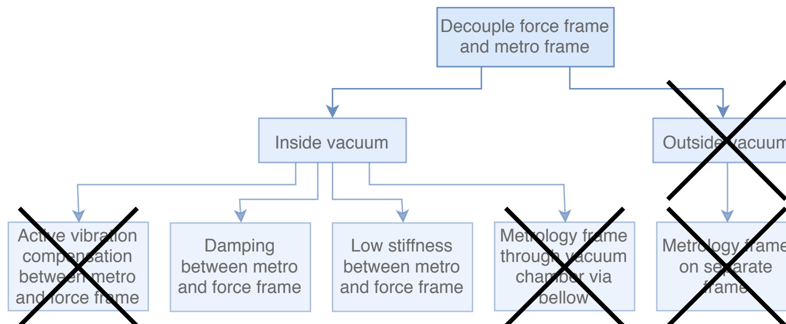

Figure 5.10: Filtering solutions of decouple force frame and metro frame

From the 'add stiffness' solutions, as depicted in Figure 5.5, a number of sub-solutions can be eliminated. From the 'stiffer column assembly', the solution 'horizontal column with vertical stage' can be scrapped. This would require a whole new system design which besides being out of the scope of this project, would also be a project of a much larger magnitude and time scale. For the 'stiffer geometry' solution the 'different stage mount' can be eliminated based on the fact that this is out of the scope. A totally new stage mount design will take up a whole separate project. The 'smaller force loop' solutions are eliminated. The 'stage on bottom vacuum chamber' does increases the stiffness of the force loop and could bring down the complexity and costs of the stage suspension. However, it introduces large design changes in the system without improving the performance by a significant amount. It also decreases the ease of maintenance, which could be compensated by introducing a door in the vacuum. However this introduces some complexity of its own. Based on these reasons it is concluded that it is

not worth the big design change. Making the cage smaller by moving the column and stage upwards is eliminated because, although it does make a stiffer stage suspension, the price that is paid is a less stiff column assembly. The fact that the lack in stiffness in the column assembly already is a significant problem in the current system, makes that this solution is not worth the risk-to-reward ratio.

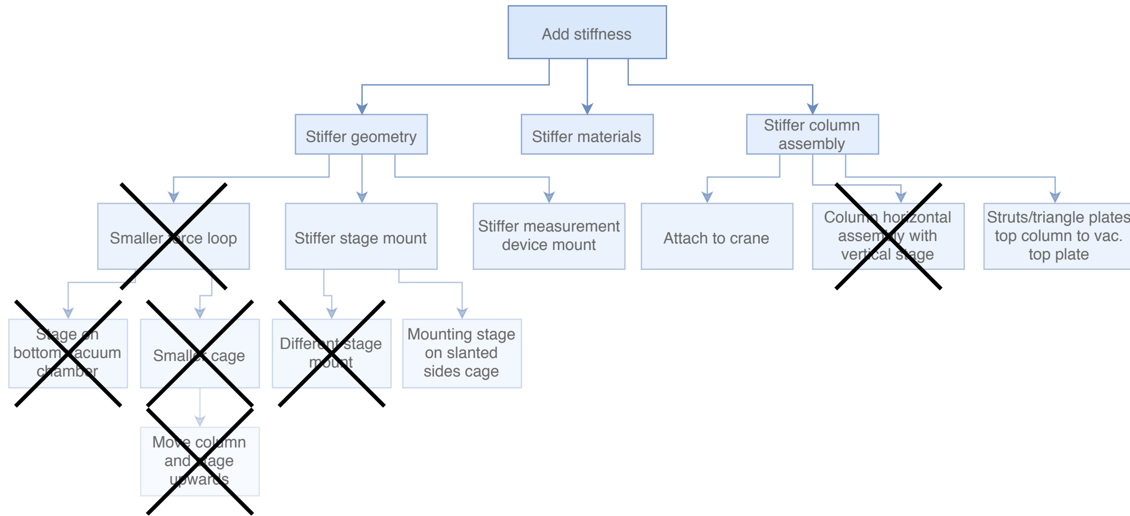

Figure 5.11: Filtering solutions of add stiffness

With the 'compensate vibration' solutions as depicted in Figure 5.6, the 'couple interferometer mechanically' solution will be eliminated. In order to measure the displacement of the stage, the interferometer should at least be distanced from the optical column with a length of equal to the stage actuation range. This is more or less the same distance as they are placed in the current system. The mechanical connection between the interferometers and the column has to quite long, which makes it harder to ensure stiffness. Also the interferometer is likely to be connected to the top plate of the suspension with some flexures. With these flexures some of the forces are reduced on the metroframe (reducing the deformation), but because in some directions stiffness is necessary the metroframe will still be coupled to the force frame. For these reasons this solution will not be very different from the current situation. So maybe some dynamic behaviour improvement can be achieved, but probably not enough to fulfill the requirements.

The solutions for the long term beam stability given by Figure 5.8 are not further reduced based on a first elimination process. However, cooling of any structures with cooling channels is preferably avoided if possible, because of the complexity and costs associated.

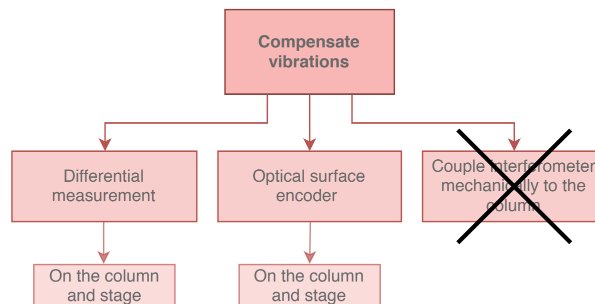

Figure 5.12: Filtering solutions of compensate vibrations

5.5 Generating concepts

With the remaining solutions after the filtering process in Section 5.4 and with using the different displacement measurement principles, two different concepts have been formulated.

5.5.1 Concept 1: Differential interferometry

The first concept uses differential interferometers to measure the relative displacement between the stage and the electron optical column. This concept has been split into two possible sub-concepts. The first one is integrating this concept in the current system, while the second sub-concept places the interferometers on a separate metrology frame inside the vacuum chamber.

Concept 1.1: Differential interferometry in current system

Concept 1 is keeping most of the current system, but adding differential interferometers and mirrors on the electron optical column. The stage suspension which houses the stage is kept, but some changes will be made to decrease the amount of vibrations in the system. For example the mounts of the interferometers will be improved compared to the current system.

With differential interferometry the relative displacement of a mirror on the electron column and the stage mirror will be measured. This can be seen in Figure 5.13. The relative displacement of those two mirrors approaches the objective measurement target: the position of the electron beam relative to the substrate. Also, any horizontal vibrations of the interferometer itself will not influence the measurement any more (the sensitivity is decreased from 1 to 0). One can also measure relative yaw with this measurement principle. How this measurement principle is integrated will be determined in a later stage.

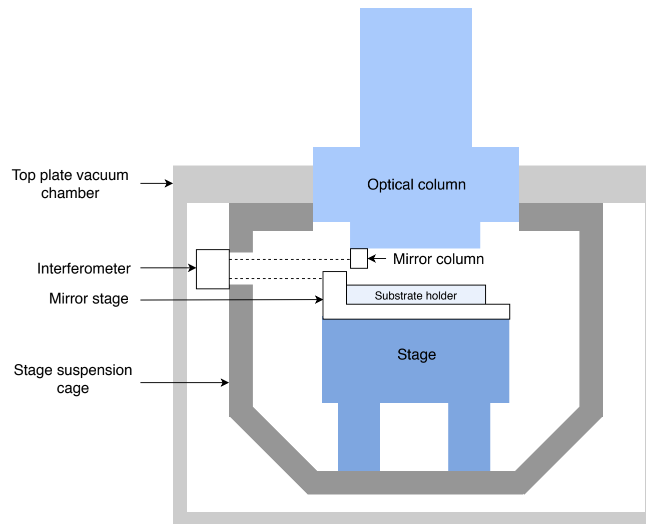

Figure 5.13: Differential interferometer with a measurement between stage and optical column

Concept 1.2: Differential interferometry on separate metrology frame in the vacuum chamber

In this concept a separate metrology frame will be added to separate and decouple the force frame and the metrology frame from each other. This frame is located inside the vacuum chamber. The exact design is not determined yet, but would probably be a heavy frame that is hanging from the vacuum chamber with very low stiffness flexure connections to act as a low pass filter.

5.5.2 Concept 2: Optical surface encoder

The second concept uses an optical surface encoder with an optical grating and an encoder. This will be implemented by placing optical grating areas on both sides of the substrate holder attached to the stage and a surface encoder attached to the sides of the electron beam column. This is illustrated in Figure 5.14a. Looking along the x-direction, the grating will be on both sides of the substrate holder, so that the holder can still be loaded from the airlock as it is done in the current system. To keep the stage symmetric to the column the grating length will be half the actuation range on both sides in the y-direction and the full actuation range in the x-direction. When the stage is actuated in y-direction only one of the halves will be used to determine position. The interferometers are attached to 2 sides of the column looking down on the two gratings. Another possibility is to do it the other way around, with the grating attached to column and the measurement device on the stage. It is possible to measure up to 6 degrees of freedom with the 2D-grating[16].

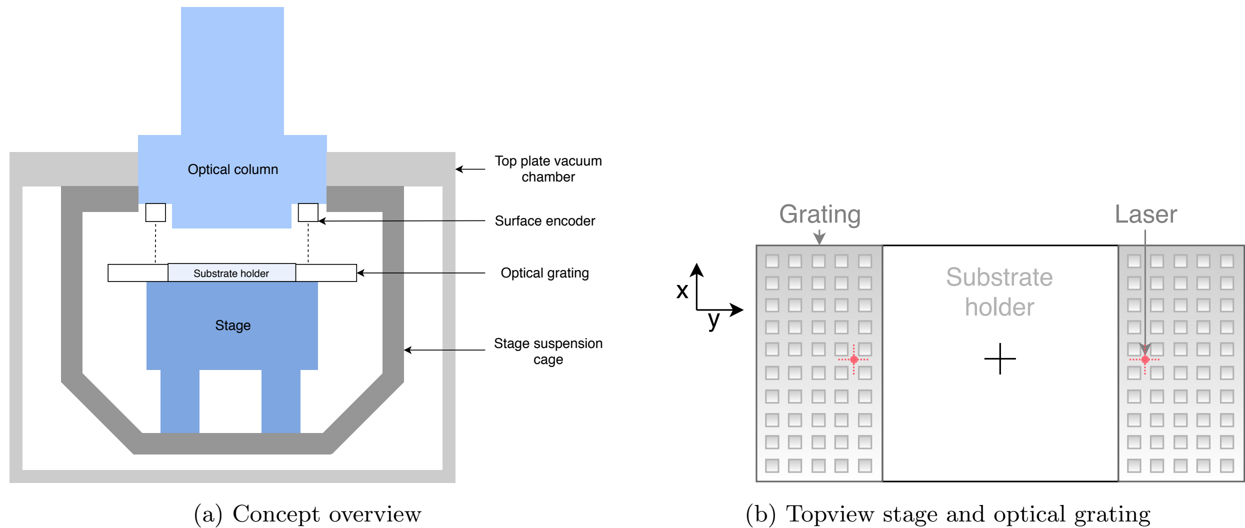

(a) Concept overview

(b) Topview stage and optical grating

Figure 5.14: Optical surface encoder measurement system with an optical grating on both sides of the stage and a interferometer on the electron beam column

5.6 Comparing concepts

To decide which concept should be chosen a appropriate comparison should be done. Concept 1 will be compared to concept 2 and the best concept will be picked.

5.6.1 Concept 1 vs. concept 2

A comparison between concept 1 (differential interferometer) and concept 2 (optical surface encoder) can be found in Table 5.1. The first comparison is the metroloop size. For both concepts the metroloop will be very small, which means the loop comprises of very few structural elements and (almost) a direct measurement is done of the desired variable (the displacement of the electron beam vs. the substrate). However, a difference between the two metrology loops is that the metroloop of the differential interferometer concept is more likely to deform compared to the optical surface encoder concept. This is due to the reasons discussed in Chapter 2. For the most part these deformations do not matter, because the differential interferometer is insensitive to most degrees of freedom. There are however a couple of DOF's that the interferometer is still sensitive for and these deformations could lead to some measurement errors. As the optical encoder is rigidly attached to the optical column, the chance of high deformations in the metroloop is small. A third comparison is done with the potential improvement of the column swing error. This error is improved in concept 1, but it is completely minimized in concept 2 which is a

	C1: Differential interferometer	C2: Optical surface encoder
Metroloop size	++	++
Potential deformations in metroloop	−	+
Improvement column swing error	+	++
Overall complexity	++	+
Costs	+	−
Integration current system	++	+
Risk	++	−−
Development time	++	−

Table 5.1: Comparison between concept 1 and concept 2

big advantage. The overall complexity and integration of the system are better for the differential interferometer, because the optical surface encoder needs large grating plates integrated in the current system. This means more space is needed and the stage suspension should be made larger which decreases the stiffness. The large optical gratings are also the reason the cost comparison is in favor of the differential interferometer, as the gratings are expensive to produce. Probably the biggest downside of the optical surface encoder concept is the risk associated with it. This also ties in with the developement time needed for this concept. Both originate from the fact that the technology is very new to the company, there is no experience currently with this measurement system. This can make the development process expensive and long.

Based on the comparison of the two concepts the differential interferometer (concept 1) will be chosen. Both concepts have very similar performance potential and could work very well, but the high risk and costs of the optical surface encoder make the differential interferometer the most favourable option out of the two.

5.6.2 Concept 1.1 vs. concept 1.2

The chosen concept in the previous section is concept 1: using a differential interferometer. Concept 1 was divided into two sub-concepts, concept 1.1 and concept 1.2. To decide which concept to choose between the two a closer look at the sensitivity of the differential interferometer will be taken. This will give an inside into how sensitive the interferometer is to certain movements. An estimation will be made of how much of these movements will be exerted on the interferometers. With this information an assessment will be made if a separate frame is necessary or not. If mounting the interferometers in the current system is possible, this would be preferred as this is the more simple concept of the two.

Sensitivity

When analysing the sensitivity of a differential interferometer, one can see that the sensitivity is zero in four of the six degrees of freedom and non-zero in two of them. This means the interferometer is sensitive for movements in two specific degrees of freedom and those are R_y and R_z. R_y is a rotation around the y axis which is also called pitch

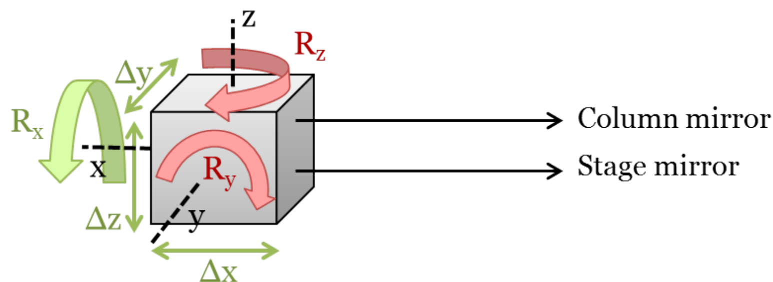

Figure 5.15: Sensitivity of a differential interferometer

and R_z is a rotation around the z-axis which is also called yaw. Figure 5.15 gives a illustration of the sensitivity in six degrees of freedom, with the color green indicating a zero sensitivity and the color red a non-zero sensitivity. Any rotation of the interferometer in those two directions would result in a optical path length error and more precisely this error is a cosine error. The cosine error is only present if there is a difference between the distance from the interferometer to the stage mirror and to the column mirror, see Figure 5.16 for an illustration of the cosine error due to a pitch movement. This will unavoidably happen when the stage is actuated. The consequential cosine error that happens is given by Equation 5.2.

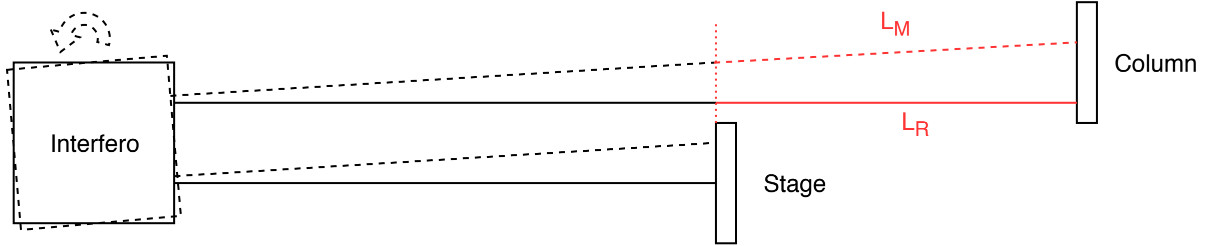

Figure 5.16: Sensitivity in pitch direction: cosine error

$$\epsilon = L_M - L_R = \frac{L_R}{cos(\alpha)} - L_R \tag{5.2}$$

The pitch and yaw errors are caused by pitch/yaw movements of the interferometer mount or pitch/yaw of the plate at which it is attached. For now the mount will be assumed to be rigidly connected to the plate and only pitching/yawing of the vacuum cover and/or the top plate of the suspension will be investigated. At first glance, the vacuum cover seems to be a good candidate to mount the interferometer to, as this is a very thick and stiff plate. If one would mount the interferometer to the vacuum chamber, the important criteria to consider is how much this plate will bent and/or rotate as this will lead to errors. To investigate this, a first order approximation will be made of the deformation of the vacuum cover plate.

Approximation

The vacuum cover is a thick plate with a hole in it. For now the assumption will be made that it is clamped on all the outer edges. It will be modelled as a very wide beam. A beam has a higher stiffness in yaw direction than in pitch direction, so only the pitch or bending of a plate will be considered for now and it will be assumed that pitch$\gg$yaw. For a first approximation the cover will be modelled as a beam that has a length that is equal to the distance from the edge of the cover to the edge of the hole and a width that is equal to the circumference of the hole. So essentially the plate with the hole has been 'rolled out' to one wide beam. This can be seen in Figure 5.17. There are three loads on the beam: the weight of the column acting as a force P on the end of the beam, the pressure of the air and the weight of the vacuum cover acting as a distributed force w over the entire beam and a moment M acting on the end of the beam caused by a rotation of the column. The beam and all the loads can be seen in Figure 5.18a. And the displacement Δx of the column that gives rise to the moment on the beam is illustrated in Figure 5.18b. The deformation caused by the loads will be worse in this scenario than it will be in reality, as in reality the column is attached to the middle of a plate that is clamped on the sides. This is a stiffer geometry than a single clamped beam and therefore the overall deformation of the plate will be less. The radius of the hole in the plate is equal to $R_{coll} = 200$ mm. With the deflection formulae described by Equation 5.3, 5.4 and 5.5 for a beam that is clamped on one side, the deflection angles due to the different loads can be calculated.

$$\theta_P = \frac{P\ell^2}{2EI} = \frac{6P\ell^2}{Ebt^3} = \frac{6 \cdot P \cdot 0.22^2}{150e9 \cdot 0.2 \cdot 2\pi \cdot 0.05^3} = 12.3P \text{ nrad} \tag{5.3}$$

$$\theta_w = \frac{w\ell^3}{6EI} = \frac{2w\ell^3}{Ebt^3} = \frac{2 \cdot w \cdot 0.22^3}{150e9 \cdot 0.2 \cdot 2\pi \cdot 0.05^3} = 0.9w \text{ nrad} \tag{5.4}$$

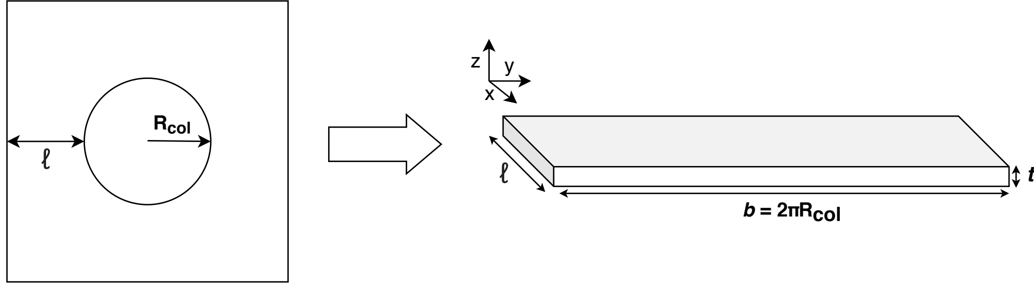

Figure 5.17: Approximation of a plate-with-hole that is clamped on all outer edges as a beam that is clamped on one side with a width b that is equal to the perimeter of the hole

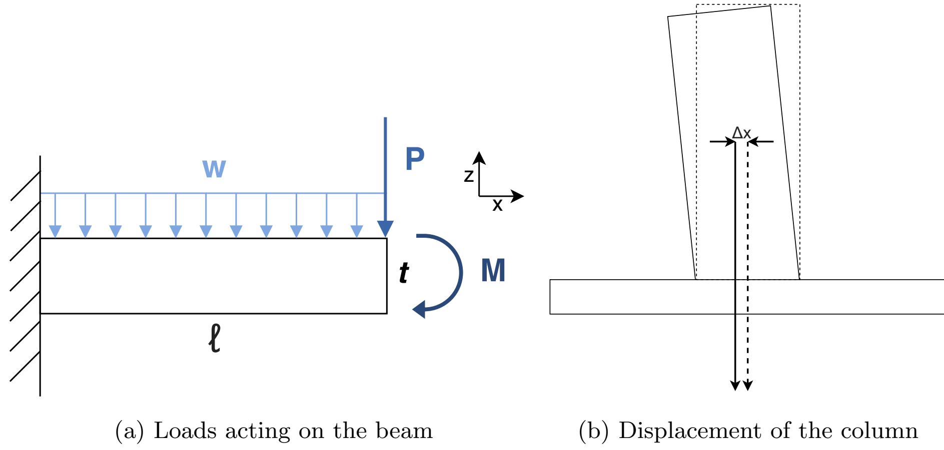

(a) Loads acting on the beam (b) Displacement of the column

Figure 5.18: Loads on the beam with the moment $M = P \cdot \Delta x$

$$\theta_M = \frac{M\ell}{EI} = \frac{12M\ell}{Ebt^3} = \frac{12 \cdot P \cdot \Delta x \cdot 0.22}{150e9 \cdot 0.2 \cdot 2\pi \cdot 0.05^3} = 112P \cdot \Delta x \text{ nrad} \tag{5.5}$$

With load P in N, w in N/m and Δx in m. The error in optical path length ϵ due to the cosine error was described by Equation 5.2, to repeat:

$$\epsilon = L_M - L_R = \frac{L_R}{cos(\alpha)} - L_R$$

The maximum length of $L_R = 160$ mm. This half the actuation range of the stage (110 mm) plus the distance between the mirror of the stage and the mirror on the column if the stage is positioned at the middle of the optical column (50 mm). One should mostly look at variations in these loads, as the static loads will not influence the beam stability. But just to see what the approximately static deformations will be, P will be taken as the weight of the column and w for the static air pressure. If $P = 2500$ N then $\theta_P \approx 31$ μrad and this leads to an optical path length error of $\epsilon \approx 0.08$ nm. So even when the force on the vacuum cover is twice that of the weight of the optical column the change in optical path length is still only 0.16 nm. $w = 10^5 \cdot 2\pi \cdot 0.2$, this is the atmospheric pressure times the circumference of the hole (the width of the beam). This will give $\theta_w \approx 113$ μrad and this leads to an optical path length error of $\epsilon \approx 1$ nm. Normal variations in air pressure are maximum about 0.1 bar. This will lead to an optical path length error of $\epsilon \approx 0.1$ nm. The weight of the vacuum cover is equal to 250 kg. This means there is an distributed load $w \approx 2000/0.22 = 9090$. This will lead to $\theta_w \approx 8$ μrad and this gives an ΔOPL of $\epsilon \approx 5$ pm. If $\Delta x = 5$ μm and $P = 2500$ N then $\theta_M \approx 1.4$ nrad and this leads to a negligible small optical path length error. Adding all the optical path length errors of the static case this will give the following total error given in Table 5.2. If the loads vary with a little less than 50% the optical path length error is still ≤ 0.5 nm.

Table 5.2: Total optical path length error due to static loads

Static load	ϵ	
Load column 250 kg	0.08	nm
Load vacuum cover 200 kg	0.005	nm
Air presure 1 bar	1	nm
Rotation column 5 μm	0	nm
Total	**$\sim$ 1.1**	**nm**

Looking at the vacuum chamber as a box, it can be noticed that the sides of the vacuum chamber are a lot thinner than the cover. The most deformation will probably take place in the sides of the vacuum chamber. If one looks at what kind of deformations are most likely, it will probably be the sides that bend a bit and this will lead to a vertical up and down movement of the vacuum cover with column. With the vertical movement the vacuum cover will move closer and further to the bottom of the vacuum chamber. This movement will probably not be very relevant in creating optical path length errors.

Based on the static deformation of the approximation of the vacuum cover, it seems possible to attach the interferometers to this plate keeping the potential ΔOPL errors $\leq$ 0.5 nm. In the next sections a finite element model using *Comsol* has been made to further investigate the deformation of both the vacuum cover and the top plate of the stage suspension.

Finite element model of the vacuum setup

To approximate the vacuum setup in a more thorough way a FEM model is made. A 3D model of the vacuum setup including the vacuum chamber, the stage suspension and the optical column has been made. All parts have appropriate dimensions, materials and weights comparable with the actual setup. The optical column is simplified the most of all the components in the model. The column has a even distribution of weight and stiffness, which in practice is not the case. For now this model will do. Only static loads have been applied to the vacuum setup to speed up the evaluation process. This of course implies that the system should not be actuated around the eigenfrequency of the setup, as this could potentially lead to much higher deformations. The model was fixed on the bottom surfaces of the little supports underneath the vacuum chamber. First the static loads of the pressure difference in vacuum was applied to all the outside surfaces and gravity was applied to all parts. After this the geometry of the model was rebuild to be the deformed mesh. Then a number of loads were applied to the system.

- A pressure variation of 4000 Pa was applied to all outside surfaces
- The weight of the stage was loaded on the bottom plate of the stage suspension, evenly distributed.
- A force of 100 N was applied to the positive x-direction on the bottom plate of the suspension, evenly distributed over the plate. The 100 N represents a constant acceleration of the stage of 2.5 m/s^2.
- A force of 200 N in z-direction was applied to the bottom plate of the vacuum chamber on the surface of a ring on which the turbo pump normally is attached to mimic the weight of the pump.
- A displacement of 10μm of the top surface of the optical column in the negative x-direction was given.

A picture of the resulting deformation is given in Figure 5.19. The resulting displacement of all the loads applied can be seen in Figure 5.19a. Due to the large deformation of the top of the column, most of the displacement in the other parts of the system is hard to see. Therefore a picture of the deformation that results from all the loads éxcept the top column displacement load is shown in Figure 5.19b. The deformation in the 'pitch' angle, meaning the angle that would lead to a pitch error of the interferometer as described earlier, was for the vacuum cover equal to $\sim$ 10μrad. This leads to an optical path length error of 8 pm. However the deformation angle of the top plate of the suspension was a lot better with the angle being $\sim$ 1μrad, giving a ΔOPL of 0.8 pm. This is under the assumption that the alignment on the mirrors is perfect. It also does not account for dynamic behaviour of the system which could potentially lead to higher deformations. Noticeably from the simulations was that the stage suspension seems

to be moving relatively parallel with the optical column. In the assembly the four struts connecting the top plate of the suspension and the vacuum cover are not simulated. This probably restricts the parallel movement between the column and stage suspension. Out of the two plates, the top plate of the suspension seem to be the most suitable place to mount the interferometers to.

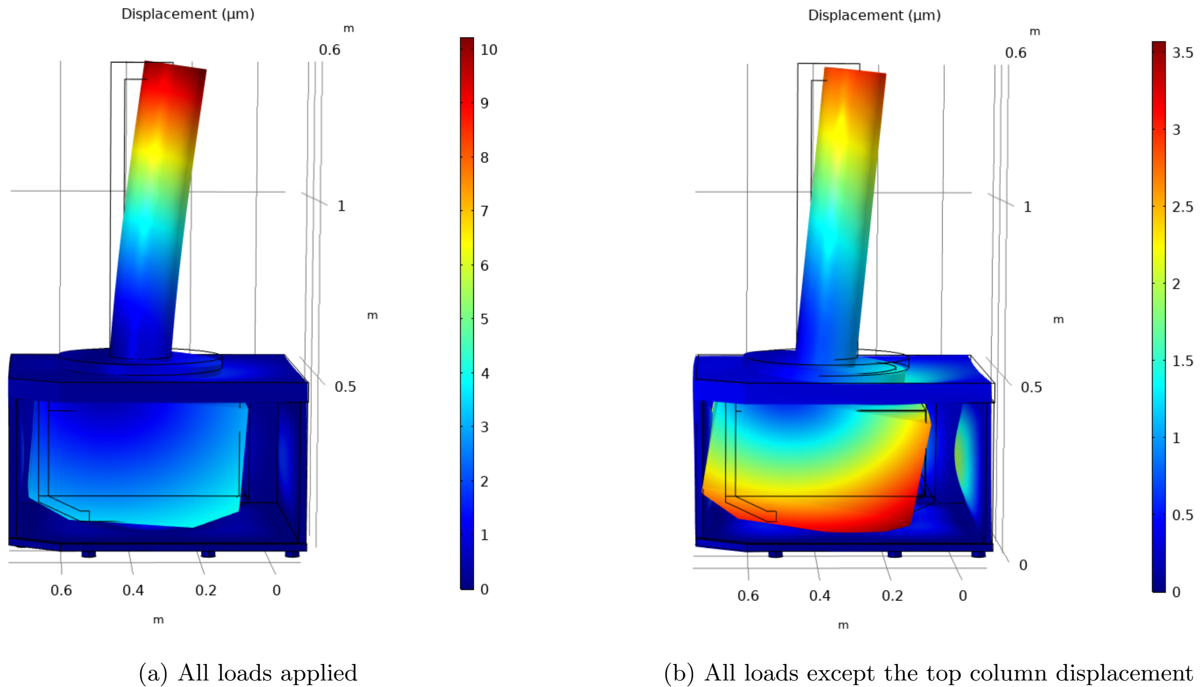

(a) All loads applied

(b) All loads except the top column displacement

Figure 5.19: Displacement of the vacuum setup

Conclusion

Based on the static load cases and leaving the stiffness and eigenfrequency of the interferometer mount itself out of consideration (so assuming a rigid connection between the interferometer and the plate it is mounted to) and assuming the system is not operated around the eigenfrequency of the vacuum setup, the following conclusions are drawn.

- There is an order of magnitude difference between the deformation of the vacuum cover: $\sim 10\mu$rad, and the deformation of the top plate of the stage suspension: $\sim 1\mu$rad.
- It seems like the whole stage suspension moves particularly parallel to the optical column, which has the positive effect of reducing measurement errors. However this will be partly impaired by the four strut connections.
- The top plate of the stage suspension seems to be the most suitable place to attach the interferometers to.
- No separate metrology frame is necessary and therefore concept 1.1 will suffice and will be the chosen concept.

Chapter 6

Detailed concept

With the general concept chosen, the detailed concept phase will start. The goal of this phase is to further elaborate the chosen concept and solve all concept issues present. Section 6.1 discusses the general design overview of the concept. After this, Section 6.2 elaborates the general optical design. Section 6.3 discusses the mounting and the alignment of all the different optical components, so the opto-mechanical design. Finally in Section 6.4 different design issues are stated and solutions are presented to these issues.

6.1 Design overview

As discussed in Chapter 5 the chosen concept is a metrology system in which a differential measurement is made between a reflector on the stage and a reflector on the electron optical column. It uses two differential x- and y-interferometers. This metrology concept comprises the following basic elements:

- 2 differential interferometers: x- and y-interferometer
- 2 reflectors on the stage
- 2 reflectors on the optical column
- 1 laser
- 3 beam benders: BB_L, BBx and BBy
- 2 beam splitters: BS1 and BS2
- brackets/optical mounts

Figure 6.1 shows an overview of the possible setup with the optical components. To obey the abbe principle the interferometers should be directly in line with the x- and y-axis as defined by the stage. The axes intersect in the middle of the optical centre of the electron optical column. Looking from the side, the laser beams on the mirrors on the stage should be in line with the writing height on the substrate.

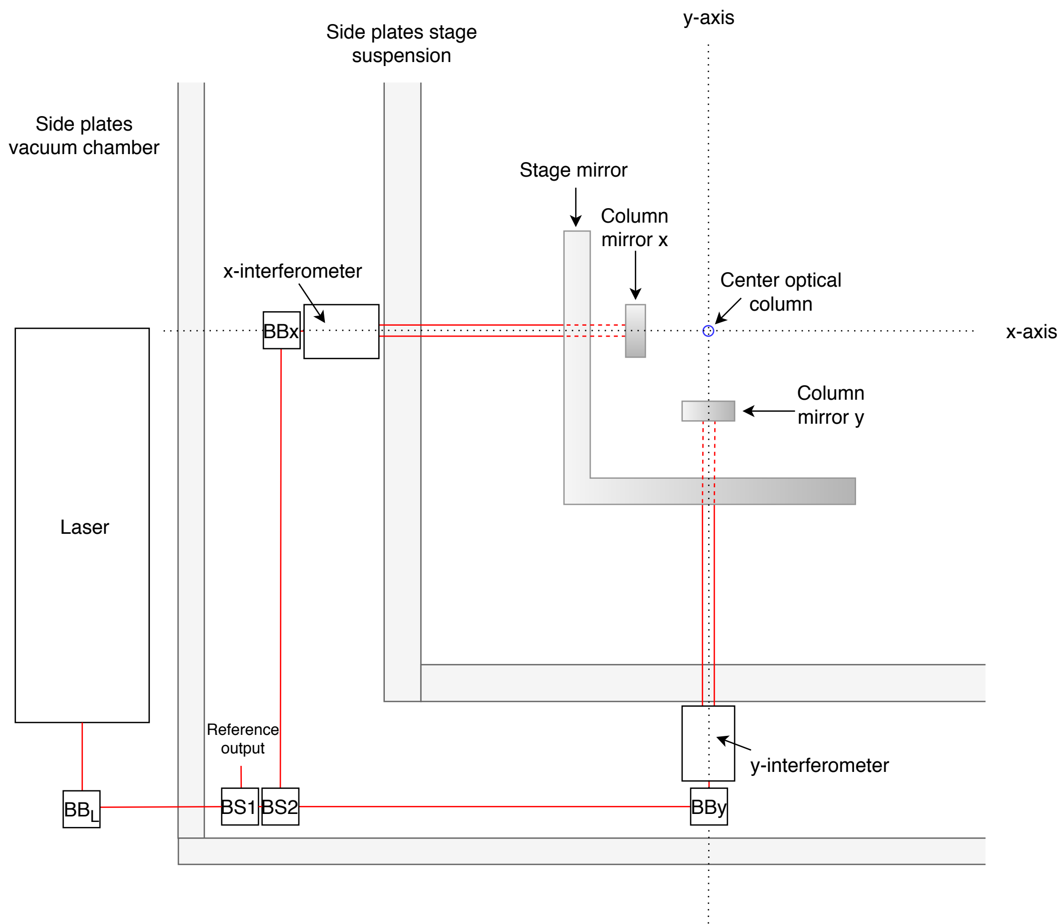

Figure 6.1: Overview concept

6.2 Optical design

6.2.1 Interferometer

The interferometers needed for the differential measurement could be either:

- Off-the-shelf
- Own design

An OTS (Off-The-Shelf) differential interferometers will probably be sufficient, there is no real direct benefit for making an own differential interferometer. It could be the case however that some customisation is needed, as the interferometer should be vacuum appropriate which not all OTS interferometers are. What is important in the interferometer design is that it is as 'monolitic' as possible. This means that all the optical components inside the interferometer such as the polarising beam splitter, cube corner and quarter wave plates should be glued or mounted together such that one big block is formed. This minimizes deformation between the different components and therefore minimizes the errors in optical path length. Another important design factor is that the common-path of the two arms of the interferometer should be as equal as possible. So each path should preferably travel the exact same distance through the same medium, in this case the exact same distance through the glass used by the optical components. An example of a great differential interferometer design is given in Figure 6.2. The principle in Figure 6.2 is based on the heterodyne type. As discussed before, this type of measurement is superior to homodyne based

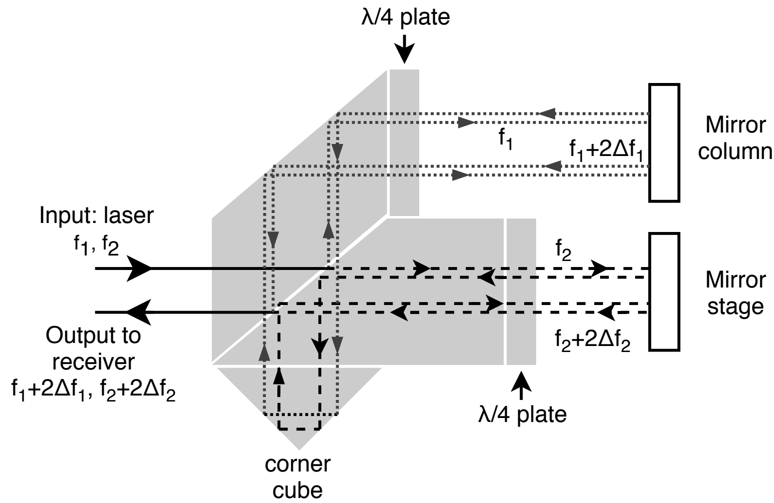

Figure 6.2: Differential interferometer design (based on the Keysight 10719A)

measurements for high precision applications. The interferometer is also doublepass, as in the current system, to increase the optical resolution. Figure 6.2 shows an 'optical differential' interferometer. This means the output signal is a direct interference between the two different measurement arms. Another option is the use of a 'digital differential' interferometer. This means both the displacement of the column mirror arm as well as the stage mirror arm are measured separately and these two measurements are subtracted from each other to find the differential displacement. This can be done be using a regular doublepass heterodyne interferometer as described in Chapter 1.3.5, but before the laser beam enters the interferometer a beam divider divides the laser beam into two separate parallel beams from which one will be directed to the stage mirror and one on the column mirror. This will give two separate displacement measurements. The optical differential method is the simpler type out of the two, as only one signal has to be read out and processed. However, the digital differential method contains more information. Both the displacement of the column mirror as well as the displacement of the stage mirror are measured with this method. If this extra information is not needed, then the preferred measurement type is the optical differential method. Another thing to consider with the interferometer design is that a yaw measurement should be made. The way this can be done is by using a two-axes (two-axes in the sense of one axis for yaw measurement and one axis

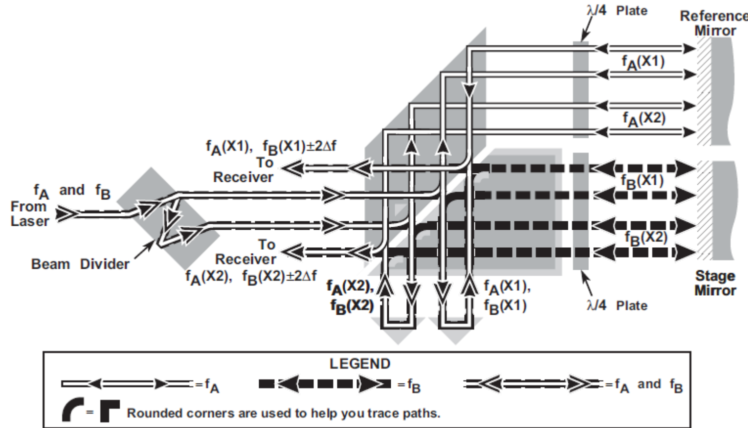

Figure 6.3: Keysight 10721A two-axes differential interferometer

for displacement) differential interferometer, as depicted in Figure 6.3. This interferometer should be used on only one axis, as yaw measurement on either the x- or y-axis is sufficient to determine the differential yaw between the stage and optical column. This means on one of the axes (x- or y-axis) a regular differential interferometer will be used and on the other a two-axes differential interferometer will be used.

6.2.2 Reflectors

The reflectors used for the two arms of the differential interferometer could be:

- Mirrors
- Retro-reflectors

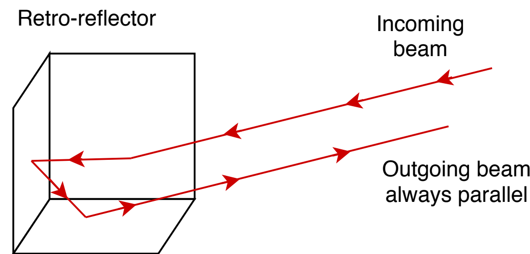

Figure 6.4: Retro-reflector: 3 reflecting surfaces at 90 degrees to each other

Retro-reflectors are in theory insensitive to any rotation of the reflector itself, as illustrated in Figure 6.4. When the retro-reflector moves perpendicular to the optical axis, the width between the two beams will become larger or smaller (but the OPL will stay the same). If translation is too large this can lead to signal degradation because the two outgoing beams of the interferometer will not perfectly overlap. The only movement that will lead to a ΔOPL is in-optical-axis movement. This means the retro reflectors should only move parallel to the measurement axis, not perpendicular. For this reason retro-reflectors are not suitable to use on the stage, because of the long actuation range perpendicular to the measurement axis. For the reflectors on the column it is possible to use retro-reflectors. However, the retro-reflectors are not really suitable to use with heterodyne interferometers because they do not change the circular polarization direction when the light is reflected twice from the reflective surfaces in the retro-reflector. They are also not suitable to use with a differential yaw interferometer. For these reasons the reflectors used for both the stage and optical column will be plane mirrors.

6.2.3 Other optical components

Laser

The laser used in the new system should be heterodyne, as this is used by the interferometers. This means the laser wavelength will still be 633 nm, because a HeNe laser and the Zeeman effect are used to create the heterodyne light. The laser beam diameter will be reduced from 6 mm to 3 mm, for multiple reasons. The first reason is because the space is limited between the optical column and the stage, so a smaller beam size is more suitable. The other reason is that the differential interferometers from keysight (that will probably be used) are only suitable for a beam size of 3 mm.

Beamsplitters and beam benders

The laser is mounted to the side op the vacuum chamber, for this reason a beam bender is necessary to bend the light before the light enters the vacuum chamber. A beam bender is another word for mirror. Two other beam benders are necessary to bend the light at the interferometer entrance. A beam dump will probably be not necessary in the new system, with the smaller laser beam size. Further more, two beamsplitters are needed in the vacuum

chamber: one for the reference output and one to split the beam for the two measurement axis. The beamsplitter for the reference signal needs to be a 15/85% beamsplitter and the other one needs to be a 50/50% beamsplitter. These optical components should be chosen in collaboration with the supplier.

6.3 Opto-mechanical design

6.3.1 Interferometer mounting

It was stated in Chapter 5.5 that the top plate of the stage suspension is the best place to mount the interferometers (and other optical components that are used inside the vacuum chamber). Mounting the optical components to the top plate of the suspension could be done in the following ways:

- Attach all the optical components with separate mounts (this is also the way it is done currently)
- Extend the top plate to two sides and attach the 2 interferometers, 2 beam benders and 2 beam splitters to this extension

From these two options extending the top plate of the suspension to two sides is the best solution. Of the two this is the most simple solution as there is no need for multiple different mounts with different attachments. It also ensures a stiff connections, not only per component, but also between the different components as they are all connected to each other via a stiff and flat surface. This gives the added benefit that the alignment between the different components could be very good, which can potentially decrease the amount of alignment procedures. The way the optical components will be mounted is displayed in Figure 6.5.

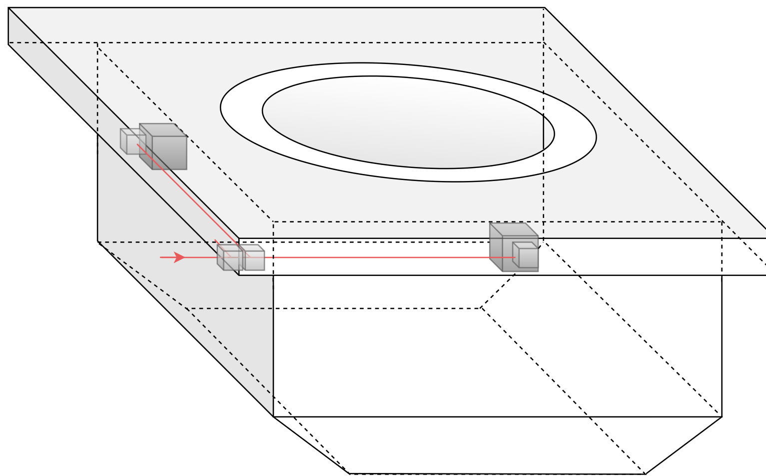

Figure 6.5: Interfero mount

6.3.2 Mirror mounting

Two mirrors are needed for the differential interferometer, one on the stage and one the optical column. The mounting of the stage mirrors will be kept the same as it is done in the current system, as this is already sufficient. This means the focus will be on designing the mirror mount for the electron optical column.

Mounting the column mirrors is an important part of the design, as this is the biggest change that is introduced, mechanically speaking, in the new system. It is also a sub-system that can potentially increase or decrease the performance of the system by a fair amount. Especially on the long term beam stability it has the power to decrease the errors in the current system by a significant amount, when designed correctly. The mirror mount could be either attached to the final lens or the height meter ring, see Figure 6.6. An important aspect of designing the mirror mount is the large thermal expansion of the optical column that needs to be accounted for. The further from the

optical center the larger the thermal expansion. This means that the mirrors should be either attached sufficiently close to the center of the column, or the thermal expansion should be compensated for in some form.

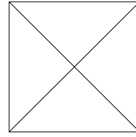

Figure 6.6: Height meter ring and final lens assembly

The first option that will be considered is mounting the mirrors close to the column center. This means that mirrors should be mounted to the final lens. The temperature variation of the final Lens is maximum ~ 0.02 K over 1 hour. The final lens is made of a μ-metal which has a CTE of $8.85E^{-6}$ K^{-1}. The closest the mirrors could reasonably be mounted is about 30 mm away from the optical center. This is shown in Figure 6.7. With this distance from the optical center an error in optical path length in one hour due to the thermal expansion of the column is equal to:

$$8.85E^{-6} \cdot 0.02 \cdot 30E^{-3} = 5.3 \text{ nm} \tag{6.1}$$

This could be an acceptable amount of expansion. There are a few problems with mounting the mirrors on the final lens. First of all it is inconvenient to mount the mirrors at that location due to the limited space. This is caused by the fact that the tubes that collect the back scattered electrons (the scintillators) are in the way. It is also undesirable to drill any holes in the final lens and have a-symmetrical structures so close to the optical center, as this could lead to interference with the electron beam. For these reasons it is preferred to mount the mirrors further away from the optical center.

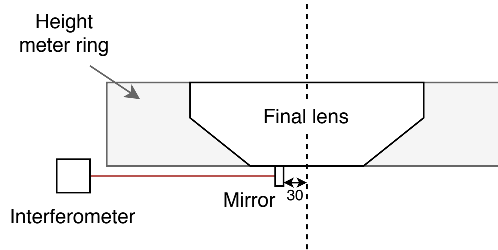

Figure 6.7: Mounting mirror directly to final lens

This means the mirror mount should be designed in such a way that the thermal expansion is compensated. A way this can be done is by making the mount from a material that has a low CTE and at the same time make sure the thermal center co-insides with the optical axis. Of course this concept only works if the expansion of the height meter ring (at which the mount will be attached) is homogeneous. The height meter ring is made of aluminum and since this has a high thermal diffusivity, this is a fair assumption to make. Figures 6.8a, 6.8b and 6.9 show three different concepts that are based on this design strategy.

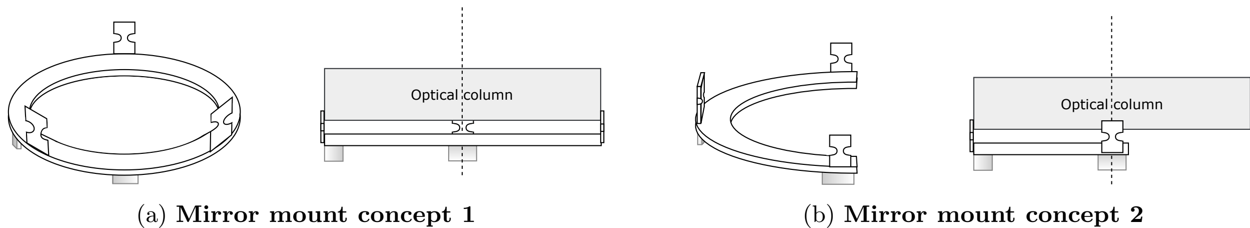

(a) **Mirror mount concept 1** (b) **Mirror mount concept 2**

Figure 6.8: Mounting the mirrors to the optical column with three notched leaf springs in two different ways. The thermal centre coincides with the optical axis

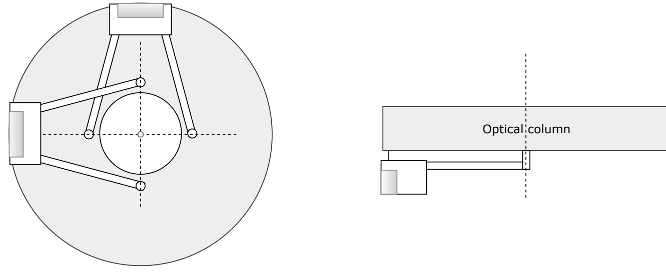

Figure 6.9: **Mirror mount concept 3:** looking from below to the optical column, two stiff rods reference the the mirrors to the centre of the optical column. Looking from the side a wire flexure connects the mount to the column.

Concept 1 and 2 are preferred over concept 3, as concept 3 involves producing more complex parts and a more complex assembly/alignment procedure. Also, concept 1 and 2 are suitable for integrating the two mirrors directly in the ring/half ring. Table 6.1 compares the remaining mirror mount concepts: concept 1 vs. concept 2. Both

Table 6.1: Comparison between Mirror mount concepts 1 and 2

	Concept 1	**Concept 2**
Design symmetry	Yes	No
Stiffness symmetry	Yes	Possibly, with use of different flexures
Manufacturability	++	+
Flexure in line with mirrors	No	Yes
Material needed	0	+

concepts are suitable candidates that could work. The deciding factor that leads to choosing mirror mount concept 1 over concept 2 is that this design is axially symmetric. As the mirror mount is still fairly close to the electron beam, a symmetric design is always preferred over a non-symmetric design to decrease any possible interference with the electron beam. This means the chosen mirror mount (concept 1) consists of a low-CTE ring that is attached to the optical column with three flexures that are attached at 120 degrees apart from each other.

6.3.3 Alignment

Alignment is an important aspect in designing an opto-mechanical system. The goal of this section is to find out for which parts alignment is necessary and in what degrees of freedom. First of all it will be investigated if alignment of the mirrors on the optical column is necessary. If this is not necessary it would simplify the design of the column mirror mount. If the assumption is made that the interferometers are aligned on the mirrors on the stage, then the limiting factor that determines if additional alignment of the column mirrors is necessary is how accurate the stage and column mirrors can be aligned to each other on manufacturing tolerances. The two degrees of freedom that matter are the yaw and pitch angles, as this will lead to a cosine error (as described earlier). The maximum yaw angle between the two mirror sets on the stage and column is indicated as the angle α_{cs} in Figure 6.10a. The maximum pitch angle between the two mirror sets is shown in Figure 6.10b as β_{cs}. The maximum allowable angle between the two mirrors (α_{cs} and β_{cs}) is mainly determined by two requirements.

1. The maximum angle between the in/out going laser beam and the interferometers is 15 arc minutes[10] $\approx$ 4 mrad. This means the maximum angle between the two mirror sets (α_{cs} and β_{cs}) is 2 mrad.
2. The worse the initial alignment between the mirrors, the more sensitive the system becomes to additional angle deviations of the optical components.

The first requirement is straight forward, this is the maximum angle that the laser beam can make with the interferometer in order for the interferometer to function properly. The second requirement will be elaborated further.

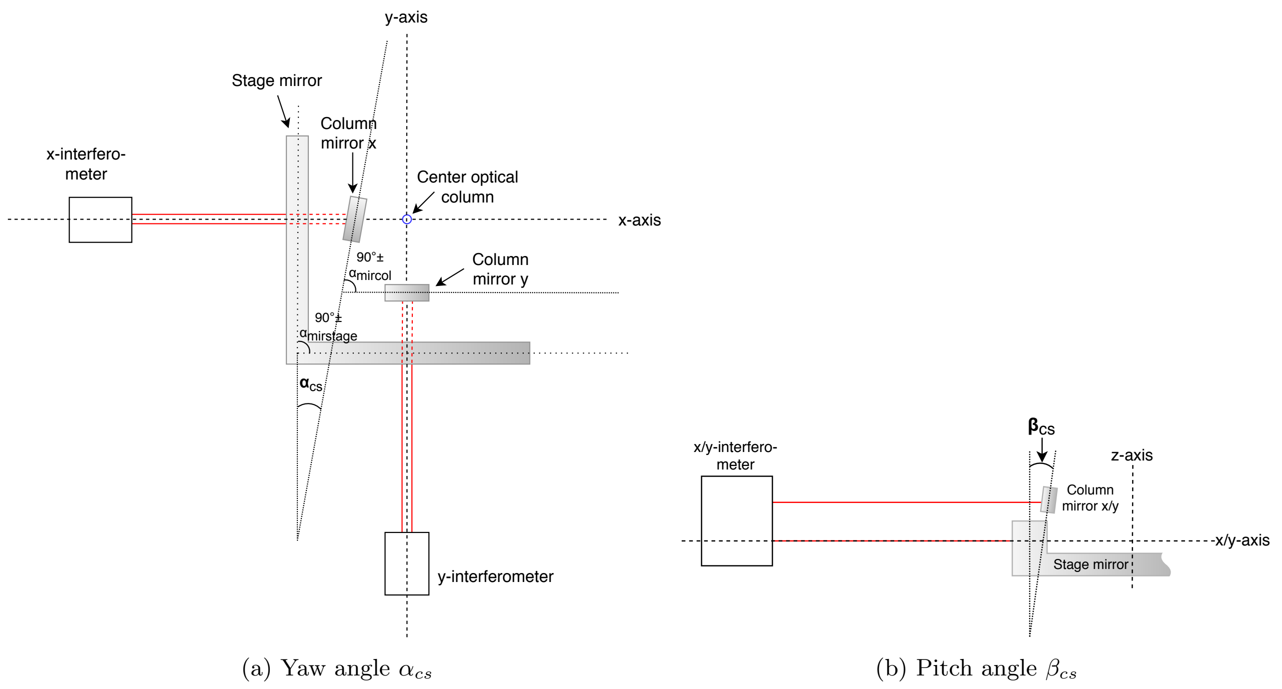

(a) Yaw angle α_{cs}

(b) Pitch angle β_{cs}

Figure 6.10: Angles α_{cs} and β_{cs} between the mirror set on the stage and mirror set on the column

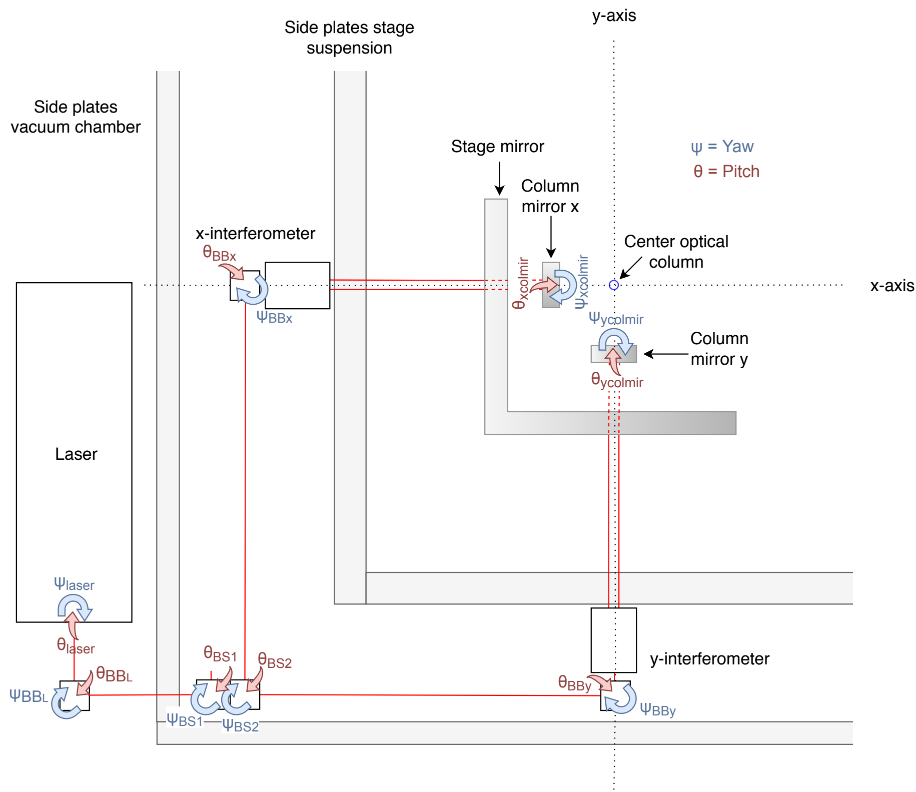

Figure 6.11: Yaw and pitch movements

With any additional angle deviation in the yaw and pitch DOF's of each optical component, the laser beam angle between the interferometer and the mirrors changes. This will give a 'dynamic' cosine error (the cosine error was described in Chapter 5.6.2). The sensitivity to these angle variations, increases the higher the initial alignment angle is between the interferometer and mirrors. The fact that the dynamic cosine errors should be kept limited, sets a requirement for what the maximum alignment angle can be. Figure 6.11 shows an overview with all the possible dynamic yaw and pitch movements of the different optical components. The relation between the error in optical path length ϵ, the dynamic yaw angle Ψ and the alignment yaw angle α_{cs} is given by Equation 6.2.

$$\begin{aligned}\epsilon &= \left(\frac{x}{cos(2\alpha_{cs}+2\Psi)}-x\right)-\left(\frac{x}{cos(2\alpha_{cs})}-x\right)\\ \epsilon &= \frac{x}{cos(2\alpha_{cs}+2\Psi)}-\frac{x}{cos(2\alpha_{cs})}\end{aligned} \tag{6.2}$$

Where x is the difference in distance from the interferometer to the mirror on the stage and on the optical column. The sensitivity of the error with a changing dynamic yaw angle can be determined by the partial derivative of Equation 6.2 with respect to the dynamic yaw angle Ψ. This is described by Equation 6.3.

$$\frac{\partial\epsilon}{\partial\Psi}=\frac{x\cdot tan(2\alpha_{cs}+2\Psi)}{cos(2\alpha_{cs}+2\Psi)} \tag{6.3}$$

The maximum distance x is half the actuation range of the stage, 110 mm, plus a distance of 50 mm when the stage is in the middle position. So this gives a maximum distance of $x = 160$ mm. If Equation 6.3 is evaluated around $\Psi = 1E^{-6}$ the graph in Figure 6.12 can be drawn. Equation 6.2 and 6.3 and Figure 6.12 are exactly the same for the dynamic pitch, in that case α_{cs} is replaced by β_{cs} and Ψ is replaced by θ. An estimate of all the dynamic

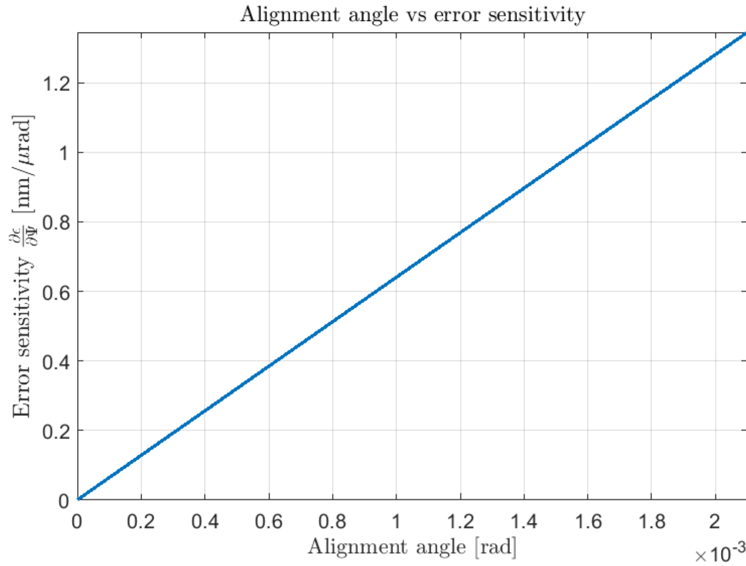

Figure 6.12: Yaw and pitch movements sensitivity vs alignment angle

yaw and pitch angles can be found in Table 6.2. The dynamic pitch angle of the entire top plate of the suspension θ_{sustp} is based on the evaluation of the comsol model discussed earlier. The dynamic yaw angle of the top plate of the suspension Ψ_{sustp} is estimated to be a factor $\frac{1}{10}$ of this (as a shear motion of the plate is less dominant than a bending motion). If the optical components are assumed to be rigidly connected to the top plate the individual dynamic yaw and pitch angles will be a small fraction of the entire top plate deformation. The laser and BB_L are attached to a separate rigid mount outside the vacuum, this will have an estimated yaw and pitch angle of a factor

$\frac{1}{10}$ of that of θ_{sustp}. As can be seen the estimated total dynamic pitch angle $\theta = 1.03\mu$rad and the dynamic yaw angle $\Psi = 0.18\mu$rad.

Table 6.2: Dynamic yaw and pitch movements

Dynamic pitch			Dynamic yaw		
θ_{sustp}	1	μrad	Ψ_{sustp}	0.1	μrad
θ_{laser}	0.05	μrad	Ψ_{laser}	0.05	μrad
θ_{BB_L}	0.1	μrad	Ψ_{BB_L}	0.1	μrad
θ_{BS1}	0.01	μrad	Ψ_{BS1}	0.01	μrad
θ_{BS2}	0.01	μrad	Ψ_{BS2}	0.01	μrad
$\theta_{BBx/y}$	0.01	μrad	$\Psi_{BBx/y}$	0.01	μrad
$\theta_{x/yColmir}$	0.1	μrad	$\Psi_{x/yColmir}$	0.1	μrad
Root square sum θ	**1.03**	**μrad**	**Root square sum Ψ**	**0.18**	**μrad**

To determine if alignment between the column mirror vs. stage mirror is necessary in pitch and/or yaw, a tolerance budget for both β_{cs} and α_{cs} has been made. The pitch tolerance budget for β_{cs} is given in Table 6.3. This will give an alignment angle in pitch between the mirror on the stage and column of 0.2 mrad. If Figure 6.12 is used it can be seen that this will give a sensitivity $\frac{\partial \epsilon}{\partial \theta} \approx 0.13$ nm/μrad. With a dynamic pitch error of 1μrad this will give an error in optical path length of 0.13 nm. This is an acceptable error (the error budget will be discussed in Chapter 8) and therefore no additional pitch alignment of the mirrors on the optical column is necessary. The

Table 6.3: Pitch tolerance for β_{cs}: pitch angle between the mirrors on the stage and on the optical column

Pitch tolerance for β_{cs}			
Parallelism superplate and column	0.01/200 mm	0.05	mrad
Orthogonality mirror stage	0.004/51 mm	0.08	mrad
Orthogonality mirror column	0.001/11 mm	0.1	mrad
Parallelism mount and optical column	0.03/300 mm	0.1	mrad
Parallelism mirror and mount	0.03/300 mm	0.1	mrad
RSS total		**0.20**	**mrad**

same procedure can be done for the yaw alignment between the two mirror sets (α_{cs}). This is shown in Table 6.4. The alignment between the rotation of the stage and the vacuum cover is done by using large pins that are fitted in holes in the stage and holes in an alignment piece that is attached to the column opening in the vacuum cover. These pins and holes show a lot of play which makes the alignment inaccurate $\sim$ 4.2 mrad. This is more than double the allowed angle deviation for the in/out going laser beam in the interferometer (the requirement was < 2 mrad). This means alignment between the two mirrors in yaw is necessary.

Table 6.4: Yaw tolerance for α_{cs}: yaw angle between the mirrors on the stage and on the optical column

Yaw tolerance for α_{cs}			
Alignment rotation stage and vacuum cover		4.2	mrad
Rotation column and vacuum cover		1	mrad
Rotation column mirror mount and column		1	mrad
Rotation mirror stage and stage		0.05	mrad
Orthogonality two mirrors stage	0.02/282 mm	0.7	mrad
Orthogonality two mirrors column	0.01/100 mm	0.1	mrad
RSS total		**4.43**	**mrad**

Besides the fact that no pitch alignment is necessary between the two mirror sets, it may also be unnecessary to align any other optical component in pitch. To see if pitch alignment of the interferometer/BB$_{x/y}$ is necessary

another tolerance table has been made, see Table 6.5. It is based on all the tolerances of the mechanical connections between the different parts. The total pitch error is 0.56 mrad, when Figure 6.12 and Table 6.2 are used again the error in optical path length will be ~ 0.32 nm. This is still an acceptable error, hence no additional alignment in pitch between the optical components is necessary.

Table 6.5: Tolerance for pitch angle between the interferometer and mirrors

Total pitch tolerance			
Pitch tolerance β_{cs} between mirror stage and mirror column		0.2	mrad
Flatness top surface height meter ring	0.01/220 mm	0.05	mrad
Flatness CSR surface (connection height meter ring)	0.01/220 mm	0.05	mrad
Parallelism CSR between connection HMR and vac. cover	0.08/440 mm	0.18	mrad
Flatness CSR surface (connection vac. cover)	0.04/440 mm	0.09	mrad
Flatness vacuum cover surface (connection CSR)	0.02/200 mm	0.1	mrad
Parallelism top and bottom surface vac. cover	0.02/200 mm	0.1	mrad
Flatness vac. cover surface (connection suspension top plate)	0.02/200 mm	0.1	mrad
Flatness suspension top plate surface (connection vac. cover)	0.02/400 mm	0.05	mrad
Parallelism suspension top plate top and bottom surface	0.02/400 mm	0.05	mrad
Flatness suspension top plate bottom surface	0.2/400 mm	0.04	mrad
Beam deviation tolerance BBx/y		0.02	mrad
Beam deviation tolerance BS1		0.02	mrad
Beam deviation tolerance BS2		0.02	mrad
Hole position tolerance in vac. cover for laser bracket bolts, distance between holes is 400 mm	0.05 mm	0.25	mrad
Hole position tolerance in laser bracket for laser bracket bolts, distance between holes is 400 mm	0.05 mm	0.25	mrad
Hole tolerances in side vac. cover 6H7	0.02 mm	0.1	mrad
Hole tolerances bracket laser 6H7	0.02 mm	0.1	mrad
Flatness bottom surface of laser bracket	0.04/400 mm	0.1	mrad
Flatness laser mount (connection laser bracket)	0.04/400 mm	0.1	mrad
Laser beam pointing static	$\pm 100\mu$rad/2	0.1	mrad
Laser beam pointing stability during startup	1 arc min./2	0.14	mrad
Beam deviation tolerance BB_L		0.02	mrad
RSS total		**0.56**	**mrad**

Alignment strategy
From the findings in the previous section it can be concluded that no additional pitch alignment between the optical components is necessary, but that alignment in the yaw direction is necessary. For the pitch 'alignment' all the components can be mounted based on the manufacturing tolerances. All the optical components on the top plate of the suspension and the laser bracket outside the vacuum will be mounted using dowel pins.

The yaw alignment strategy is the following. To align the two mirrors and the interferometer to each other, two of the three components should have an alignment mechanism. As the stage mirror is rigidly mounted to the stage and this is preferably kept that way, the other two components will have to be aligned with the stage mirror. This means both the column mirror and the interferometer need some alignment mechanism. If the two mirrors on the column are manufactured with the use of two orthogonal flat surfaces integrated in the mount, then (as can be seen from Table 6.4) the estimated orthogonality between the two mirrors is 0.1 mrad. This means that it is not necessary to align the individual column mirrors, but that the mirror mount as a whole can be aligned. The second component that needs to be aligned is the combination of $\mathrm{BB}_{x/y}$ and the interferometer. Either the beam bender ($\mathrm{BB}_{x/y}$) is integrated in the housing of the interferometer, or it is a separate component. Either way, the part that has to be used to align the laser beam is the beam bender. If the beam bender is a separate part the interferometer should move with it to ensure requirement 1 (discussed in the beginning of Section 6.3.3) is complied. All the other optical components (the laser, BB_L, BS_1 and BS_2) can be mounted in 'yaw' using the dowel pins, as the $\mathrm{BB}_{x/y}$ can

compensate for all the yaw misalignment between these components. To align the $BB_{x/y}$ and the mirrors column and stage, the following alignment strategy will be adhered to (visualised in Figure 6.13):

1. The BB_x and the BB_y will be aligned in yaw to the mirror on the stage.
2. The column mirror mount will be aligned as a whole in yaw to the BB_x and the BB_y simultaneously.

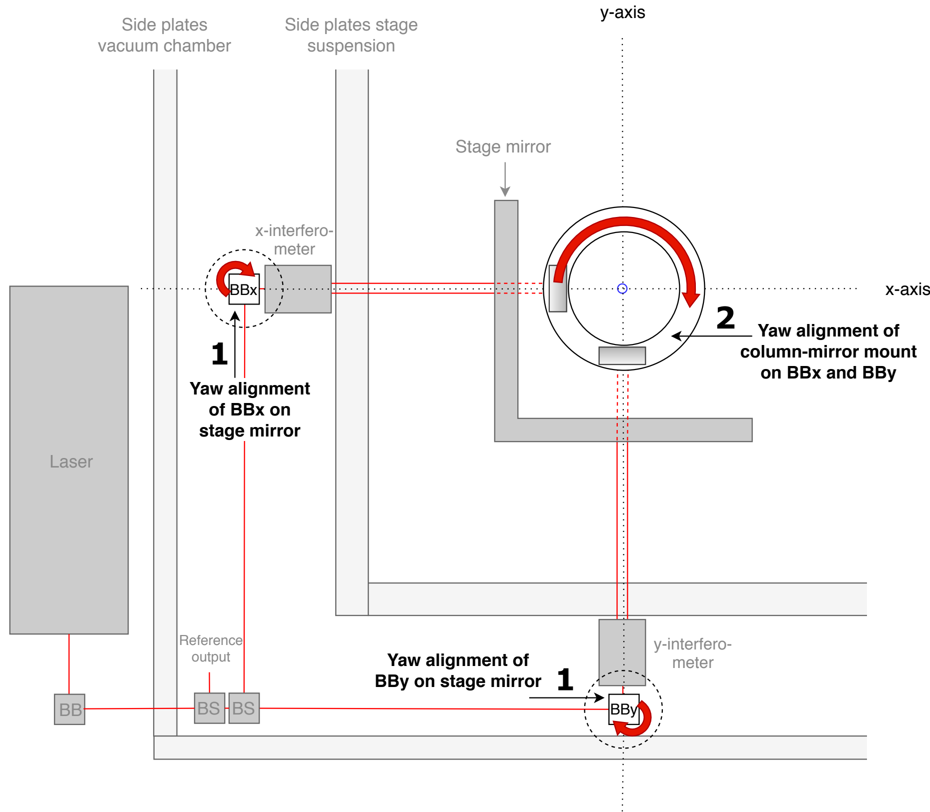

Figure 6.13: Alignment strategy

6.3.4 Laser mounting

The laser is currently mounted just outside the vacuum chamber on a bracket that is attached to the side of the vacuum cover plate. This houses the laser but also the first beam bender BB_L. In the current system both the laser and the BB_L can be aligned in pitch and yaw separately. Table 6.5 showed that no separate alignment of the optical components in pitch is necessary. The yaw alignment between the optical components is done by adjusting the BB_x and BB_y and the column mirror mount. This means that no separate alignment in either pitch or yaw is necessary for the laser and the BB_L and they can be mounted directly to the bracket. To achieve the right distance between the bracket and the BB_L in order to guide the laser beam properly, some rigid and flat connection should be designed between them.

6.4 Design issues and solutions

6.4.1 Height constraint

One of the 'problems' with the current concept that needs to be solved is the space that is needed between the stage and the bottom of the optical column. There is a height constraint between the stage and the height meter ring

that needs to be obeyed. Figure 6.14 shows the column/stage setup of the current system with the addition of the differential interferometer. Both the interferometers from Keysight that are considered (the Keysight 10719A and

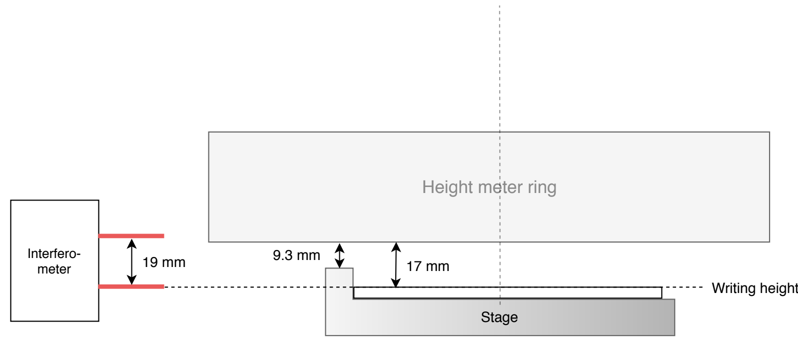

Figure 6.14: Current situation

10721A) have a distance between the two laser beams of 19.05 mm. The total space available between the stage and the height meter ring is equal to 17 mm. To obey the abbe-principle the laser beam that is pointed at the stage mirror should be in line with the writing height on the substrate. This means there is currently too little space underneath the height meter ring for the second laser beam to be pointed at the column mirror. A second problem is that the top of the stage mirror is currently 7.7 mm above the writing height, leaving only 9.3 mm of space for the column mirror and column mirror mount. To solve these spatial problems a few solutions have been thought of.

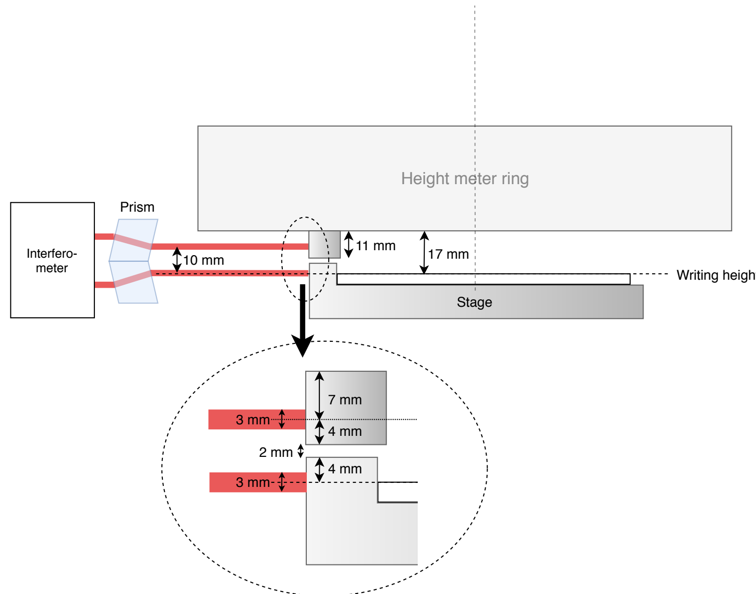

Figure 6.15: New situation

The new column/stage setup is shown in Figure 6.15. To address the problem that the distance between the two outgoing laser beams is too large (the 19 mm) a double prism is added, creating an offset on both laser beams and therefore reducing the distance between them to about 10 mm. These are mounted just after the two laser beams leave the interferometers. To solve the problem that there is only 9.3 mm left between the current stage mirror and the height meter ring, the following adjustments are made:

- The height of the mirror on the stage is reduced with 3.7 mm such that distance from the writing height to the top of the mirror is only 4 mm.

- The mirror mount on the optical column is mounted 'in' the height meter ring such that the mount itself does not take up any space underneath the height meter ring.
- The column mirror only takes up 11 mm underneath the height meter ring, leaving a 2 mm gap between the stage mirror and column mirror.

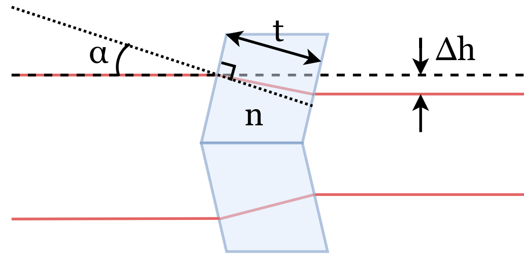

Figure 6.16: Prism

The dimensions for the double prism can be seen in Figure 6.16 and determined with the following approximation.

$$\Delta h \approx \alpha t \frac{n-1}{n} \tag{6.4}$$

With n the index of refraction, α the incident angle between the laser beam and the normal of the prism surface, t the thickness of the prism and Δh the translation of the laser beam. Assuming the prism is made of glass, $n \approx 1.5$. $\Delta h = \frac{19-10}{2} = 4.5$ mm and if $\alpha = \frac{1}{2}\pi$ then t should be around 8.6 mm. The added double prism is insensitive to movements in all degrees of freedom and if the index of refraction changes with temperature only a translation (a change in Δh) will be the result. This means the double prism does not add any additional errors in measurement of the optical path length.

6.4.2 Column swing

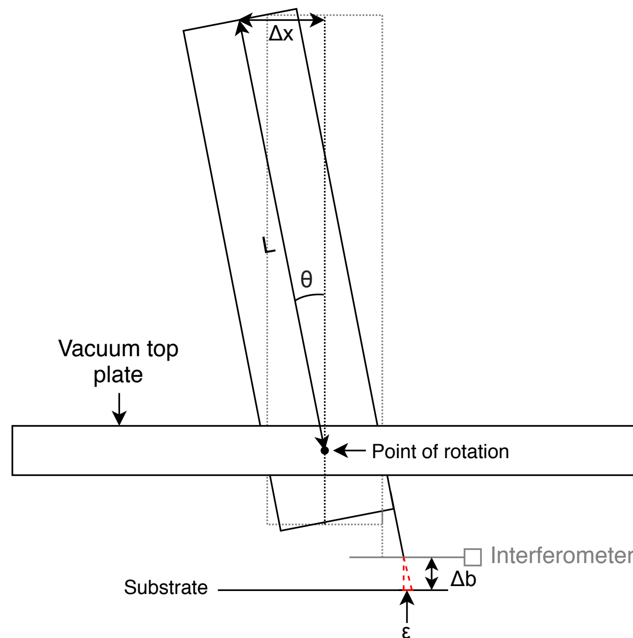

Figure 6.17: Error column swing

As discussed before the swing motion of the optical column can lead to large measurements errors directly after a stage step. As the relative displacement is measured in the new system this error is significantly reduced already, but unfortunately not enough to the extend that writing can start immediately. This is caused by the fact that the measurement on the optical column is done from a certain distance from the substrate. In Figure 6.17 this is visualised as Δb. When the column rotates around the point of rotation an error occurs in the beam position on the substrate. When the small angle approximation is used this error is equal to:

$$\epsilon = \Delta b \frac{\Delta x}{L} \tag{6.5}$$

If $\Delta x = 4$ μm, $L = 900$ mm and $\Delta b = 10$ mm then $\epsilon = 44$ nm. This is more than a factor 10 smaller than observed in Chapter 4.2, but still very high. This is therefore a design issue for which solutions should be found. To improve the error produced by the swing motion of the column a few solutions have been thought of. Two main routes can be taken, either prevent/reduce the swinging motion or compensate for the error it gives (or a combination of both).

The first way that has been explored to improve the column swing error is by increasing the stiffness of the optical column assembly. A simplified model of the vacuum cover plus the optical column has been made. In this model the mass distribution has been done in such a way that it is representative for the real situation, as in the actual system the top part of the optical column is particularly heavy. In the model the column has been divided into 7 parts that all have a different mass. The stiffness distribution is not a very accurate representation of the actual column assembly. In this model all the connections are rigid and the stiffness is the same for all the parts, which in reality is not the case. This means the eigenfrequencies found by using this model are going to be higher than the actual system. The goal of making this model is to compare different situations with each other, rather than looking at the specific numbers. Four different situations have been analysed. These include the current unsupported situation of the optical column and three different situations in which the column is supported. The eigenfrequencies of the current situation for the different mode shapes are given by Figure 6.18b. The first two mode shapes are the swinging motion of the optical column and one of the two is shown in Figure 6.18a. The first two eigenfrequencies are around 33 Hz, which is a factor 2.5 higher than the actual (presumed) first eigenfrequency of 13 Hz. This means that the overall stiffness of the actual column assembly is 6.25 (using Equation 6.6) times lower, but additionally to this it is likely that the stiffness distribution along the column is not homogeneous. Since the first eigenfrequency is that much lower in the actual assembly it could be that the bottom half is relatively less stiff than the upper half of the column, but this is not necessarily true. To increase the stiffness of the column

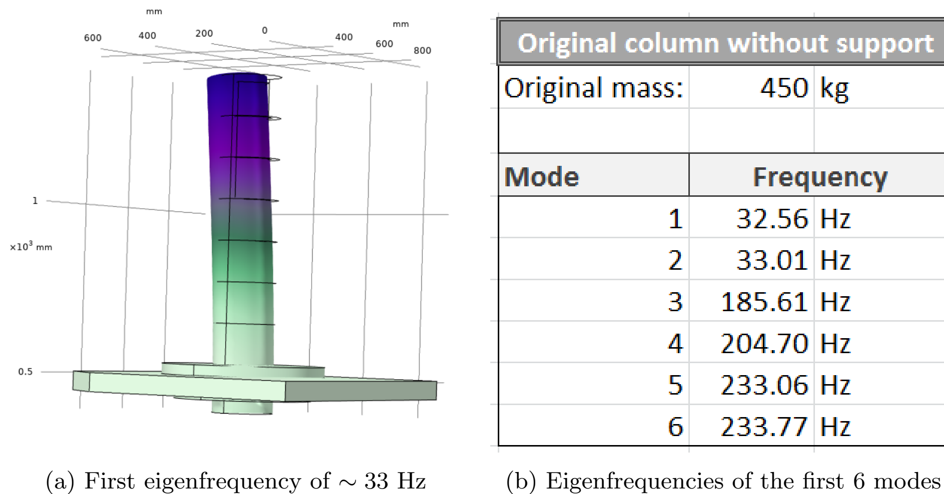

Original column without support		
Original mass:	450	kg
Mode	Frequency	
1	32.56	Hz
2	33.01	Hz
3	185.61	Hz
4	204.70	Hz
5	233.06	Hz
6	233.77	Hz

(a) First eigenfrequency of ~ 33 Hz (b) Eigenfrequencies of the first 6 modes

Figure 6.18: First six eigenmodes of the original column assembly

assembly three triangular plate at 120 degrees apart are added connected to the top of the vacuum cover and the side of the column. The thickness of these plates is varied and with 15 and 20 mm and to reduce the weight, holes

are added in the 20 mm thick plates. The first eigenmode of the 20 mm thick plate assembly can be seen in Figure 6.19a and the one with added holes is displayed in Figure 6.19b. In Figure 6.20 the eigenfrequencies of the six mode shapes that correspond with the mode shapes of the original column assembly are given. Each figure gives the added mass compared to the original setup and the relative increase in mass with the 'mass factor'. It also shows the relative increase in eigenfrequency (compared to the original situation of figure 6.18b), this is labeled as the 'frequency factor'. The 'stiffness factor' is the relative increase in stiffness and is determined from the mass factor and the frequency factor via the relation:

$$\frac{f_2}{f_1} = \frac{\sqrt{\frac{k_2}{m_2}}}{\sqrt{\frac{k_1}{m_1}}}$$

$$\frac{k_2}{k_1} = \left(\frac{f_2}{f_1}\right)^2 \cdot \frac{m_2}{m_1} \tag{6.6}$$

This stiffness factor is given with the assumption that the stiffness distribution is homogeneous. However, if the column assembly is relatively less stiff in the lower half of the column, the added triangular plates would increase the stiffness by an even higher factor. In the same frame of mind, if the stiffness distribution in the actual system is leaning towards a relatively higher stiffness in the lower half of the column, the added side plates could have a less dramatic effect than estimated. This is something that should be investigated further. From Figure 6.20a and

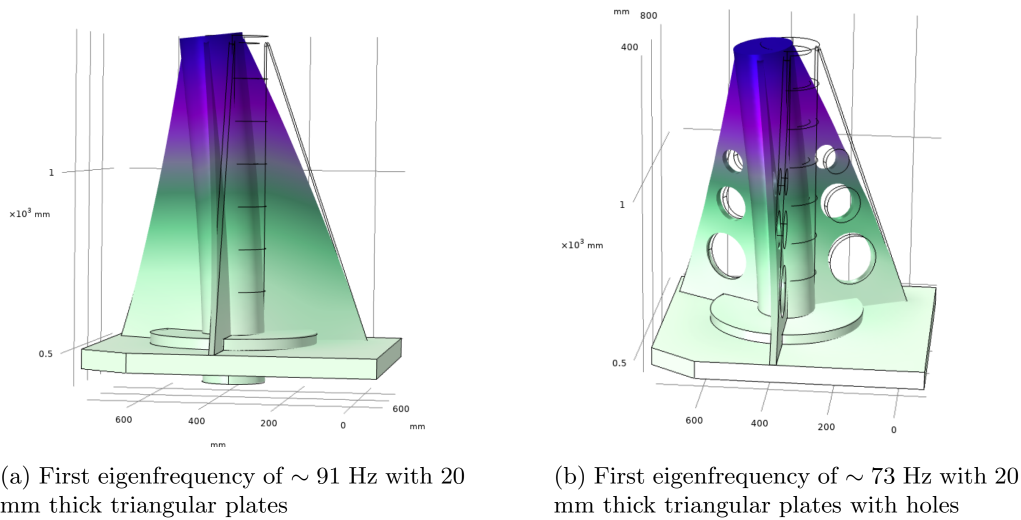

(a) First eigenfrequency of ∼ 91 Hz with 20 mm thick triangular plates

(b) First eigenfrequency of ∼ 73 Hz with 20 mm thick triangular plates with holes

Figure 6.19: First eigenmodes of the different supported column assemblies

6.20b it can be noticed that a thicker plate increases the eigenfrequency and stiffness. Looking only between these two situations the 10 mm thicker plate leads to a first eigenfrequency that is ∼ 10% higher, a mass that is ∼ 4% higher and a stiffness that is ∼ 25% higher. In Figure 6.20c holes are added in the thicker plate of 20 mm. This leads to a same increase in mass as the thinner plate, namely 51 kg. However in this situation the stiffness factor is lower compared to the 15 mm plates of Figure 6.20a (∼ 22% lower) and therefore also the eigenfrequency (∼ 12% lower). So it is better to decrease the weight of the plates by decreasing the thickness rather than by making holes in the plates.

Added sides 15mm thick				
Added mass:	51	kg		
Mass factor:	1.113			
Mode	Frequency		Frequency factor	Stifness factor
1	82.96	Hz	2.55	7.23
2	85.65	Hz	2.59	7.50
3	265.47	Hz	1.30	1.87
4	199.71	Hz	1.08	1.29
5	326.39	Hz	1.40	2.18
6	328.38	Hz	1.40	2.20

(a) With 15 mm thick plates

Added sides 20mm thick				
Added mass:	68	kg		
Mass factor:	1.151			
Mode	Frequency		Frequency factor	Stifness factor
1	91.18	Hz	2.80	9.02
2	94.81	Hz	2.87	9.50
3	280.59	Hz	1.37	2.16
4	201.61	Hz	1.09	1.36
5	357.55	Hz	1.53	2.71
6	360.40	Hz	1.54	2.74

(b) With 20 mm thick plates

Added sides 20 mm thick with holes				
Added mass:	51	kg		
Mass factor:	1.113			
Mode	Frequency		Frequency factor	Stifness factor
1	73.41	Hz	2.25	5.66
2	75.13	Hz	2.28	5.77
3	245.54	Hz	1.20	1.60
4	202.87	Hz	1.09	1.33
5	315.86	Hz	1.36	2.04
6	317.55	Hz	1.36	2.05

(c) With 20 mm thick plates with holes

Figure 6.20: The first six eigenmodes that correspond with the first six eigenmodes of the original column assembly and the relative increased stiffness, mass and eigenfrequency.

Another option to improve the column swing error is by compensating for it in some form. A possible way this could be done with the differential interferometers is by measuring both the displacement of the stage mirror and the column mirror separately. In that case the displacement of the electron optical column is known. Since by far the most likely movement of the electron optical column will be the swinging motion, this information could be used to make a feedforward correction on the electron beam that is determined with the use of a calibration procedure. To avoid using this correction (incorrectly) on long term effects, such as thermal drift between the optical column and interferometer, a high-pass filter could be used.

Chapter 7

Column mirror design

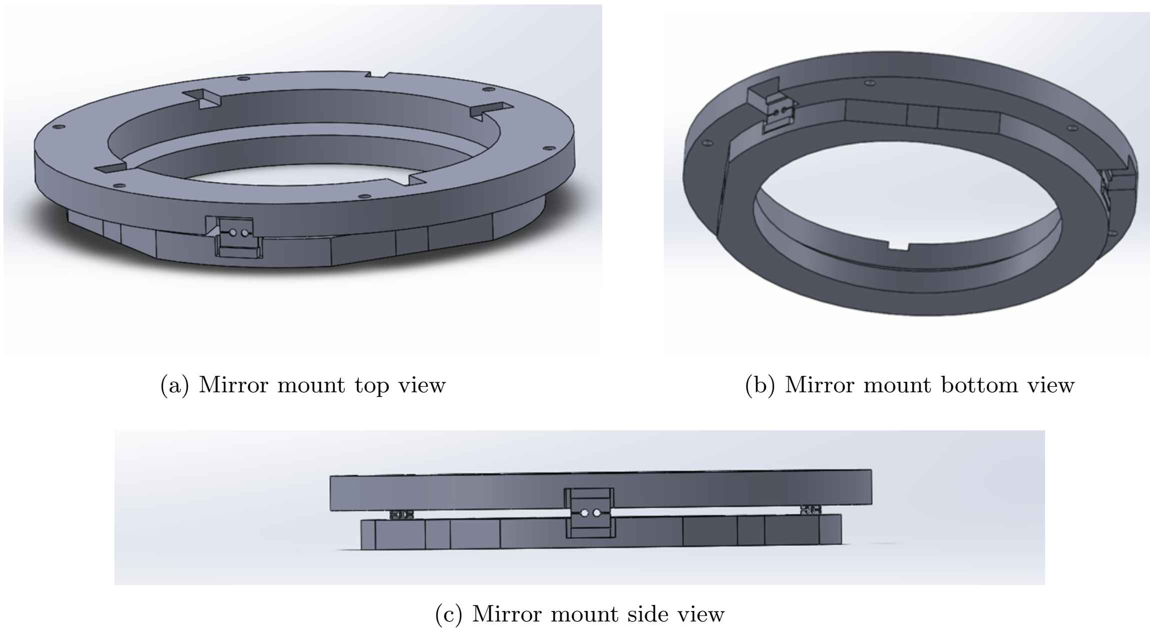

(a) Mirror mount top view

(b) Mirror mount bottom view

(c) Mirror mount side view

Figure 7.1: Mirror mount design

Figure 7.1 shows the column mirror mount design. The mount consists of two rings that are attached with 3 flexures. The top ring is called the alignment ring and is used as a flange to align the mirrors in yaw. The lower ring is called the mirror ring and houses the mirrors. Each design aspect will be discussed further in the next sections.

7.1 Flexure design

As discussed in the previous chapter, the mirrors will be attached to the optical column with three flexures that are at 120 degrees apart from each other. The requirements for the flexure mechanism are the following:

- The mechanism should be exactly constraint to make the expansion homogeneous and avoiding high stress
- The thermal center should be co-inside with the optical axis of the electron optical column
- The mechanism should be symmetric with connection 120 degrees apart

One mechanism that meets the requirements consist of something that creates two 'screws' that have opposite rotational components from each other. A 'screw' is an admissible movement that exists of two DOF's (Degrees Of Freedom), a rotational component and a translational component, that are coupled[20]. The admissible movement

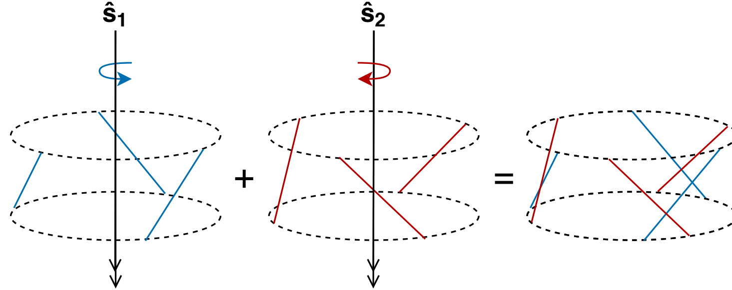

Figure 7.2: Two screws with opposite rotational freedom together constraint 6 DOF's

is a rotation around the screw and a translation parallel to the the screw. In Figure 7.2 the two opposite screws are drawn ($\hat{\boldsymbol{s}}_1$ and $\hat{\boldsymbol{s}}_2$). The blue and red lines are constraint lines. The resulting mechanism is exactly constraint and exists of 3 pairs of crossed constraint lines. This means for each flexure mechanism two constraints lines can be drawn. Each mechanism that suffice the desired constraint lines is adequate. The crossing point of the constraint lines can be shifted arbitrarily, as long as they cross each other. Figure 7.3a shows the desired constraint lines and Figure 7.3b shows different solutions that suffice the desired constraints. The first mechanism is a notched leaf flexure, the second is a triangle flexure and the third mechanism exists of two stiff rods parallel with the constraint lines.

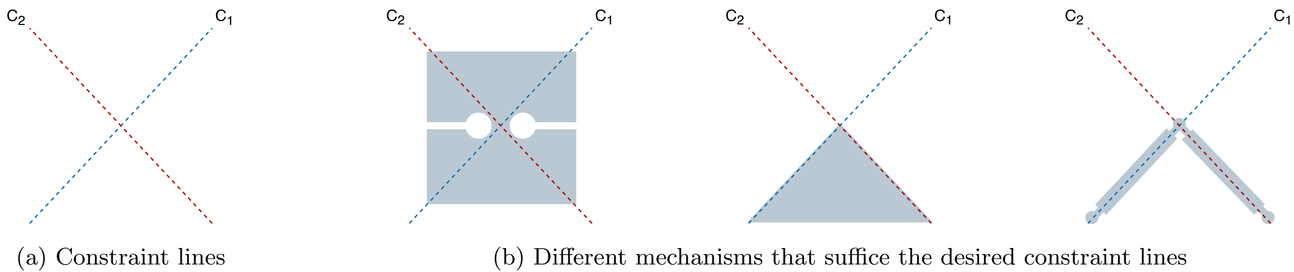

(a) Constraint lines (b) Different mechanisms that suffice the desired constraint lines

Figure 7.3: The required constraint lines and different mechanisms that fulfill the constraints

The mechanism that uses two separate stiff rods is the most complex of the three to produce and assemble and therefore will be eliminated. The remaining two mechanisms are both very suitable and easy to implement. Out of the two the notched leaf spring will be picked, mainly for the reason that with this concept additional torsional stiffness is easier added. The fact that the flexures are orientated at 120 degrees and the two mirrors are at 90 degrees from each other, makes it impossible to align both mirrors with a flexure. To add the most stiffness perpendicular to the mirrors ideally one would like to align the mirrors with the flexures, but the fact that this is not possible is the price that was paid for symmetry. To optimize the amount of stiffness perpendicular to both mirrors, the optimum gives an orientation at which one of the flexures is orientated at 45 degrees to both mirrors. This is visualized in Figure 7.4a. The flexure dimensions are given in Figure 7.4b. The ratio between the hole diameter D and the width between the two holes h is the elastic hinge parameter β:

$$\beta = \frac{h}{D} \tag{7.1}$$

The design rule of thumb for the elastic hinge parameter is that it should be $0.01 < \beta < 0.5$ [21]. If β is higher than 0.5 the notch in the flexure is no longer functioning as a hinge. If β is smaller than 0.01 it is hard to manufacture.

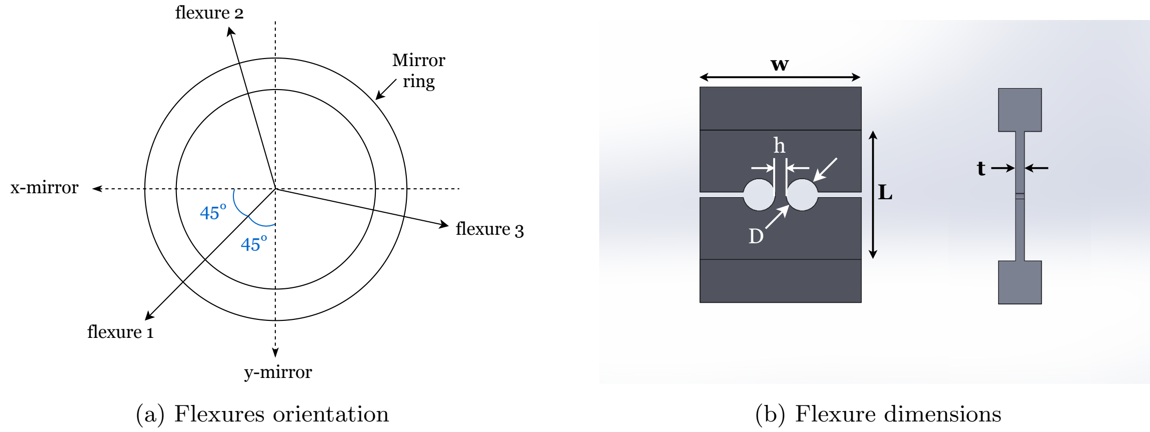

(a) Flexures orientation (b) Flexure dimensions

Figure 7.4: Flexures orientation and dimensions

Two materials will be considered for the flexures, aluminum and steel. These are materials that are easily accessible and machinable and that are suitable materials to use as flexures. For aluminum the 7075 alloy will be used and for the steel S355 structural steel (even if another type of steel or stainless is used, the yield strength and Young's modulus are similarly valued). An indicator of a suitable flexure material is the resilience. This is the ratio between the yield strength and the Young's modulus[24].

$$\text{Resilience} = \frac{\sigma_y}{E} \tag{7.2}$$

In general, the higher the resilience the better the material is suited to use for a flexure. In Table 7.1 the two materials are compared. Solely based on the resilience the aluminum 7075 is a better suited flexure material. The

Table 7.1: Flexure materials

Material	σ_y [MPa]	E [GPa]	Resilience $\cdot 10^{-3}$
Steel S355	355	200	1.8
Aluminum 7075	505	70	7.2

dimensions of the flexure as depicted in Figure 7.4b in combination with the material should lead to a flexure that is a trade-off between two opposite goals. On the one hand it should be as flexible as possible such that it allows the deformation difference between the two rings without too much stress build up, but on the other hand it should be as stiff as possible to ensure a high eigenfrequency of the mirror mount. Another trade-off criteria is the use of space, there is a limited space for the entire mirror mount so this should be taken into account when choosing the flexure dimensions. To determine all the dimension an optimization process is required. For a limited amount this has been done, but further optimization might be necessary. The dimensions for the two flexures with different materials are given in Table 7.2. As it can be noticed, only the thickness t is different for the two materials. The elastic hinge parameter $\beta = 0.33$ for both flexures.

Table 7.2: Flexure dimension for different materials

Dimension [mm]	Steel S355	Aluminum 7075
w	15	15
L	15	15
h	1	1
D	3	3
t	0.5	0.8

7.2 Alignment system

In Chapter 6.3 it was determined that the column mirrors should be aligned in yaw on the optical column. The way this will be done is by rotating the entire mount, the alignment between the separate mirrors will be determined by the tolerances of the manufacturing process. This means no separate alignment between the individual mirrors will be done. The yaw alignment of the mirror mount is done with the alignment ring that is used as a flange fitted around the optical column. This ring is shown in Figure 7.9b. The ring can be rotated and when the desired orientation is achieved, bolted down with six bolts. The bolts will have springs attached to them to keep pretension between the ring and the column.

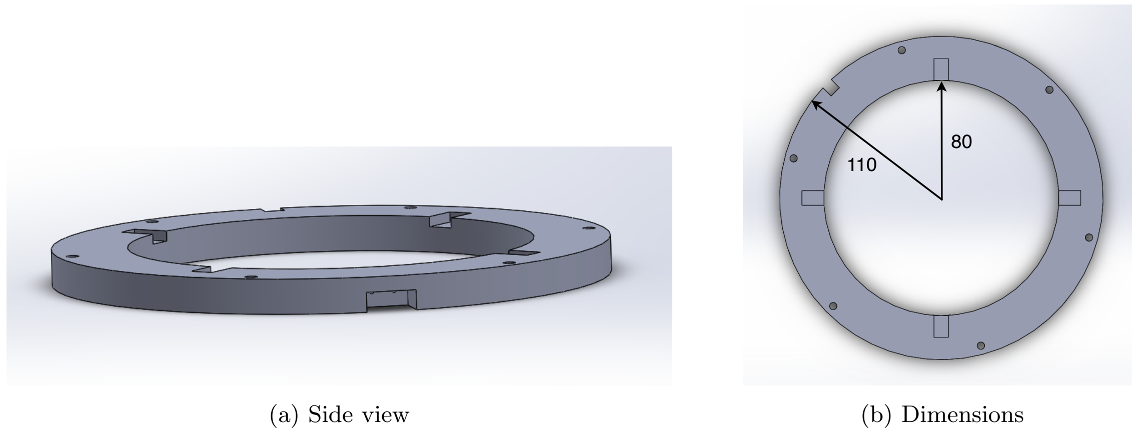

(a) Side view (b) Dimensions

Figure 7.5: Alignment ring of the column mirror mount

As discussed in Chapter 6.4 to solve the height constraint issue, the mirror mount will be mounted 'in' the optical column. This means the top part of the mirror mount will be integrated in the height meter ring. This is depicted in Figure 7.6. Part of the outside of the height meter ring will be removed in order to fit the alignment ring of the column mirror mount around it. To match the thermal expansion of the height meter ring and to ensure

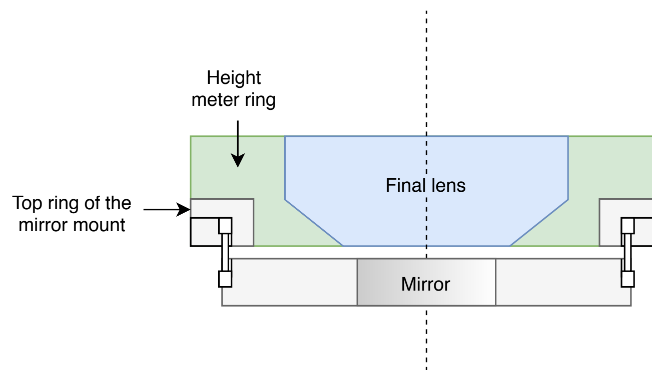

Figure 7.6: Mounting the alignment ring of the mirror mount

the temperature distribution in the top ring is also homogeneous, the ring will be made out of the same material as the height meter ring which is Aluminum 7075. To fit in the height meter ring four compartments are taken out of the top side of the ring (as depicted in Figure 7.9b) to make room for the four glass tubes that run through the height meter ring. Figure 7.7 show how the column mirror mounts are integrated in the current system. In this view the stage mirrors have not been adjusted jet so the height between the column mirrors and the stage mirror is not completely accurate.

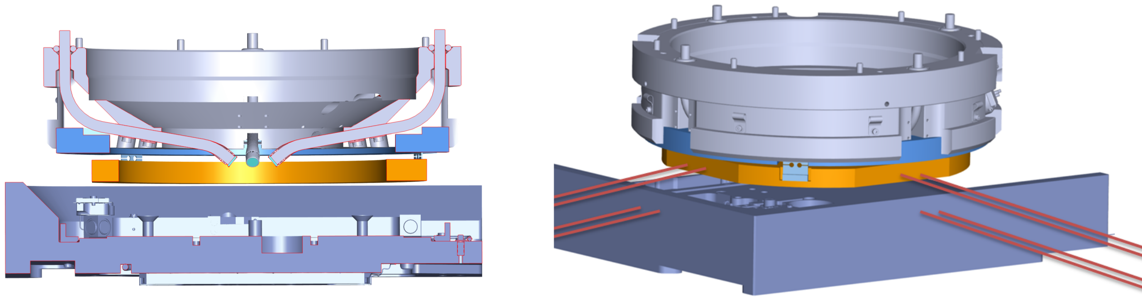

Figure 7.7: Mirror mount integrated in current system

Alignment mechanism
To rotate the alignment ring relatively to the height meter ring an alignment mechanism is used. A small compartment will be cut out of the alignment ring as shown in Figure 7.8a and the alignment mechanism used is a lever. The lever consists of a rod with two different sized balls on it, the principle of using this kind of lever is based of (*J. Nijenhuis et al.*, 2005 [22][23]). In their design they use a long stick with two balls which they actuate by hand as a 'joystick' to rotate and laterally move the mount of a mirror. The way this type of lever will be implemented and used in this system is slightly different and is shown in Figure 7.8b. The lever will not be actuated by hand, but

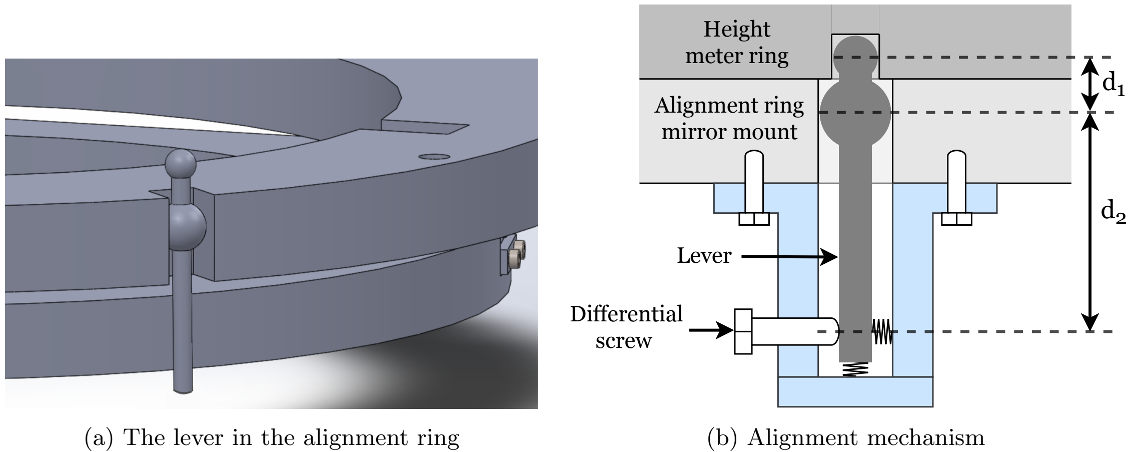

(a) The lever in the alignment ring (b) Alignment mechanism

with a fine threaded or differential screw. The upper ball will be inserted in a hole in the height meter ring and the lower ball will be inserted in the cut out of the alignment ring. Two springs connect the rod with the housing of the alignment mechanism. These springs provide pretension between the rod and the differential screw and between the upper ball and the height meter ring. The housing is bolted down to the alignment ring. When the differential screw is tightened the movement of the differential screw is translated to a movement of the alignment ring relative to the height meter ring.

They gear ratio of the lever is equal to:

$$\text{gear ratio} = \frac{d_1}{d_2} \tag{7.3}$$

If $d_1 = 10$ mm and $d_2 = 40$ mm then the ratio is equal to $\frac{1}{4}$. If the desired angular alignment resolution is ~ 0.1 mrad, then the resolution of the movement of the upper ball should be $\sim 10\mu$m. This means the resolution of the differential screw, the pitch, should be $10 \cdot 4 = 10\mu$m. The angular range of alignment mechanism should be $\sim$ 6mrad, 1.5 times the expected misalignment of 4 mrad. This means the alignment range of the alignment ring should be 0.6 mm and this means the range of the differential screw should be ~ 2.5 mm.

7.3 Mirror design

The mirror design is kept as simple as possible. The mirrors are integrated in a ring which will have two flat surfaces. The mirror design is visualised in Figure 7.9b. Depending on which material will be used for the ring, the mirrors will either be the flat surfaces themselves or the mirrors will be glued to the flat surfaces. In the latter case a small cavity will be made in the flat surfaces leaving three small contact areas. The separate mirrors will then be glued with some glue from the sides to these three contact points. The expected dimensions of the mirror ring can be seen in Figure 7.9a. These dimensions can be changed while evaluating the dynamic performance of the design.

Figure 7.9: Mirror design

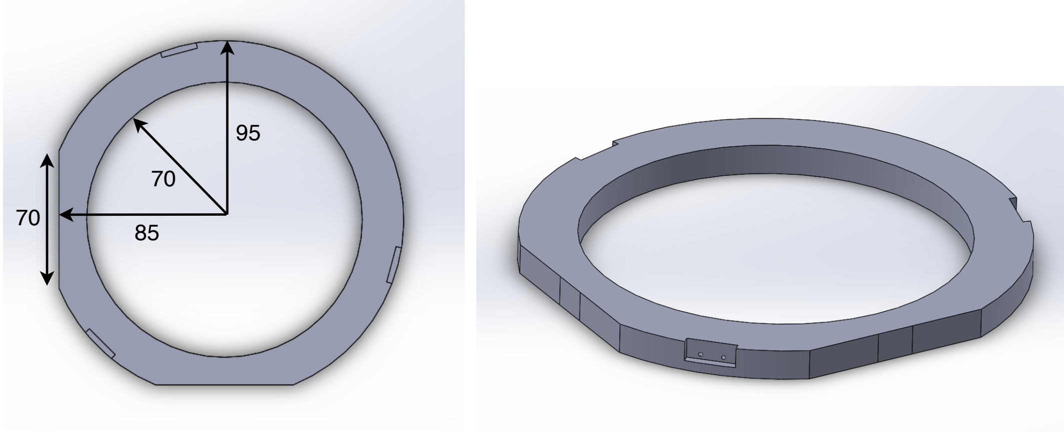

(a) Mirror ring dimensions

(b) Top part of the column mirror mount

Mirror material

The material of the mirror ring should have a low CTE. Two materials will be considered for now, Invar36 and Zerodur. Invar is more cost friendly than Zerodur, so if Invar is an option this would be preferred. If the temperature variation of the mirror $\Delta T = 0.1$ K, then the thermal expansion when Invar is used is equal to:

$$\Delta x = 1.2E^{-6} \cdot 0.1 \cdot 85E^{-3} = 10.2 \text{ nm} \tag{7.4}$$

This means an optical path length error equal to 10.2 nm. This is equal to the whole allowed budget according to the requirements. For this reason Invar is not a suitable option. With Zerodur the thermal expansion is equal to:

$$\Delta x = 0.02E^{-6} \cdot 0.1 \cdot 85E^{-3} = 0.17 \text{ nm} \tag{7.5}$$

The optical path length error is a lot smaller with Zerodur and stays within the 10 nm/h budget with a large margin. Another advantage of using Zerodur is that the mirrors can be integrated directly into the mirror ring as the two flat surfaces. One thing that needs to be taken into account when choosing for Zerodur, is that this material is non-conducting (of electricity). If this is not addressed the mirror ring will have charge build up. This electric potential will influence the electron beam and eventually a potential breakdown will occur. To create a conducting layer on the ring it will be entirely coated in aluminum. This additionally makes the mirror surfaces reflective, hitting two birds with one stone.

7.4 Dynamic behaviour analysis

A short dynamic behaviour analysis of the column mirror mount will be made in the coming sections. Further development and optimization is needed to finalize the column mirror design, but a good start has been made.

7.4.1 Eigenfrequency analysis

Table 7.3: First six eigenfrequencies of the mirror mount

Steel flexure		**Aluminum flexure**	
Mode	Eigenfreq. [Hz]	Mode	Eigenfreq. [Hz]
Shear	662.07	Shear	527.22
Shear	664.33	Shear	527.36
First order bending	955.36	Rotation	847.69
First order bending	1020.3	First order bending	894.97
Rotation	1102.4	First order bending	955.58
Second order bending	1349.6	Second order bending	1172.8

An overview of the first six eigenmodes with corresponding eigenfrequencies is given by Table 7.3. Overall for both materials the first eigenfrequencies are already very high, which is desirable. The higher the eigenfrequency the less chance that this frequency will be excited during operation and the smaller the amplitude will be of any vibration. The steel flexure shows higher eigenfrequencies than the aluminum flexure. It can be seen that not all the modes are expressed in the same ascending order for the aluminum and steel flexure. The rotation mode for the steel flexure is excited at a much higher eigenfrequency than it does for the aluminum flexure. The first modes for the two different flexure materials are shown in Figure 7.10, they are both shear motions.

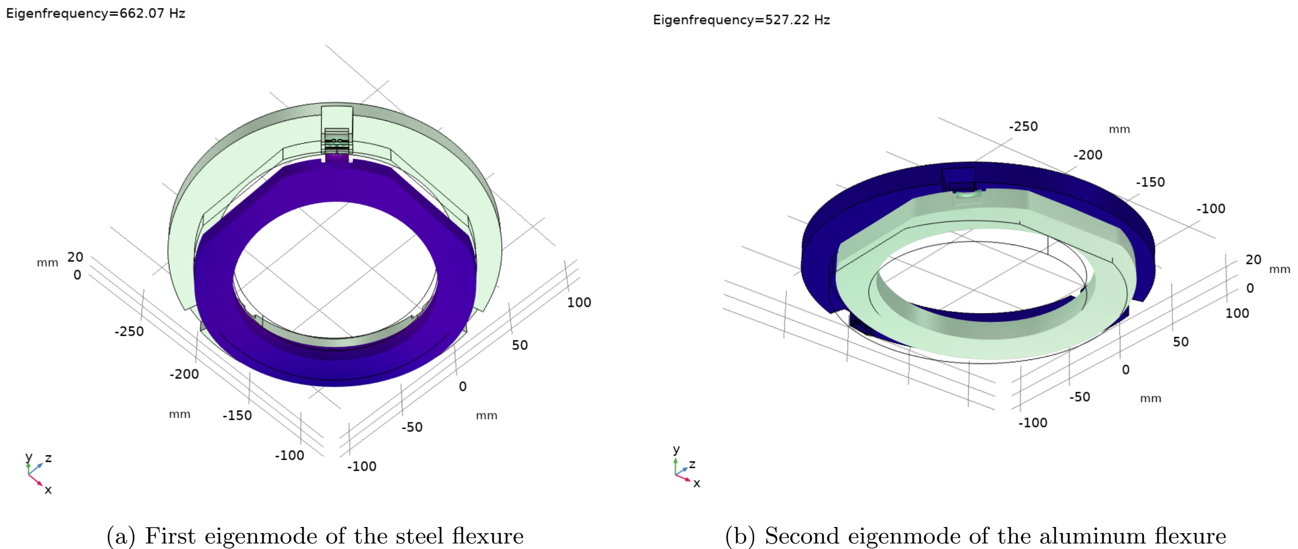

(a) First eigenmode of the steel flexure

(b) Second eigenmode of the aluminum flexure

Figure 7.10: First eigenmodes of the two different flexures

7.4.2 Steady state behaviour

If a temperature difference of $\Delta T = 0.1$ K is applied to the mirror mount system the mount and flexures will expand. The resulting steady state thermal expansion due to ΔT is shown in Figure 7.11a for the mirror mount with the aluminum flexures. The mirror ring will experience a downwards movement because the flexures expand, but this does not negatively influence the displacement measurement of the mirrors. The stress due to this thermal expansion is depicted in Figure 7.11b. The stress is maximum 0.5 MPa which is very low. Even with a $\Delta T = 20$ K the stress experienced in the flexures is < 30 MPa. This means the most important criteria for the stress in the flexures are the manufacturing tolerances during assembly of the mirror mount system.

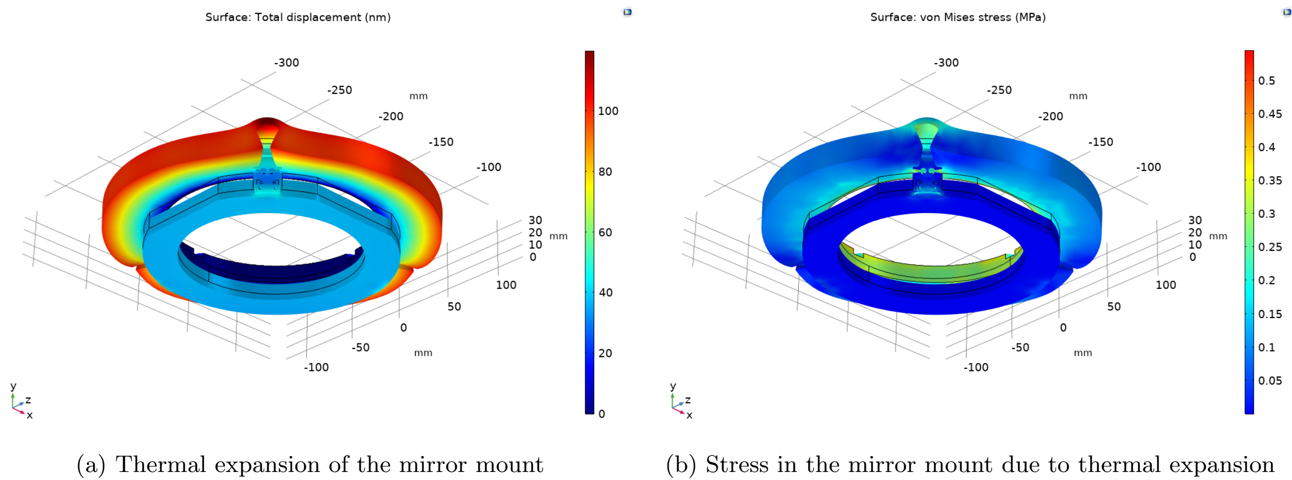

(a) Thermal expansion of the mirror mount

(b) Stress in the mirror mount due to thermal expansion

Figure 7.11: Steady state thermal expansion with $\Delta T = 0.1$ K for the mount with aluminum flexures

Figure 7.12a shows the static deformation due to gravity. The mirrors are moved down with about 160 nm. As this is a static situation and the mirrors are mostly moved in a straight line down, it does not influence the interferometer measurements. The associated stress is depicted in Figure 7.12b and is very low (< 1.5 MPa).

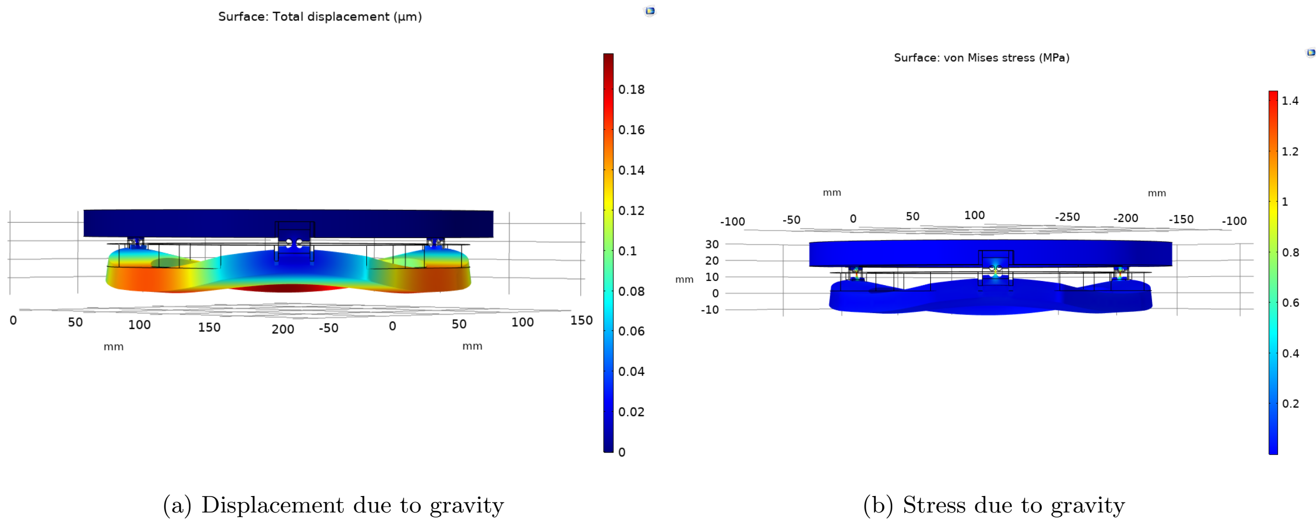

(a) Displacement due to gravity

(b) Stress due to gravity

Figure 7.12: Deformation due to gravity with the aluminum flexures

To investigate the possible deformation of the flexure during assembly a lateral deformation of 0.05 mm is applied to both the aluminum and steel flexure. The resulting stress is displayed in Figure 7.13. For the steel flexure the stress is twice as high as for the aluminum flexure. The steel flexure is a factor 3.9 away from the yield strength, while the aluminum flexure is a factor 11 away from the yield strength. With higher deformations the steel flexure may be too stiff compared to its yield strength, while the aluminum flexure has a much higher margin for higher deformations. Of course this is something that can be looked into further and optimised. Because of this margin the aluminum flexure seems the more suitable out of the two for now, even though the eigenfrequencies are slightly lower.

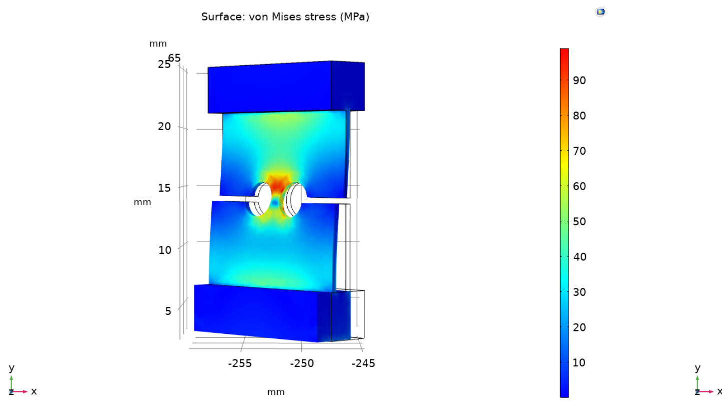

(a) Steel flexure

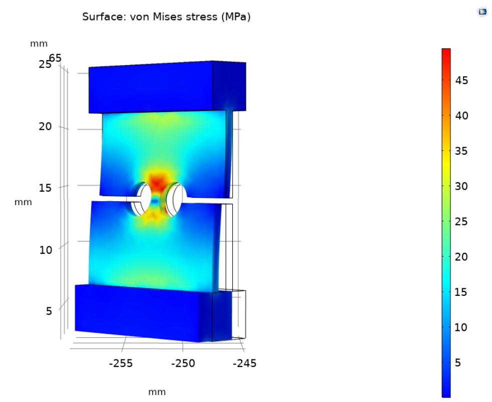

(b) Aluminum flexure

Figure 7.13: Stress in the flexure due to a 0.05 mm lateral displacement

Chapter 8

Concept analysis: error budget

8.1 Beam stability

To evaluate the beam stability of the new concept for the short term and long term new errorbudgets have been made. Designing the new system and using an error budget to see if the requirements are met is an iterative process. For the static non-repeatable errors a new error budget has been made, depicted in Table 8.1. The parameters that are changed compared to Table 4.4 are the non-repeatable yaw angle, by measuring the yaw angle the uncertainty is reduced from 10μrad to 0.01 μrad[10]. The other parameter that has changed is the optics cyclic error, to reduce the error from 1 nm to 0.1 nm it is recommended to use a cyclic error correction procedure. These changes lower the non-repeatable static errors from 1.4 nm to 1.18 nm. For the short term dynamic error budget it was evaluated

Table 8.1: Non-repeatable static errors with error source new system

Contributor	**Unc.**	**unit**	**Prob. dist.**	**Div.**	**Sens.**	**Perf.**	**unit**	**[%]**	**Remarks**
Alignment/Abbe errors	0.71	nm						36.2	
Pitch error non-repeatable	10	μrad	Normal, 2s	2.00	0.1	0.50	nm	18.1	0.1 mm offset
Roll error non-repeatable	10	μrad	Normal, 2s	2.00	0.1	0.50	nm	18.1	0.1 mm offset
Yaw error non-repeatable	0.01	μrad	Normal, 2s	2.00	0.1	0.001	nm	0.0	0.1 mm offset
Instrumentational errors	0.94	nm						63.8	
Laser stability	0.002	ppm	Uniform	1.73	800.00	0.92	nm	31.8	
Optics cyclic error	0.1	nm	Uniform	1.73	1.00	0.06	nm	0.2	Periodic error
Measurement resolution	0.155	nm	-	1.00	1.00	0.16	nm	1.7	$\lambda/4096$
Non-repeatable static errors	1.18	nm						100.0	

in Section 4.3 that 'other noise sources' in the system led to an error of $\sim$ 2.1 nm. The dynamic metrology errors present in the new system are equal to the dynamic pitch and yaw errors discussed in Section 6.3.3. With a pitch alignment of $\sim$ 0.6 mrad and a dynamic pitch angle of $\sim$ 1 μrad the error in optical path length is 0.4 nm. The estimated yaw alignment is calculated by taking the root sum square of all tolerances. This is given by Table 8.2.

Table 8.2: Total yaw angle between optical components

Yaw angle	mrad
Orthogonality stage mirrors	0.7
Orthogonality column mirrors	0.1
Rotation mirror stage and stage	0.05
Alignment column mirrors	0.1
Alignment interferometer	0.1
RSS	0.72

A yaw alignment of 0.72 mrad combined with an dynamic yaw error of ~ 0.2 μrad gives an optical path length error of 0.1 nm. The RSS of the two errors is $\sqrt{0.4^2 + 0.1^2} = 0.41$ nm. This will be rounded up to 0.5 nm. The error budget for the short term beam stability is represented by Table 8.3. The total short term beam stability is equal to 3.34 nm. This means the stability is improved from < 5 nm to < 3.5 nm, so the requirement is met. The

Table 8.3: Short term beam stability error budget new system

Error source	**nm**	[%]
Non-repeatable static error	1.18	35.3
Dynamic errors	2.16	64.7
- Metrology	0.5	3.5
- Other noise sources	2.1	61.2
Total error	3.34	100

long term error budget for the new system can be found in Table 8.4. From the evaluation in Section 4.3 it was concluded that an error of about 45 nm was caused by thermal drift and 5 nm by other error sources. This 5 nm is therefore also shown in the new error budget as 'other error sources'. The thermal drift error sources are based on evaluations in Section 4.2.3 and 7.3. To account for any other metrology drift that is not represented in the error table, an extra error source of 1 nm is added as 'other metrology drift'. The total long term beam stability is equal to 8.8 nm and this means the stability is improved from < 50 nm to < 9 nm. This is a huge improvement (more than 5 times) and it means the user requirement is met. The thermal drift is improved from ~ 45 nm to ~ 3.8 nm, this is improved of almost a factor 12!

Table 8.4: Long term beam stability error budget new system

Error source	**nm**	[%]
Thermal drift	3.8	43.2
- Optics	1	11.4
- Substrate	1.3	14.7
- Mirror column	0.2	2.3
- Mirror stage	0.3	3.4
- Other metrology drift	1	11.4
Other error sources	5	56.8
Total error	8.8	100

8.2 Other user requirements

Overlay

The overlay will be improved with the use of the yaw measurement this improves the error from 7 nm to 0.07 nm. Another way the overlay is improved is through the improvement of the non-repeatable static errors in Table 8.1. This does not bring that big of a change, only an improvement of 0.22 nm. This brings the total contribution of the interferometer down from 7.13 nm to $\sqrt{0.07^2 + 1.18^2 + 0.125^2} = 1.19$ nm. This is an improvement of the error contribution of the metrology of a factor of 6.

Throughput

For the throughput no real numbers can be given. However the initial measurement error due to a column swinging motion is reduced an order of magnitude from ~ 500 nm to ~ 45 nm. This could be improved further by creating a stiffer column assembly and possibly use a double axis differential interferometer to measure the displacement of the column mirror separately and use feedforward correction.

Chapter 9

Conclusion

The aim of this thesis was to improve the beam stability of the system in the short and long term by redesigning the metrology system. The beam stability for the short term (time $\leq$ 1 s) should be improved from $\leq$ 5 nm to $\leq$ 3.5 nm. The long term beam stability ($\leq$ 1 h) should be improved from $\leq$ 50 nm to $\leq$ 10 nm. A powerful aspect of the metrology is that every accurate displacement measurement can be corrected for with the high deflection bandwidth of the electron beam. For the short term stability it was found that a significant part is caused by vibrations on the metrology (about 50%). These vibrations cause measurement errors because the interferometers are very sensitive (sensitivity of 1) to any movements parallel to the measurement axis. For the long term beam stability it was found that thermal errors contribute up to 90% of the total error and that they are mostly caused by thermal drift between the interferometer and the mirror on the stage. The proposed design is a metrology system that uses a differential interferometers that measure the relative displacement between a mirror on the stage and a mirror on the electron optical column. This decreases the sensitivity of the interferometer from 1 to 0 to movements parallel to the measurement axis. It decreases the sensitivity of the metrology to vibrations and thermal expansion by a significant amount. To ensure the thermal expansion of the column mirrors is minimized, a thermal insensitive mirror mount was designed. The mirrors are integrated in a ring that is made from a material with a low coefficient of thermal expansion (Zerodur). This ring is attached to the optical column with three notched leaf springs that ensure the thermal center coincides with the center of the optical column. The evaluated first eigenfrequency of the column mirror mount is $\sim$ 500 Hz. The proposed design improves the short term beam stability from $\leq$ 5 nm to $<$ 3.5 nm, so the requirement is met. The long term beam stability is improved from $\leq$ 50 nm to $<$ 9 nm, so also this requirement is met.

Chapter 10

Recommendations

This thesis project approached the design process by evaluating the system as a whole rather than zooming in on one specific part. This makes the project very wide, but less deep. The proposed design was elaborated to a great extend, but not into full detail. To really implement this design, further elaboration is needed. For example the mounting of all the optical components (except the column mirrors) was not worked out into detail. This is something that should be done in collaboration with the optical component supplier. Also, no technical drawing is made with all the tolerances on it for the flatness/parallelism of the mounting surface and the positions of the dowel pin holes. The beam benders BB_x and BB_y should be aligned in the yaw direction, so they should have some sort of alignment mechanism. This thesis does not elaborate this further. It is recommended to use a similar type of alignment mechanism as for the column mirrors. This means the use of a flange with a lever and differential screw. This would allow alignment, but would still ensure a stiff connection if the mount is bolted down.

Another design aspect that should be elaborated further is the improvement of the column swing error. First of all the dynamic behaviour of the column should be investigated further. This means a more in-depth evaluation should be made about how large the errors are that are caused by this motion and the nature and frequency of this motion. The Comsol model made in this thesis could be worked out further to more accurately represent the real system. After investigating the dynamic behaviour more in-depth solutions should be thought of to increase the stiffness and eigenfrequency of the column and how these can be implemented in the current system. The use of a two-axes differential interferometer is also a promising solution to improve the column swing errors.

The proposed design uses a differential yaw interferometer on one of the measurement axes. How this information is used is not described in this thesis. This information should be used in some way to correct for the measured yaw. It is recommended to use it as an additional electron optics correction as this is probably the most simple way to implement it. The signal could be decomposed into a additional x and y correction on the beam error feedback.

During the error source evaluation the absolute accuracy of the system (when solely looking at the static errors) was in the order of 200 nm. This is a large error and if a higher absolute accuracy is desired, calibration of the system shall be necessary. This could be done by creating a 'golden standard' for which all the dimensions are fully measured and which is then used to calibrate the system.

A last recommendation concerns the use of material in the current system. With the introduction of the differential measurement the sensitivity of the interferometers to movements parallel to the measurement axis became 0. This means the displacement measurement is not influenced by thermal expansion between the interferometer and the mirrors. Therefore the use of Invar for the suspension top/bottom plate, the vacuum cover and the CSR are no longer necessary. It is recommended to use other materials for these parts. For example the vacuum cover could be made out of regular steel and the suspension plates out of aluminum (the same material the side plates of the suspension are made of). This will decrease the overall costs of the system as Invar is an expensive material to use.

Bibliography

[1] P. Tipler, G. Mosca. *Physics for scientists and engineers.* Sixths edition, W. H. Freeman and Company, 2008.

[2] Z. Cui. *Nanofabrication: Principles, Capabilities and Limits.* Second edition, Springer International Publishing Switzerland, 2017.

[3] Raith nanofabrication.
`https://www.raith.com/products/ebpg5200.html`

[4] J. Orloff. *Handbook of charged particle optics.* Second edition, CRC Press Taylor & Francis Group, 2009.

[5] R. Leach, S. Smith. *Basics of Precision Engineering.* CRC Press, Taylor & Francis Group, 2018.

[6] ASM International Materials Properties Database Committee, technical editor: Fran Ceverna. *ASM ready reference: thermal properties of metals.* ASM International, 2002.

[7] SCHOTT AG *Thermal Expansion of ZERODUR.* SCHOTT AG folder, 2013.

[8] A.Tesar, B.Fuchs. *Zerodur Polishing Process for High Surface Quality and High Efficiency.* Optcon '92 Optical Fabrication and Testing Workshop, 1992.

[9] Agilent Technologies. *Agilent Laser and Optics User's Manual, Volume I.* Fifth edition, Agilent Technologies Inc., 2007.

[10] Agilent Technologies. *Agilent Laser and Optics User's Manual, Volume II.* Fifth edition, Agilent Technologies Inc., 2007.

[11] A. Rosenbluth, N. Bobroff. *Optical sources of nonlinearity in heterodyne interferometers* Precision engineering, Volume 12, Issue 1, 1990.

[12] S. Cosijns, H. Haitjema, P. Schellekens. *Modeling and verifying non-linearities in heterodyne displacement interferometry* Precision engineering, Volume 26, Issue 4, 2002.

[13] Keysight Technologies. *Keysight 5517 Laser Head User's Guide* First Keysight Edition, Keysight Technologies, 2014.

[14] K. Bustraan. *Design Principles.* Mikroniek, Issue 2, 2010.

[15] W. Gao, S. Kim, H. Bosse, H. Haitjema, Y. Chen a, X. Lu, W. Knapp, A. Weckenmann, W. Estler, H. Kunzmann. *Measurement technologies for precision positioning* CIRP Annals - Manufacturing Technology,Volume 64, Issue 2, 2015.

[16] V. Badami. *Encoders graduating to extreme precision.* Mikroniek, Issue 2, 2019.

[17] X. Li, W. Gao, H. Muto, Y. Shimizu, S. Ito, S. Dian. *A six-degree-of-freedom surface encoder for precision positioning of a planar motion stage.* Precision Engineering, Volume 37, Issue 3, 2013.

[18] H. Kunzmann, T. Pfeifer, J. Flügge. *Scales vs. Laser Interferometers: Performance and Comparison of Two Measuring Systems*. CIRP Annals, Volume 42, Issue 2, 1993.

[19] HEIDENHAIN. *Exposed Linear Encoders*. Catalogue, 2014.

[20] J. Hopkins, M. Culpepper. *Synthesis of multi-degree of freedom, parallel flexure system concepts via Freedom and Constraint Topology (FACT) – Part I: Principles*. Precision Engineering, Volume 34, Issue 2, 2010.

[21] JPE. *Precision Point. To the point precision engineering knowledge*. fourth edition, 2019.

[22] J. Nijenhuis, P. Giesen. *Mechanisms enabling observation of Jupiter like planets in deep space*. SPIE proceedings, Volume 5877, Optomechanics, 2005.

[23] J. Nijenhuis, P. Giesen. *A major step forward back in time with the ESO Star Separator system*. SPIE proceedings, Volume 5877, Optomechanics, 2005.

[24] R. Roopa, P. Navin Karanth , S. Kulkarni. *Effect of flexure beam geometry and material on the displacement of piezo actuated diaphragm for micropump*. IOP Conference Series: Materials Science and Engineering, 2018.